A comparative study of neuroepithelial cells and O_2 sensitivity in the gills of goldfish (*Carrasius auratus*) and zebrafish (*Danio rerio*)

By Peter C. Zachar

Thesis submitted to the
Faculty of Graduate and Postdoctoral Studies
University of Ottawa
in partial fulfillment of the requirements for the
Ph.D. Degree in the
Ottawa-Carleton Institute of Biology

30 September, 2013

ACKNOWLEDGEMENTS

First and foremost, I'd like to thank Michael Jonz for accepting me into his lab and providing continued guidance and support over these past five years. Thank you for your constant availability and input on experiments and new findings. I came into your lab an uninitiated undergraduate, and I come out a research-worn electrophysiologist. I also thank the members of my committee, John Lewis, Steve Perry, and Bill Willmore, for their insight and guidance in bringing my experiments to fruition. Thanks to Les Buck for acting as my external examiner, and to Tuan Bui for agreeing to participate in my defence.

Second, I thank all past and present Jonz lab members, except Sara. Thanks to Ben, but not Sara, for being a sounding board for my ideas, and for making the lab that much more fun to be in. I also thank all my friends for feigning interest in what I've been doing for the last five years, and for their endless optimism. Very special thanks to my wonderful wife Gerri for her continued love and support, and for listening to me talk about ion channels for hours.

Finally, I thank my family for their love, patience, and guidance. Thanks to my dad for his practical advice, and to my mom for teaching me never to quit. I couldn't have achieved what I have without you.

TABLE OF CONTENTS

LIST OF TABLES AND FIGURES

1. General Introduction

2. Expression of the vesicular acetylcholine transporter and associated innervation in the gill

3. Characterization of ion channels and O_2 sensitivity in neuroepithelial cells of the goldfish gill

LIST OF ABBREVIATIONS

$[Ca^{2+}]_i$	Intracellular calcium ion concentration
µm	Micrometer
µM	Micromolar
4-AP	4-Aminopyridine
5-HT	5-Hydroxytryptamine
A594	Alexafluor 594
ACh	Acetylcholine
aFA	Afferent filamental artery
aff.	Afferent filamental aspect
AMP	Adenosine monophosphate
ATP	Adenosine triphosphate
Ba^{2+}	Barium
$BaCl_2$	Barium chloride
Ca^{2+}	Calcium
CaCl	Calcium chloride
Ca_V	Voltage-dependent calcium channel
CB	Carotid body
cc	Common carotid artery
Cd^{2+}	Cadmium
CO	Carbon monoxide
CO_2	Carbon dioxide
CsCl	Cesium chloride
CSN	Carotid sinus nerve
CTCF	Corrected total-cell fluorescence
da	Dorsal artae
dpf	Days post-fertilization
ec	External carotid artery
EDTA	Ethylenedinitriotetraacetic acid
eFA	Efferent filamental artery
eff.	Efferent filamental aspect
EGTA	Ethylene glycol tetraacetic acid
FCS	Fetal calf serum
FITC	Fluorescein isothiocyanate
gpn	Glossopharyngeal nerve
H+	Proton
H2O2	Hydrogen peroxide
H2S	Hydrogen sulfide
HIF-1α	Hypoxia-inducible factor 1-α
HO-2	Haemoxygenase-2
I	Current
I_A	A-type voltage-dependent potassium current
ic	Internal carotid artery
I_{KB}	Background potassium channel current
I_{KCa}	Calcium-activated potassium channel current
I_{KV}	Voltage-dependent potassium channel current

ILCM	Inter-lamellar cell mass
I_{Total}	Total whole-cell current
K^+	Potassium
K_B	Background potassium channel
K_{Ca}	Calcium-activated potassium channel
KCl	Potassium chloride
KH_2PO_4	Potassium phosphate monobasic
K_V	Voltage-dependent potassium channel
MgATP	Magnesium adenosine triphosphate
$MgCl_2$	Magnesium chloride
mM	Millimolar
ms	Millisecond
mV	Millivolts
Na_2HPO_4	Sodium phosphate dibasic
NaCl	Sodium chloride
NADPH	Nicotinamide adenine dinucleotide phosphate
NEB	Neuroepithelial body
NEC	Neuroepithelial cell
nm	Nanometers
NR	Neutral red
O_2	Oxygen
pb	Pseudobranch
pA	Picoamps
PBS	Phosphate-buffered saline
P_{O2}	Partial pressure of oxygen
P_{WO2}	Partial pressure of oxygen in water
s	Second
S.D.	Standard deviation
S.E.M.	Standard error of the mean
sysa	Systemic aorta
TASK	Two-port acid-sensitive K^+ channel
TEA	Tetraethylammonium
V	Voltage
va	Ventral aorta
VAChT	Vesicular acetylcholine transporter
V_m	Membrane potential
vn	Vagus nerve

ABSTRACT

Serotonin (5-HT)-containing neuroepithelial cells (NECs) of the gill filament are believed to be the primary O_2 chemosensors in fish. In the mammalian carotid body (CB), 5-HT is one of many neurotransmitters believed to play a role in transduction of hypoxic stimuli, with acetylcholine (ACh) being the primary fast-acting excitatory neurotransmitter. Immunohistochemistry and confocal microscopy was used to observe the presence of the vesicular acetylcholine transporter (VAChT), a marker for the presence of ACh, and its associated innervation in the gills of zebrafish. VAChT-positive cells were observed primarily along the afferent side of the filament, with some cells receiving extrabranchial innervation. No VAChT-positive cells were observed in the gills of goldfish; however, certain key morphological differences in the innervation of goldfish gills was observed, as compared to zebrafish. In addition, in zebrafish NECs, whole-cell current is dominated by an O_2-sensitive background K^+ current; however, this is just one of several currents observed in the mammalian CB. In zebrafish NECs and the CB, membrane depolarization in response to hypoxia, mediated by inhibition of the background K^+ (K_B) channels, is believed to lead to activation of voltage-gated Ca^{2+} (Ca_V) channels and Ca^{2+}-dependent neurosecretion. Using patch-clamp electrophysiology, I discovered several ion channel types not previously observed in the gill chemosensors, including Ca^{2+}-activated K^+ (K_{Ca}), voltage-dependent K^+ (K_V), and voltage-activated Ca^{2+} (Ca_V) channels. Under whole-cell patch-clamp conditions, the goldfish NECs did not respond to hypoxia (P_{O2} ~ 11 mmHg). Employing ratiometric calcium imaging and an activity-dependent fluorescent vital dye, I observed that intact goldfish NECs respond to hypoxia (P_{O2} ~ 11 mmHg) with an increase in intracellular Ca^{2+} ($[Ca^{2+}]_i$) and increased synaptic vesicle activity. The results of these experiments demonstrate that (1) ACh appears to play a role in the zebrafish, but not goldfish gill, (2) goldfish NECs likely signal hypoxic stimuli primarily via the central nervous system

(CNS), (3) goldfish NECs express a broad range of ion channels as compared to the NECs of zebrafish, and (4) goldfish NECs rely on some cytosolic factor(s) when responding to hypoxia (P_{O2} ~ 11 mmHg). This thesis represents a further step in the study of neurochemical and physiological adaptations to tolerance of extreme hypoxia.

RÉSUMÉ

Les cellules neuroépithéliales (CNEs) des filaments de branchies, contenant de la sérotonine (5-HT), sont soupçonnées d'être les chimiorécepteurs d'oxygène primaires chez les poissons. Dans le corps carotidien des mammifères (CC), le 5-HT est l'un des nombreux neurotransmetteurs soupçonnés de jouer un rôle dans la transmission de stimulus hypoxique, avec l'acétylcholine (ACh) étant le neurotransmetteur excitateur à action rapide primaire. L'immunohistochimie et la microscopie confocale ont été utilisées sur des préparations de branchies de poisson zébré afin d'observer la présence de transporteurs d'acétylcholine vésiculaire (VAChT), un indicateur de la présence d'ACh, et l'innervation associée avec la présence d'ACh. Les cellules positives pour les VAChTs, se retrouvaient principalement sur le côté afférent du filament, et quelques cellules recevaient de l'innervation extrabranchial. Aucunes cellules positives pour les VAChTs ont étés identifiées dans les branchies de poissons rouges; cependant, une comparaison de l'innervation des branchies des poissons rouges et des poissons zébrés a révélé d'importantes différences morphologiques. En outre, dans les CNEs de poissons zébrés, le courant de la cellule entière est dominé par un courant de K^+ de fond, sensible à l'oxygène; comparativement, ceci est seulement l'un des plusieurs courants observés chez le CC des mammifères. Chez le poisson zébré et le CC, la dépolarisation membranaire en réponse à l'hypoxie, par l'entremise de l'inhibition des canaux de K^+ de fond, est soupçonnée d'engendrer l'activation des canaux voltage-dépendants de Ca^{2+} (Ca_v) et la neurosécrétion dépendante de Ca^{2+}. La technique d'électrophysiologie « patch-clamp », m'a permis de découvrir plusieurs types de canaux ioniques encore jamais observés dans les chimiorécepteurs de branchies, tel que des canaux K^+ activés au Ca^{2+} (K^{Ca}), des canaux voltage-dépendants de K^+ (K_v) et de Ca^{2+} (Ca_v). Lorsque la cellule entière était en « patch-clamp », les CNEs de poissons

rouges n'ont pas réagit face à l'hypoxie (P_{O2} ~ 11 mmHg). Avec l'imagerie calcique quotientométrique, accompagnée d'un colorant fluorescent dépendant d'activité cellulaire, j'ai observé que les CNEs de poissons rouges réagissent à l'hypoxie avec une élévation de Ca^{2+} intracellulaire et une augmentation dans l'activité des vésicules synaptiques. Les résultats de ces expériences démontrent que (1) l'ACh semble jouer un rôle chez les poissons zébrés, mais non chez les poissons rouges, (2) les CNEs de poissons rouges semblent signaler la présence de conditions hypoxiques par le système nerveux central, (3) les CNEs du poisson rouge possèdent une plus grande variété de canaux ioniques que celles du poisson zébré, et (4) les CNEs du poisson rouge dépendent sur un certain facteur cytosolique lorsqu'elles répondent à l'hypoxie (P_{O2} ~ 11 mmHg). Cette thèse constitue une nouvelle étape dans l'étude des adaptations neurochimiques et physiologiques de la tolérance extrême de l'hypoxie.

1. General Introduction

Excerpted from: Zachar, P.C., Jonz, M.G., 2012. Neuroepithelial cells of the gill and their role in oxygen sensing. Respir. Physiol. Neurobiol. 183, 301-308.

1.1. Introduction

Oxygen is critical for survival in all but the most extremophilic organisms. It acts as the final electron acceptor in the mitochondrial electron transport chain, enabling synthesis of adenosine triphosphate (ATP), which itself is a key player in maintenance of cellular homeostasis and in numerous metabolic pathways. Consequently, it is not surprising that many higher organisms, such as vertebrates, have evolved highly sensitive mechanisms for monitoring internal and external levels of oxygen (O_2) in order to exert reflex cardioventilatory changes.

Aquatic vertebrates face unique challenges in meeting their metabolic O_2 requirements. Whereas decreased O_2 availability is generally limited in terrestrial vertebrates to conditions such as altitude, exercise, or disease, aquatic vertebrates exist in an aqueous, and relatively less oxygenated, environment. Thus, in fish low O_2 (hypoxia) has become the primary environmental stressor that ultimately drives compensatory cardioventilatory responses (Milsom et al., 2002).

Over the course of vertebrate evolution, a variety of strategies for sensing arterial and environmental hypoxia have emerged (Milsom and Burleson, 2007). In mammals, the carotid body (CB) is a densely populated organ with chemoreceptive type I (glomus) cells that detect changes in blood O_2 and CO_2/H^+. In fish, neuroepithelial cells (NECs) of the gills are the putative O_2/CO_2 chemoreceptors, but are diffusely distributed within this tissue and may monitor both arterial and environmental changes in O_2 and CO_2. As will be described, NECs bear morphological, biochemical and physiological similarities with type I cells and are considered to be their homologues and evolutionary precursors.

1.2. The homology of O_2 chemoreceptors in vertebrates

The sites of O_2 sensing in vertebrates, from fish to amphibians to mammals, reflect a common phylogenetic origin. In the vertebrate embryonic state, there are six pairs of aortic arches that receive blood from the ventral aorta, and return it to the systemic circulation through paired dorsal aortae (Fig. 1A). The six aortic arches may be modified over the course of embryonic development to form distinct patterns at the adult stage, as illustrated in Figure 1.1. In teleosts, the first pair of arches (I) degenerates and is absent, the second (II) is modified into a non-respiratory structure known as the pseudobranch, and the remaining four (III-VI) pairs of arches are modified to perfuse the gills (Jonz and Nurse, 2009). The gill arches are thus designed to maximize respiratory surface area for gas exchange in an aqueous environment. They give rise to a system of primary filaments and secondary lamellae, where NECs are situated throughout a thin epithelial layer. The gills generally receive innervation from cranial nerves VII (facial), IX (glossopharyngeal), and X (vagus) (Sundin and Nilsson, 2002). Premetamorphic anurans (i.e. frogs and toads) develop internal gills associated with the same four aortic arches and cranial nerves as in fish. Despite the significant differences in gross morphology of the gills of larval amphibians, they also contain NECs (Saltys et al., 2006).

The primary site of peripheral O_2 sensing in mammals is the CB, located at the bifurcation of the internal and external carotid arteries (Fig. 1C) (López-Barneo et al., 2008). The CB is thus homologous with the first gill arch in fish. It is extensively perfused by a capillary network and innervated primarily by afferent glossopharyngeal fibres of the carotid sinus nerve (González et al., 1994). In addition, the CB receives innervation by efferent fibres that are important in mediating inhibitory feedback during hypoxia (Campanucci and Nurse,

2007). The CB is composed of chemoreceptive type I cells that are derived from the neural crest (Pardal et al., 2007).

The condensed nature of the mammalian CB stands in contrast to the diffuse distribution of gill NECs, which are found on all four gill arches. It was proposed that these arrangements are indicative of an evolutionary trend towards grouping of O_2-sensitive cells from their diffuse distribution across the gills to a single, peripheral O_2-sensing organ, and that this was associated with the emergence of air breathing in terrestrial vertebrates (Milsom and Burleson, 2007).

1.3. Neuroepithelial cells (NECs) as O_2 chemoreceptors

1.3.1. Distribution and innervation

The NECs are found in the gill within a thin epithelial layer covering the efferent aspect (i.e. facing the incident flow of water) of the filaments and lamellae, and have been observed in all fish species studied (Perry et al., 2009). Their position in the efferent epithelium places the NECs in a prime location to sample changes in the partial pressure of O_2 in the water (P_{WO2}) as it passes over the gills; however, given their proximity to the efferent filament artery, there is strong evidence for an additional role as internal sensors of arterial P_{O2} (Jonz and Nurse, 2006; Perry et al., 2009).

Neuroepithelial cells typically contain neurotransmitters, such as serotonin (5-hydroxytryptamine or 5-HT), as well as dense-core synaptic vesicles in which these are stored (Fig. 2) (Dunel-Erb et al., 1982; Perry et al., 2009). Studies in teleosts, such as trout, zebrafish and goldfish, have shown that NECs are closely apposed to nerve fibres originating from multiple sources (Dunel-Erb et al., 1982; Bailly et al., 1992; Jonz and Nurse, 2003; Bailly et al., 2009). Innervation patterns generally indicate that NECs form synapses with catecholaminergic

nerve fibres with ultrastructural characteristics of afferent or efferent nerve terminals (Dunel-Erb et al., 1982; Bailly et al., 1992, 2009). These nerves are extrinsic, having their cell bodies localized within the cranial nerve ganglia. An additional source of NEC innervation includes indolaminergic neurons intrinsic to the gill filaments that may also present afferent terminals (Bailly et al., 1992; Jonz and Nurse, 2003; Bailly, 2009). These neurons, in turn, form synapses with a contractile segment of the filament artery and may indicate a mechanism of vascular control (Bailly et al., 1989; Sundin, 1995; Jonz and Nurse, 2003). Moreover, in the zebrafish, denervation experiments with gills in explant culture demonstrated that NECs of the filaments are innervated by intrinsic serotonergic neurons and extrinsic nerve fibres, while lamellar NECs receive only the latter (Jonz and Nurse, 2003). Overall, the functional significance of these different patterns of NEC innervation in the gill is presently not clear, but it may suggest that NECs of both the filaments and lamellae participate in centrally-mediated reflex responses to hypoxia, such as hyperventilation. While there is presently limited functional evidence to support these proposed mechanisms, developing zebrafish exhibit adult-like reflex hyperventilatory responses to hypoxia only after gill NECs are innervated by extrinsic nerve fibres (Jonz and Nurse, 2005). Filament NECs may additionally control local vascular responses in the gill, such as vasoconstriction (Bailly, 2009; Jonz and Nurse, 2009).

As noted above, gill NECs are also innervated by nerve fibres with ultrastructural features of efferent nerve terminals (Bailly et al., 1992, 2009), suggesting a putative pathway of modulation of the NEC response to hypoxia, or an additional paracrine role for NECs. In mammals, pulmonary NEBs receive both afferent and efferent innervation (Brouns et al., 2009), and efferent innervation of the CB is important in feedback inhibition during hypoxia (Campanucci and Nurse, 2007).

Some fish, including goldfish and crucian carp, are able to change their gill structure in response to temperature and O_2 availability (Sollid and Nilsson, 2006). When acclimated to relatively low environmental temperatures, these species develop an inter-lamellar cell mass (ILCM), which essentially covers the gill lamellae. This effect is reversible by either acclimating the fish to a higher environmental temperature, or by exposing the fish to hypoxia (Sollid and Nilsson, 2006). It has been shown that goldfish producing the ILCM are still able to respond to hypoxia (Tzaneva and Perry, 2010). Under these conditions, the lamellar NECs were redistributed to the edge of the lamellae and maintained innervation. It was suggested that these results indicate a role for lamellar NECs in sensing external PO_2 (Tzaneva and Perry, 2010); however, in these experiments O_2-chemoreceptive NECs of the filaments remained exposed and unaffected during formation of the ILCM. It has also been demonstrated that developing zebrafish hyperventilate despite the complete absence of lamellae (Jonz and Nurse, 2005) and trout do not produce lamellar NECs (Saltys et al., 2006). The role of lamellar NECs in O_2 sensing may, therefore, be limited or species specific.

1.3.2. Physiological evidence of O_2 sensitivity

The gills were first implicated in O_2 sensing by observing increased afferent activity in excised gill arches in response to hypoxia. Recordings from the glossopharyngeal and vagus nerves in gill arches isolated from yellowfin tuna and trout showed increased neuronal discharge in response to decreased P_{O2} in both the external solution, and in solution perfused through the gill vasculature (Milsom and Brill, 1986; Burleson and Milsom 1993). This observation indicated the presence of internally and externally-oriented chemoreceptors of the gill.

Similarly, afferent activity from excised American bullfrog tadpole gills increases in response to hypoxia, further implicating the gills as an important O_2-sensing organ (Straus et al., 2001).

The neurochemical origin of gill neuronal discharge in response to hypoxia remains largely uncharacterized. In rainbow trout, perfusion of excised gills with neurotransmitters commonly found in the mammalian CB, including acetylcholine (ACh), dopamine, and 5-HT, elicits increased afferent activity resembling that observed during hypoxic stimulation (Burleson and Milsom, 1995a). Furthermore, exogenous application of these neurochemicals via injection to the dorsal aorta caused physiological changes normally associated with hypoxia, including changes to heart and ventilatory rate (Burleson and Milsom, 1995b). While 5-HT appears to be the most prominent neurotransmitter, NECs retain a suite of neurochemicals, including ACh, that may mediate activation of afferent nerves (Milsom and Burleson, 2007; Perry et al., 2009). Taken together, these studies provide compelling evidence that the neurochemical profile of O_2 sensing in fish is diverse in its composition; however, without knowledge of which neurotransmitters are specifically released from NECs during acute hypoxic stimulation, it is difficult to speculate as to which is primarily involved in O_2 sensing.

In the type I cells of the mammalian CB, the proximal effect of a decrease in P_{O2} is the inhibition of background K^+ (K_B) channels (Fig. 3A, Buckler, 1997), which regulate resting membrane permeability and cell excitability. A stimulus that inhibits these K_B channels, such as hypoxia, is able to depolarize the cell membrane by inhibiting the resting outward K^+ current, which in turn leads to a host of intracellular events tied to membrane potential (V_m). In a similar manner, whole-cell conductance of NECs is dominated by an O_2-sensitive K^+ conductance through K_B channels (Fig. 3B, Jonz et al., 2004). Patch-clamp experiments in isolated cells from zebrafish show that the 5-HT-positive filament NECs respond to acute changes in hypoxia (25

mmHg) by ion channel inhibition and membrane depolarization (Jonz et al., 2004). The NEC response to acute hypoxia occurs immediately, with inhibition of K^+ current precisely tied to reduction of P_{O2} (Fig. 3C). Similar experiments show O_2 sensitivity in the NECs of channel catfish; however, the specific channel type involved in transduction was not characterized (Burleson et al., 2006). These studies demonstrate that K_B channels are an important initial step in the transduction of hypoxia in zebrafish NECs, as they are in mammalian chemoreceptors.

1.3.3. Ion channels of excitable membranes

Resting membrane potential (V_m) is primarily generated by K^+-selective ion channels known as "leak" or background K^+ (K_B) channels. These K_B channels are open rectifiers, meaning their open state is independent of V_m, and they allow K^+ ions to flow down their electrochemical gradient out of the cell, carrying positive charge with them and resulting in a V_m of ~ -60 mV in most cell types. As mentioned in the previous section, a subfamily of K_B channels known as two-pore acid-sensitive K^+ (TASK) channels are believe to be primarily responsible for membrane depolarization in response to hypoxic stimuli in the mammalian carotid body (Buckler, 1997). In the type I cells of the mammalian carotid body, it is believed that hypoxic stimuli act on a combination of membrane-delimited and cytosolic sensing factors to inhibit outward K^+ current through K_B channels (Kumar & Prabhakar, 2012). This inhibition results in depolarization of V_m.

Depolarization of the plasma membrane results in the activation of a variety of voltage-dependent ion channels, most notably voltage-activated Ca^{2+} (Ca_V) channels. Once activated, Ca_V channels open, allowing Ca^{2+} to flow down its electrochemical gradient into the cytosol. The corresponding increase in intracellular Ca^{2+} concentration ($[Ca^{2+}]_i$) facilitates Ca^{2+}-

dependent synaptic vesicle fusion and neurotransmitter release (Fu *et al*., 2002). Increased $[Ca^{2+}]_i$ may have other potentially damaging effects on cellular function, including gene up- or down-regulation, thus making mechanisms of Ca^{2+} sequestration or modulation of membrane depolarization particularly important in cells and organisms prone to prolonged exposure to excitatory stimuli.

One such mechanism, observable in vascular (Roberts *et al*., in press) and neuronal cells (Pérez *et al*., 2013), relies on the presence of Ca^{2+}-activated K^+ (K_{Ca}) channels in the plasma membrane. In these cells, a rise in $[Ca^{2+}]_i$ allows Ca^{2+} ions to interact with K_{Ca} channels, activating an outward Ca^{2+}-dependent K^+ conductance (I_{KCa}) that facilitates membrane repolarization following stimulus. The rapid repolarization of V_m imparted by K_{Ca} channels helps to prevent excitotoxicity that would be caused by prolonged membrane depolarization and increased $[Ca^{2+}]_i$.

In addition to Ca_V channels, membrane depolarization may activate a variety of voltage-dependent K^+ (K_V) channels. In the membranes of excitable cells, conductance through K_V channels is rapidly activating and inactivating, resulting in a transient outward K^+ conductance (Bekar *et al*., 2004; Kollo *et al*., 2008). This type of conductance is carried by A-type K_V channels, and also contributes to the repolarization of the plasma membrane. Its transient nature implies that its role is to provide relatively short-term mediation of membrane depolarization, relying on other mechanisms (i.e. K_{Ca} channels) for longer-term repolarization.

1.3.4. Molecular mechanisms of O_2 sensing

There remains much controversy as to the identity of the molecular O_2 sensor that initiates ion channel inhibition at the plasma membrane in mammalian chemoreceptors, and there

appears to be no universal sensor that operates across species. While very little is known about putative O_2 sensors in fish, it is useful to consider potential mechanisms from the mammalian literature to guide future comparative investigations. The proposed models of O_2 sensors may be divided into two broad categories: those that are membrane-delimited and confined to sense O_2 at the plasma membrane, and those that occur elsewhere in the cell, such as the mitochondrion or cytosol, and are potentially linked with metabolism. In all cases, these putative sensors must communicate with membrane ion channels either directly or indirectly.

1.3.4.1. Membrane-delimited mechanisms

Haemoxygenase-2 (HO-2) has received much attention for its potential role as a molecular O_2 sensor, due in large part to its use of O_2 to convert heme into iron, biliverdin, and carbon monoxide (CO) (Shibahara et al., 1985). The presence of CO has been observed to activate K_{Ca}-type K^+ channels (Williams et al., 2004), indicating that a drop in P_{O2} would lead to a decrease in CO production by HO-2, inhibiting K^+ conductance through K_{Ca} channels. However, knock-out mice lacking HO-2 showed no difference in CB O_2 sensitivity (Ortega-Saenz et al., 2006). In addition, while O_2-sensitive K_{Ca}-type channels are present in the rat CB, it is generally believed that they are not the primary contributors to type I cell depolarization in response to hypoxia (Buckler, 2010). Haemoxygenase-1, another member of the haemoxygenase family, is present in zebrafish and *Takifugu* spp. (Wang et al., 2008).

An alternative model proposes that sensing of hypoxia may occur through the production of reactive oxygen species, such as hydrogen peroxide (H_2O_2), by a membrane-bound nicotinamide adenine dinucleotide phosphate (NADPH) oxidase. In NEBs from mice deficient in the NADPH oxidase subunit, $gp91^{phox}$, O_2 sensitivity is lost (Fu et al., 2000). However,

knock-out studies in mice targeting the same subunit of NADPH oxidase have shown that O_2 sensitivity remains unaltered in pulmonary myocytes (Archer et al., 1999).

Data from zebrafish may suggest that the O_2 sensor is membrane-delimited (Jonz et al., 2004). Patch-clamp recordings were done in the whole-cell configuration, which causes dialysis of the NEC and dilution of cytosolic factors. Yet zebrafish NECs retain their O_2 sensitivity under these conditions, suggesting an O_2 sensor that is not soluble or diffusible in the cytosol.

1.3.4.2. Mitochondrial or cytosolic mechanisms

Perhaps the earliest candidate for the molecular O_2 sensor was mitochondrial dysfunction. Indeed, decouplers of the electron transport chain, such as cyanide and rotenone, lead to increased neuronal discharge from the CB (Mills and Jobsis, 1972). It was initially proposed that the increase in $[Ca^{2+}]_i$ required for type I cell neurosecretion came, at least in part, from the mitochondria (Duchen and Biscoe, 1992). This theory preceded the discovery of O_2-sensitive K_B channels in the CB, which offered a more complete model of Ca^{2+} entry through Ca_V channels following plasma membrane depolarization (Buckler and Vaughan-Jones, 1994). Mitochondrial dysfunction ultimately leads to the halting of ATP synthesis. This has two proposed effects: closure of ATP-regulated K_B channels (Varas et al., 2007), or activation of AMP-activated protein kinase leading to phosphorylation and inhibition of membrane ion channels (Wyatt et al., 2008). However, the CB appears to retain its ability to respond to hypoxia despite exposure to metabolic inhibitors (Ortega-Saenz et al., 2003), and type I cells dialysed with artificially high concentrations of ATP likewise retain their O_2 sensitivity (Lopez-Barneo et al., 1988).

Hypoxia-inducible factor 1-α (HIF-1α) has also received some attention as a potential O_2 sensor (Kline et al., 2002). Under normoxic conditions, HIF-1α is hydroxylated using available

O_2 and degraded by the proteasome. When O_2 levels drop, HIF-1α is retained in the cytosol and may modulate the function of ion channels in the plasma membrane. Mice in which HIF-1α has been knocked-out, however, have relatively unchanged CB O_2 sensitivity (Ortega-Saenz et al., 2007). Hypoxia-inducible factor 1-α has been observed in several fish species, including zebrafish, rainbow trout, and sea bass (see Shen et al., 2010).

A more recent addition to the gallery of potential O_2 sensors is hydrogen sulfide (H_2S). Olson et al. (2006) proposed that the balance between cellular production and oxidation of H_2S is disrupted by decreased O_2 availability, such that hypoxia will lead to intracellular H_2S accumulation. Hydrogen sulfide has been shown to have many vasoactive and neuroprotective effects, in addition to its effects at the neural synapse (Kimura et al., 2005). It was subsequently demonstrated in trout that intrabuccal application of H_2S mimicked hypoxia by inducing cardio-ventilatory changes (Olson et al., 2008). Additionally, enzymatic production of H_2S in homogenized gills was inhibited by O_2, and isolated zebrafish NECs were observed to depolarize upon exogenous application of H_2S (Olson et al., 2008). In mice, deletion of H_2S synthetic enzymes leads to a blunted hypoxic response in the CB, furthering the case for its involvement in O_2 sensing (Peng et al., 2010).

1.4. Summary

The diffuse organization of NECs along the filaments and lamellae in some species constitutes a potentially complex network of O_2-sensitive chemosensors ideally distributed to sense subtle changes in either environmental or arterial P_{O2}, or both. In zebrafish and goldfish, for example, as many as five populations of gill NECs were identified with diverse morphological and biochemical features (Jonz and Nurse, 2003; Saltys et al., 2006). In addition,

the different innervation patterns of lamellar and filament NECs observed in zebrafish suggest that they are capable of affecting different responses to hypoxia. It is possible that NECs of the lamellae signal primarily via the central nervous system, as their innervation is of extrinsic origin. Innervation of filament NECs is also primarily extrinsic in origin, but their innervation by intrinsic neurons associated with a contractile segment of the filament artery suggests an additional role in modulation of local blood flow within the gill. Future studies may reveal the significance of the diversity and innervation of gill NECs and their precise roles in O_2 sensing.

It is possible that there is more than one molecular O_2 sensor at work in gill NECs. The proposed O_2 sensors are varied not only in their intracellular location, but potentially also in their sensitivity to hypoxia. In mammalian models, different O_2 sensors may contribute to the overall sensitivity of CB type I cells within different ranges of P_{O2} (Prabhakar, 2006). Similarly, this could be true for the gill NECs. Moderate levels of acute hypoxia, such as those used in patch-clamp experiments (Jonz et al., 2004), may be detected by membrane-delimited sensor(s) associated with ion channels, whereas more severe hypoxia might disrupt mitochondrial function and initiate associated O_2 sensing pathways coupled with metabolism. Ion channels are regulated by P_{O2} levels below 80 mmHg, while mitochondrial respiration is not limited by O_2 until extracellular P_{O2} falls below 2-3 mmHg (López-Barneo et al., 2001). Regardless of whether there are single or multiple molecular O_2 sensors at work, definitive identification has yet to be achieved in NECs. It is conceivable that multiple, overlapping O_2 sensors with variable sensitivities to hypoxia may present an advantage for regulating cardioventilatory changes in fish, which naturally experience a broad range of environmental P_{O2} levels.

It is also worth noting that, while the NECs have primarily been investigated for their role in O_2 sensing, they have also been implicated in the response to other chemostimuli. Zebrafish

NECs have been shown to respond to hypercapnia with a similar inhibition of K_B current as in hypoxia (Qin et al., 2010). In addition, exposure of zebrafish NECs to high CO_2 increases $[Ca^{2+}]_i$ (Abdallah *et al*., 2012). The NECs of the first and second gill arch of rainbow trout have also been implicated in sensing ammonia (Zhang et al., 2011). This "polymodal" sensitivity is also characteristic of the mammalian CB and NEBs (Kumar and Bin-Jaliah, 2007), and may indicate a further evolutionary link between these peripheral O_2 sensing structures and the NECs.

Nothing is known about O_2 chemoreceptors in anoxia-tolerant organisms. Studies aimed at understanding how O_2 sensing mechanisms differ in organisms tolerant of prolonged O_2 deprivation may shed light on how adaptation has occurred at the cellular level.

1.5. Hypotheses

1.5.1. Vesicular acetylcholine transporter expression in the gill

In this chapter, I discuss the presence of the vesicular acetylcholine transporter (VAChT) in the gills of zebrafish and goldfish. I hypothesized that the serotonergic NECs of zebrafish and goldfish would also contain ACh, as indicated by the expression of VAChT. In addition, I predicted that the innervation pattern of goldfish NECs would differ from that of zebrafish. To test these hypotheses, I employed immunohistochemistry and confocal microscopy, as well as acute explant cultures to characterize sources of innervation in the goldfish gill.

1.5.2. Ion channels and O_2 sensitivity in neuroepithelial cells of the goldfish gill

I hypothesized that ion channels expressed in the plasma membrane of goldfish NECs would differ from those of zebrafish. I also hypothesized that goldfish NECs express an O_2-sensitive background K^+ conductance similar to that observed in zebrafish. I tested these

hypotheses using the patch-clamp electrophysiological technique on NECs isolated from gill tissue.

With respect to Ca^{2+} dynamics, I hypothesized that $[Ca^{2+}]_i$ would increase in response to hypoxia in goldfish NECs. In addition, I predicted that this increase would facilitate Ca^{2+}-dependent synaptic vesicle fusion (necessary for neurosecretion), and was the result of extracellular Ca^{2+} influx. To test these hypotheses, I employed ratiometric Ca^{2+} imaging and a fluorescent vital dye to observe $[Ca^{2+}]_i$ and synaptic vesicle activity in response to hypoxia.

Figure 1.1. Phylogenesis of the vertebrate aortic arches, with associated innervation from the glossopharyngeal (*gpn*) and vagus (*vn*) nerves. Innervation is bilateral, but is displayed individually for clarity. A) The embryonic condition, with six aortic arches (I-VI) connecting the ventral aorta (*va*) to paired dorsal aortae (*da*). Numerals correspond to homologous structures in B and C. B) In teleosts, the first aortic arch is absent, the second is modified into the non-respiratory pseudobranch (*pb*), and aortic arches III-VI become gill arches 1-4, respectively. The *pb* and first gill arch receive *gpn* innervation, whereas all four arches receive *vn* innervation. C) In mammals, the ventral aorta is modified to the common carotid (*cc*), which bifurcates to the external and internal carotids (*ec*, *ic*, respectively). The right *da* is lost. The *va* is modified to become the systemic aorta (*sysa*). The site of the carotid body, the *cc*, receives *gpn* innervation. Right subclavian artery (*rsa*), left subclavian artery (*lsa*). Adapted from Milsom and Burleson (2007), and Jonz and Nurse (2009).

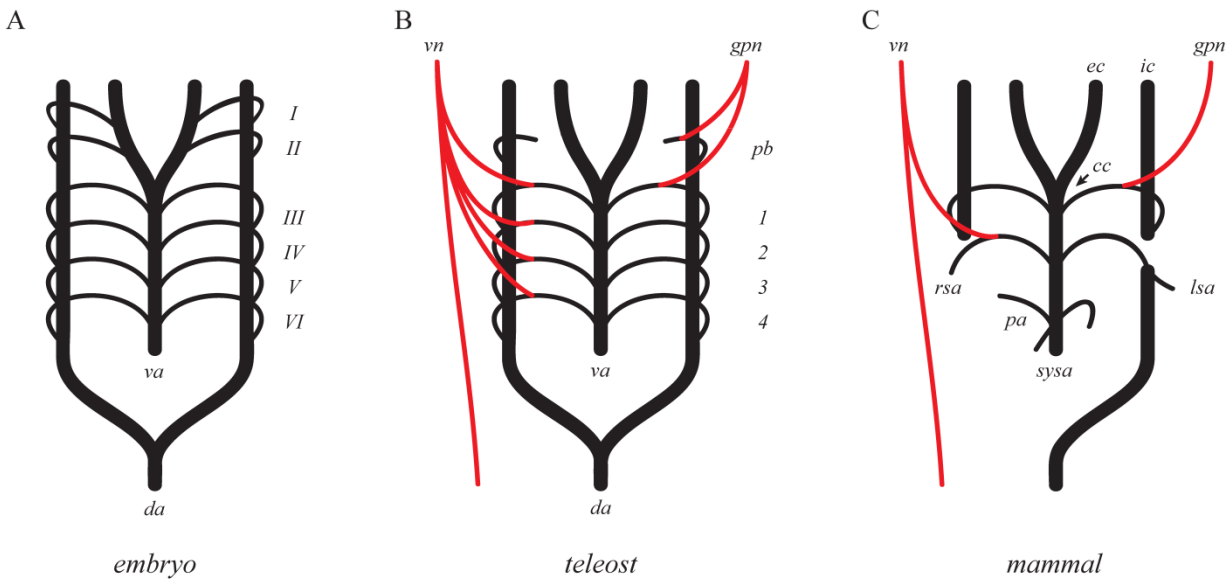
A
I
II
III
IV
V
VI
va
da
embryo
B
vn
gpn
pb
1
2
3
4
va
da
teleost
C
vn
ec
ic
gpn
cc
rsa
lsa
pa
sysa
mammal

Figure 1.2. Neuroepithelial cells (NECs) and their associated innervation in the goldfish. A) NECs of the filament (arrow) and lamellae (arrowhead) express serotonin (5-HT, green) and a synaptic vesicle protein (SV2, white), and both are intimately associated with nerve fibers (zn-12, red); B) 5-HT labeling of the NECs colocalizes with synaptic vesicles, indicating potential for neurosecretion; C) Characteristic 5-HT labeling of NECs. Scale bar, 20µm. Tissue was prepared for immunohistochemistry, and imaged by confocal microscopy, following procedures similar to Jonz and Nurse (2003).

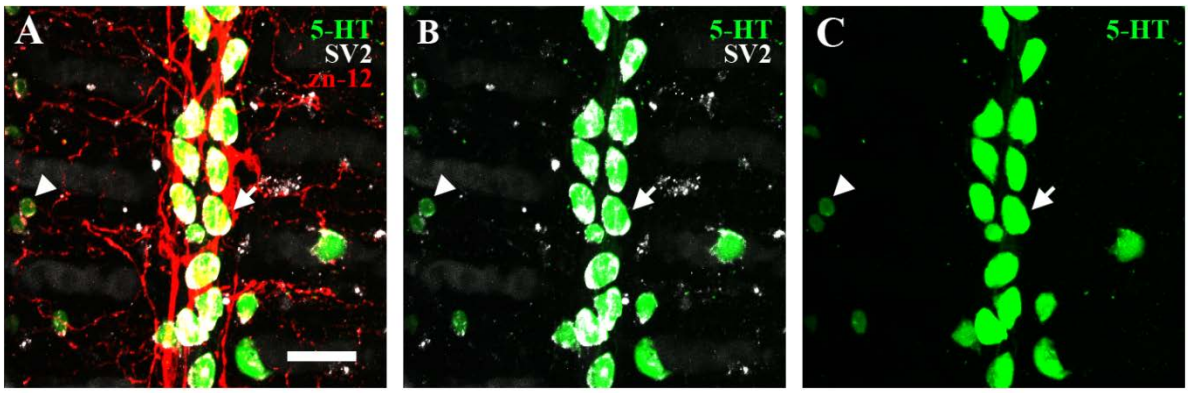
A
5-HT
SV2
zn-12
B
5-HT
SV2
C
5-HT

Figure 1.3. Patch-clamp recordings from carotid body (CB) type I cells and zebrafish filament neuroepithelial cells (NECs). A) Type 1 cells of the rat CB have an O_2-sensitive voltage-independent K^+ current through background K^+ channels. Left panel shows the current-voltage (I-V) relationship with inhibition of whole-cell current under hypoxia. Right panel shows the difference current (control – hypoxia), revealing the O_2-sensitive, open-rectifier-type current which reverses around the equilibrium potential for K^+ (E_K). Modified from Buckler (1997) with permission. B) Filament NECs of the zebrafish have a similar O_2-sensitive K^+ current. Left panel shows the I-V relationship, with hypoxia-induced inhibition of whole-cell current. Right panel shows the difference current, reversing at E_K. C) Filament NECs are highly tuned to hypoxia. Normalized current, elicited by periodic depolarizing steps to +30 mV, begins to drop immediately with P_{O2} (solid line). B and C are reprinted from Jonz et al. (2004) with permission.

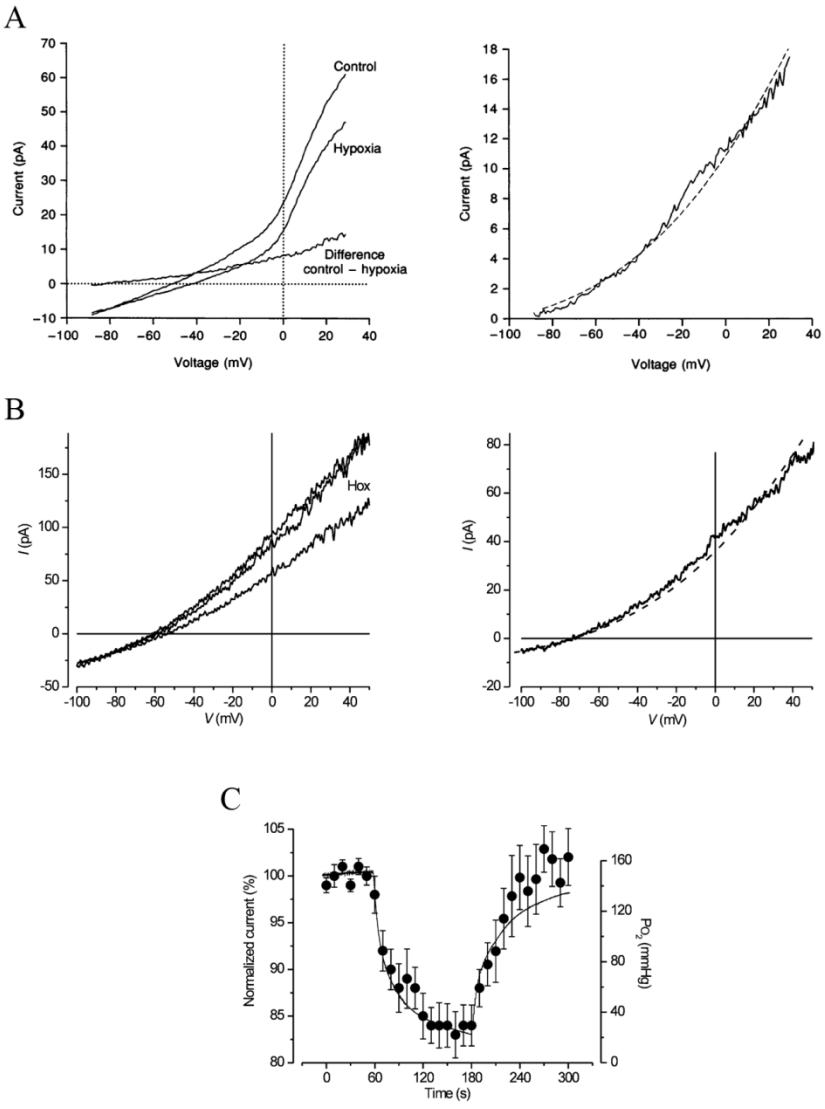
A
Control
Hypoxia
Difference
control – hypoxia
Current (pA)
Voltage (mV)
B
Hox
I (pA)
V (mV)
C
Normalized current (%)
Time (s)

2. Expression of the vesicular acetylcholine transporter and associated innervation in the gill

2.1. INTRODUCTION

The ability to detect and respond to changes in environmental O_2 partial pressure (P_{O2}) is of the utmost importance to the continued survival of all but the most extremeophilic organisms. Over the course of evolution, several different strategies of O_2 chemosensing have emerged, including the advent of the carotid body, the primary O_2-sensory organ in mammals (Kumar & Prabhakar, 2012), neuroepithelial bodies (NEBs) of the pulmonary epithelium (Domnik & Cutz, 2011), and the amphibian carotid labyrinth (Kusakabe, 2002). In fish, neuroepithelial cells (NECs) of the gill are believed to be the primary peripheral O_2 chemoreceptors (Perry *et al*., 2009; Zachar & Jonz, 2012). The NECs of fish gills are identified by their expression of synaptic vesicles and the neurotransmitter serotonin (5-HT), and are divided into filamental and lamellar populations (Jonz & Nurse, 2003), although only the former group has been identified as functionally O_2 and CO_2 sensitive (Jonz et al., 2004; Qin et al., 2010). The filamental NECs of zebrafish are innervated by both nerve fibers originating from neuronal cell bodies at the proximal end of the filament and nerve fibers originating from extrabranchial cell bodies, whereas innervation of lamellar NECs appears to originate from only the latter (Jonz & Nurse, 2003).

While 5-HT has been implicated as a primary neurotransmitter in O_2 sensing in NEBs (Fu *et al*., 2002), in the carotid body its role is secondary to other compounds, such as dopamine, ATP, and acetylcholine (ACh; Kumar & Prabhakar, 2012). In the mammalian carotid body, ACh appears to be the primary fast-acting neurotransmitter involved in the response to hypoxia (Shirahata *et al*., 2007; Nurse, 2010), though species-specific differences between its role as an excitatory (Diamond, 1955; Fitzgerald *et al*., 1997) or inhibitory (Docherty *et al*., 1979; Eyzaguirre & Monti-Bloch, 1980) compound on chemodischarge have been observed. In

rainbow trout, ACh has been observed to increase afferent neuronal activity from the gill arch (Burleson & Milsom, 1995a), as well as increasing heart rate and ventilatory frequency (Burleson & Milsom, 1995b). Additionally, cells expressing the vesicular acetylcholine transporter (VAChT), as well as serotonergic NECs, were observed in the amphibious fish *Kryptolebias marmoratus* (Regan et al., 2011) and zebrafish larvae (Shakarchi et al., 2013), whose behavioral responses to hypoxia were mediated by serotonergic and cholinergic systems. Neurons expressing VAChT were also described in the gills of goldfish and trout (Porteus *et al*., 2013).

This study aimed to further characterize the presence of ACh activity in the gills of adult zebrafish, as indicated by VAChT expression. We combined immunohistochemistry and confocal microscopy and investigated the distribution of VAChT immunoreactive cells within the gill, whether these cells expressed other markers associated with NECs (i.e. synaptic vesicles), and whether they received innervation similar to that of serotonergic NECs. While zebrafish are a common model for the study of O_2 chemoreception and neurochemical pathways, it is also valuable to look at other models with varying tolerances to O_2 deprivation. The goldfish (*Carassius auratus*) is tolerant to extreme hypoxia (Bickler & Buck, 2007), and even anoxia, and provides a compelling point of comparison to zebrafish, as there may be morphological differences in the gill that underlie or contribute to their increased tolerance of prolonged O_2 starvation. Indeed, we demonstrate that while zebrafish display extensive VAChT immunolabelling in the gill, goldfish gills are devoid are VAChT-positive cells.

2.2. METHODS

2.2.1 Animals

Adult zebrafish (*Danio rerio*; AQUAlity Tropical Fish Wholesale Inc., Mississauga, ON, Canada) and goldfish (*Carrasius auratus*; Mt. Parnell Fisheries, Pennsylvania, PA, USA) were maintained at 28.5°C and 18°C, respectively. All procedures for animal use were carried out according to institutional guidelines, adhering to those of the Canadian Council on Animal Care (CCAC).

2.2.2 Confocal immunofluorescence

Techniques for tissue extraction, immunolabelling, and confocal imaging were modified from those previous described (Jonz & Nurse, 2003). Zebrafish and goldfish were stunned with a blow to the head and killed by decapitation. Heads were stored in ice-cold phosphate-buffered saline (PBS) containing (mM): NaCl 137, Na_2HPO_4 15.2, KCl 2.7, and KH_2PO_4 1.5; pH 7.8 (Jonz & Nurse, 2003) until dissection. Whole gill baskets were removed, rinsed in PBS, and fixed by immersion in 4% paraformaldehyde (Sigma) for 24 h at 4°C. Fixed gill baskets were rinsed with PBS and permeabilized with 2% Triton X-100 in PBS for 24-48 h at 4°C.

Neuroepithelial cells (NECs) of the gill were identified using antibodies against serotonin (5-HT) and the synaptic vesicle protein SV2 (Jonz & Nurse, 2003). The NECs of zebrafish display immunoreactivity for SV2, and the majority of these cells also express 5-HT (Jonz & Nurse, 2003). Nerve fibers were identified using a zebrafish-derived antibody targeted to a neuron-specific human natural killer 1- (HNK1) like antigen (zn-12) (Trevarrow *et al*., 1990; Jonz & Nurse, 2003). The presence of acetylcholine activity was indicated by immunoreactivity for the vesicular acetylcholine transporter (VAChT) (Roghani *et al*., 1994; Shakarchi *et al*.,

2013). Polyclonal rabbit anti-5-HT (Sigma) was used at a dilution of 1:250 and visualized with goat anti-rabbit secondary antibodies conjugated to Alexa Fluor 405 (Alexa 405, 1:50, Molecular Probes). Monoclonal mouse anti-zn-12 and anti-SV2 (Developmental Studies Hybridoma Bank, University of Iowa, IA, USA) were used at a dilution of 1:100 and visualized with goat anti-mouse secondary antibodies conjugated to Alexa Fluor 594 (Alexa 594, 1:100, Molecular Probes). These antibodies were used previously to characterize NECs and innervation in both zebrafish and goldfish (Jonz & Nurse, 2003; Saltys *et al*., 2006). Polyclonal guinea pig anti-VAChT (EMD Millipore) was used at a dilution of 1:50 and visualized with rabbit anti-guinea pig secondary antibodies conjugated to FITC (1:50, Molecular Probes). In zebrafish, preabsorption of the VAChT antibody with a control peptide (EMD Millipore, CAT#AG260) eliminated VAChT immunoreactivity in the gill. In addition, VAChT labeled neuronal cell bodies and nerve fibers in the nodose ganglion (Shakarchi *et al*., 2012; Appendix I). All antibodies were diluted with PBS.

Whole gill arches were incubated in primary antibodies for 24 h at 4°C. Tissue was rinsed with PBS and left in secondary antibodies for 1-2 h at room temperature in the dark. Whole gill arches were mounted on glass slides in Vectashield (Vector Laboratories Inc., Burlingame, CA, USA) to minimize photobleaching. Whole-mounted specimens were imaged on a confocal system (LSM 510, Zeiss) equipped with lasers with peak outputs of 405, 488, and 543 nm. Images were collected using ZEN confocal software (Zeiss). Each image is presented as a composite of serial optical sections (0.5-3 µm sections, ~50 µm depth). Image processing and manipulation was done using ZEN 2012 (Zeiss) and Adobe Photoshop CS6 (Adobe Systems Inc., San Jose, CA, USA).

2.2.3 Morphometric analysis

Confocal images of gill filaments showing immunoreactivity for 5-HT and VAChT were analyzed for cell diameter and counted. Measurements and counts were done within the distal 200 µm of gill filaments. Cell diameter was measured in ZEN 2012 (Zeiss) and analyzed using Prism 5 (GraphPad Software, La Jolla, CA, USA). Diameter measurements and cells counts were compared using the Student's *t* tests, and are presented as mean ± S.E.M.

2.2.4 Denervation experiments

Gill baskets were removed from adult goldfish under sterile conditions in PBS. Gill arches from the right side of the fish were separated from the gill basket and placed in L-15 medium supplemented with 2% fetal calf serum and 4% penicillin/streptomycin (Gibco, Carlsbad, CA, USA), and maintained in an air atmosphere at 28°C. After 24 h, 2 ml of supplemented L-15 was replaced with fresh medium. After 48 h, explants were fixed and processed for immunohistochemistry. For controls, fresh gill tissue was removed from the left side of the gill basket of the same individuals immediately after sacrifice, fixed and processed directly for immunohistochemistry.

2.3. RESULTS

2.3.1. Vesicular acetylcholine transporter in the gills of zebrafish

Two major populations of cells expressing the vesicular acetylcholine transporter (VAChT) were identified in gill epithelia of zebrafish, based on their location relative to incident water flow (Figure 2.1). The first population of VAChT immunoreactive cells resided within the epithelium of the efferent aspect of the filament, exposed to the incident water flow through the

gills and adjacent to the efferent filamental artery (eFA), the latter of which carries oxygenated blood from the lamellae (Figure 2.1B, eff.). The second population of VAChT-positive cells was found within the afferent filamental epithelium, exposed to environmental water but sheltered from direct flow, and adjacent to the afferent filamental artery (aFA), which carries deoxygenated blood to the lamellae (Figure 2.1B, aff.). On both the efferent and afferent sides of the filament, VAChT-positive cells were more concentrated near the distal ends of the filament and became less so towards the proximal region, near the gill arch. In addition, synaptic vesicle (SV2) immunoreactivity was observed on the afferent filamental aspect, though it did not colocalize with VAChT labeling (Figure 2.1C, arrowheads). VAChT immunoreactivity also did not appear to colocalize with filamental or lamellar 5-HT-positive NECs.

Cells immunopositive for VAChT were more numerous along the distal 200 μm of the afferent filamental aspect (30.8 ± 3.1 per filament), as compared to the efferent aspect (10.2 ± 0.6 per filament; Figure 2.2A). This region of the filament corresponded to the highest density of serotonergic (5-HT) neuroepithelial cells (NECs), as well as VAChT-positive cells. In addition, VAChT immunoreactive cells were smaller than the 5-HT-positive NECs, with a mean diameter of 6.9 ± 0.3 μm, compared to 9.2 ± 0.2 μm for the NECs (Figure 2.2B). The VAChT-positive cells did not colocalize with 5-HT or SV2 immunoreactivity (Figure 2.3). Labeling of the VAChT-positive cells within the efferent filamental epithelium was observed along the periphery of the filament, distinct from the labeling pattern of 5-HT-positive NECs, which occured along the central axis or midline of the filament (Figure 2.3B).

The distribution of VAChT-positive cells relative to NECs is further illustrated at the distal tip of the filament (Figure 2.4). In addition, the presence of SV2 in the afferent filamental epithelium is further evidenced in this region (Figure 2.4A, arrowhead). Furthermore, VAChT

labeling is again distinct from SV2 (Figure 2.4A, arrow). When the image from Figure 2.4A was rotated 90° along the length of the filament, the VAChT-positive cells were clearly more numerous along the afferent aspect (Figure 2.4B). The 5-HT-positive NECs were observed throughout the depth of the filament in this region (Figure 2.4C, arrowheads), intermingling with VAChT cells. In addition, VAChT-immunoreactive cells were observed to span the tip of the filament, located within ~2-10 µm of the 5-HT-positive NECs (Figure 2.4C, arrows).

2.3.2. Innervation of VAChT-positive cells in zebrafish

On the efferent side of the filament, some VAChT-positive cells were located within ~1-2 µm of nerve fibers labeled by the zebrafish-derived neuronal marker zn-12 (Figure 2.5). While many VAChT-positive cells observed deeper within the efferent filamental epithelium did not appear to make contact with zn-12-positive nerve fibers (Figure 2.5B,C; arrowheads), some VAChT-positive cells near the surface of the efferent filamental epithelium came within ~1-2 µm of filamental innervation (Figure 2.5C, arrow). These nerve fibers appeared to be of the type that were observed to degrade during previous denervation experiments (Jonz & Nurse, 2003), indicating that they are likely of extrabranchial origin. Immunoreactivity for zn-12 had not been previously observed on the afferent filamental aspect (Figure 2.6). Within the afferent filamental epithelium, most VAChT-positive cells did not appear to make direct contact with zn-12-positive nerve fibers (Figure 2.6A, arrowhead); however, in some cases, VAChT-positive cells appeared to sit adjacent to labeled nerve fibers (within ~2 µm) (Figure 2.6B, arrow).

2.3.3. Innervation and negative VAChT-immunolabelling in the gills of goldfish

The gills of goldfish showed no VAChT immunoreactivity (Figure 2.7). Antibody specificity was verified in zebrafish gills (not shown) and glial neurons (Shakarchi *et al*., 2012; Appendix I).

Denervation experiments in goldfish revealed the presence of intrinsic and extrinsic innervation of the gill filament (Figure 2.8). Arches fixed immediately following dissection showed zn-12 immunoreactivity along the central axis of the filament, as well as lamellar innervation (Figure 2.8A). Arches fixed following 48 hours in explant culture exhibited degradation of lamellar zn-12 immunoreactivity (Figure 2.8B). Innervation of the central axis of the filament appeared to originate from intrabranchial neuronal cell bodies at the proximal end of the filament (Figure 2.8D, arrowheads). Persistent filamental nerve fibers resembled the chain neurons observed in zebrafish gills (Jonz & Nurse, 2003), as their innervation showed nerve fibers connecting cell bodies along the length of the filament (Figure 2.8E, arrows). Closer inspection of NEC innervation following denervation confirmed the persistence of central chain neurons (Figure 2.9D, arrow). In intact filaments, the chain neurons (Figure 2.9C, arrow) appeared to send nerve fiber projections up to the filamental NECs, into the lamellae to the lamellar NECs, and deeper into the filamental epithelium (Figure 2.9C, arrowheads). These projections all degraded following explant culture (Figure 2.9B&C). All innervation to the lamellar NECs degraded following explant culture (Figure 2.8E, arrowheads).

2.4. DISCUSSION

In this study, we identified cells in adult zebrafish containing the vesicular ACh transporter (VAChT). Most notably, VAChT immunoreactivity did not colocalize with the serotonergic NECs, but was limited to a separate population of cells on both the efferent and

afferent filamental aspects. Some VAChT-positive cells appeared to be innervated by zn-12 immunoreactive nerve fibers, while the majority did not. Also of note is the lack of colocalization between VAChT and SV2 immunoreactivity in the zebrafish gill. The synaptic vesicle marker SV2 appears to be widely conserved in vertebrates (Buckley & Kelly, 1985); however, it is possible that it does not label some neurosecretory cells (Pumplin & Getschman, 2000). In addition to indicating the presence of ACh, the VAChT antigen is itself a protein found in the membranes of vesicles (Prado *et al*., 2002), thus the VAChT-positive cells described in this study are likely neurosecretory. As there is no electrophysiological data characterizing the sensory capabilities of the VAChT-positive cells, it remains unclear whether they constitute a novel population of cholinergic NECs. It is also possible that the SV2-positive 5-HT-negative NECs observed in this study and previously (Jonz & Nurse, 2003) are progenitors to the VAChT-positive cells, as their location along the periphery of the filament bears morphological similarity to the VAChT-positive cells. Future experiments aimed at observing this proposed transition are required.

2.4.1. Physiological significance of acetylcholine in zebrafish gills

In larval zebrafish, the appearance of VAChT-positive cells in the gills occurs at ~ 21 days post-fertilization (d.p.f.), which corresponds to the onset of ventilatory sensitivity to ACh (Shakarchi *et al*., 2013). In larvae, as in the present study, VAChT-immunopositive cells were distinct from the 5-HT-positive NECs (Shakarchi *et al*., 2013). In addition, only 5-HT-positive NECs of larval zebrafish appear to receive innervation at ~ 7 d.p.f., coinciding with a dramatic increase in O_2 sensitivity in the gills (Jonz & Nurse, 2005). Taken together, these observations do not implicate the VAChT-positive cells as primary peripheral O_2 sensors.

The presence of ACh in the gill is nevertheless significant, as it is among the primary candidates for mediation of neurotransmission in the mammalian carotid body (Shirahata *et al*., 2007). More importantly, its role as a stimulant of afferent neuronal activity in trout gills (Burleson & Milsom, 1995a), as well as triggering of hyperventilation in the trout (Burleson & Milsom, 1995b) and larval zebrafish via nicotinic ACh receptors (Sharakchi *et al*., 2012), indicates that ACh plays an important modulatory role in the O_2 sensing pathway of fish.

The proximity of VAChT-positive cells described in this study to the NECs, efferent and afferent filamental arteries, lamellae, and zn-12-positive innervation offers multiple potential avenues for the release and action of ACh. The morphological arrangement of peripheral O_2 sensing in the gills of fish represents a much more diffuse chemosensory system than the mammalian carotid body (Perry *et al*., 2009; Kumar & Prabhakar, 2012; Zachar & Jonz, 2012). It is possible that, in the same way the NECs are spread over the length of the gill filament in fish, cells containing accessory neurotransmitters (i.e. ACh) would be arranged similarly. In this case, the role of the VAChT-positive cells might be to modulate the response of NECs to hypoxia in a paracrine mechanism. In the mammalian CB, both muscarinic and nicotinic ACh receptors on type I cells provide a mechanism by which ACh can modulate their response to hypoxia by increasing intracellular Ca^{2+} through either membrane depolarization or Ca^{2+} entry through the receptors themselves (Wyatt & Peers, 1993; Dasso *et al*., 1997).

Acetylcholine is also a vasoactive neurotransmitter in the gills of fish (Jonz & Zaccone, 2009). Acetylcholine has been shown to cause vasoconstriction in the efferent filamental artery and arterioles feeding blood flow to the lamellae in trout (Sundin & Nilsson, 1997). Though this mechanism appears to be mediated by cholinergic innervation in trout, it is possible that the VAChT-positive cells observed in zebrafish gills play a similar role. Release of ACh from

VAChT-positive cells in the efferent filamental epithelium, located adjacent to the central axis of the filament near the lamellae, may act on cholinergic receptors regulating blood flow from the lamellae into the filamental artery. Vasoconstriction in this region would increase time spent by deoxygenated blood in the lamellae, leading to higher O_2 saturation of the blood.

Acetylcholine has also been implicated in a proposed process known as "lamellar recruitment", whereby the number of lamellae that receive perfusion is dictated by respiratory demand (Booth, 1978, 1979). In trout gills, injection of acetylcholine into the blood stream caused a reduction in the number of perfused lamellae (Booth, 1979). It is possible that ACh plays a similar role in zebafish; however, if its role is to modify vascular tone in response to hypoxia, it seems unlikely that ACh would cause vasoconstriction of the afferent filamental artery despite the significantly higher abundance of VAChT-positive cells directly adjacent to it. Instead, perhaps ACh is released into the blood from this population of VAChT-positive cells in response to hypoxia and acts on efferent arterioles to increase perfusion time through the lamellae. Alternatively, ACh can also act as a vasodilator through the activation of nitric oxide (NO) production via endothelial nitric oxide synthase (eNOS) (Jin & Loscalzo, 2010). The VAChT-positive cells of the afferent filamental epithelium may act to dilate the afferent filamental artery in response to hypoxia, increasing blood flow through the gill.

The proximity of some VAChT-positive cells to zn-12 immunoreactive nerve fibers on both the efferent and afferent sides of the filament implies that they may be able to send signals to or receive information from the central or peripheral nervous system. On the efferent filamental aspect, zn-12 nerve fibers that come into close proximity with VAChT-positive cells were of the type that degenerate following explant culture (Jonz & Nurse, 2004). These nerve fibers were concluded to be of extrabranchial origin, implying that signals carried by them pass

to or are generated from the central nervous system (Jonz & Nurse, 2004). Ultrastructural characterization is required to determine whether the VAChT-positive cells do in fact form synapses with zn-12 immunoreactive nerve fibers. Should future physiological experiments show the VAChT-positive cells to be a novel population of O_2 chemosensors, this potential extrinsic innervation would provide a signaling pathway for central integration of hypoxic stimuli. As zn-12 immunoreactive nerve fibers have not previously been observed on the afferent filamental aspect, it is unclear whether these are of intrinsic or extrinsic origin.

2.4.2. Adaptive implications of goldfish gill morphology

Goldfish did not show immunoreactivity for VAChT in their gills similar to that observed in zebrafish. Thus far, there is no information on the effect of ACh in the gills of goldfish. Though some VAChT labeling has been reported in nerve fibers of the goldfish gill (Porteus *et al*., 2012), it is possible that the absence in goldfish of VAChT-positive cells like those observed in the gills of zebrafish and mangrove rivulus (Regan *et al*., 2011) is adaptive, as their natural environments differ greatly. Goldfish are tolerant of a wide range of environmental O_2 partial pressures (P_{O2}), including extreme hypoxia (Burggren, 1982). They have evolved several adaptations to cope with extreme O_2 starvation, including a blood O_2 affinity that is relatively high (P_{50} = 2.6 mmHg; Burggren, 1982) as compared to other less hypoxia-tolerant species, such as sculpins (P_{50} ~ 22-58 mmHg; Mandic *et al*., 2009) and rainbow trout (P_{50} = 22.9 mmHg; Bushnell *et al*., 1984). Goldfish also produce ethanol as a result of anaerobic metabolism, which is much more easily excreted across the gills (Chamberland & Rioux, 2010). If ACh does in fact play a role in extending or intensifying the response to hypoxia in zebrafish (eg. via vasoconstriction/dilation, modulation of NEC activity), this role is perhaps less important or

absent in anoxia-tolerant species, such as goldfish, which have evolved other methods of coping with extreme O_2 starvation (eg. blood O_2 affinity). Further characterization of VAChT immunoreactivity in the gills of other anoxia-tolerant fish species will help clarify this possibility.

Differences in gill morphology extended to the innervation pattern of NECs in the goldfish gill. Lamellar NECs in goldfish gills appeared to receive innervation originating from extrabranchial neuronal cell bodies, much like those of zebrafish (Jonz & Nurse, 2003). In addition, following denervation, zn-12 immunoreactive neurons and nerve fibers originating from cell bodies at the proximal end of the filament persisted over the length of the efferent filamental aspect. These nerve fibers resembled those of the chain neurons of zebrafish filaments (Jonz & Nurse, 2003). Notably, goldfish gills appeared to lack a nerve bundle running adjacent to the efferent filamental artery and making direct contact with the NECs, as is observed in zebrafish (Jonz & Nurse, 2003). In zebrafish, this nerve bundle originates from intrabranchial cell bodies. Intact tissue from goldfish gills showed zn-12 immunoreactive nerve fibers forming connections between the chain neurons and filamental NECs which degraded following explant culture. This may indicate that filamental goldfish NECs receive primarily extrabranchial innervation, and that their physiological response to changes in environmental O_2 is primarily mediated by the central nervous system, and may not include the local vascular changes as proposed in the zebrafish gill (Jonz & Nurse, 2003).

The present study has characterized the presence of VAChT-containing cells in the gills of zebrafish, their associated innervation, and their absence in goldfish gills. In addition, we have observed key differences in the innervation of goldfish NECs as compared to zebrafish. The distribution and morphology of the VAChT-positive cells in zebrafish suggests that they

may play a role in modulation of vascular tone in the gill, as well as potentially interacting with the serotonergic NECs either through central innervation or via paracrine signaling. It is also possible that the VAChT-positive cells are themselves a novel population of O_2 chemosensors; however, future physiological studies are required to evaluate this role. Innervation of the serotonergic NECs of goldfish appears to be predominantly of extrabranchial origin, suggesting that central integration of the hypoxic stimulus is primarily responsible for physiological changes in this species. The lack of VAChT-positive cells in the gills of goldfish as compared to other species may be indicative of species-specific differences, perhaps due to evolutionary adaptation of tolerance to varying environmental O_2 availability.

Figure 2.1. Zebrafish express the vesicular acetylcholine transporter (VAChT) in their gills. A) General view showing serotonin (5-HT, blue) and synaptic vesicle (SV2, red) immunoreactivity. All 5-HT immunoreactive cells are also immunopositive for SV2; however, some SV2-positive cells do not express 5-HT (arrow). B) VAChT immunoreactive cells (green) are distinct from 5-HT positive cells, and appear to be more abundant on the afferent filamental aspect (*aff.*). C) VAChT-positive cells do not colocalize with SV2 immunoreactivity on either the efferent (*eff.*) or afferent filamental aspect. Cells positive for SV2 were also found on the afferent filamental aspect (arrowheads). D) Overview of 5-HT, SV2, and VAChT immunoreactivity in the zebrafish gill. Scale bar = 50 µm.

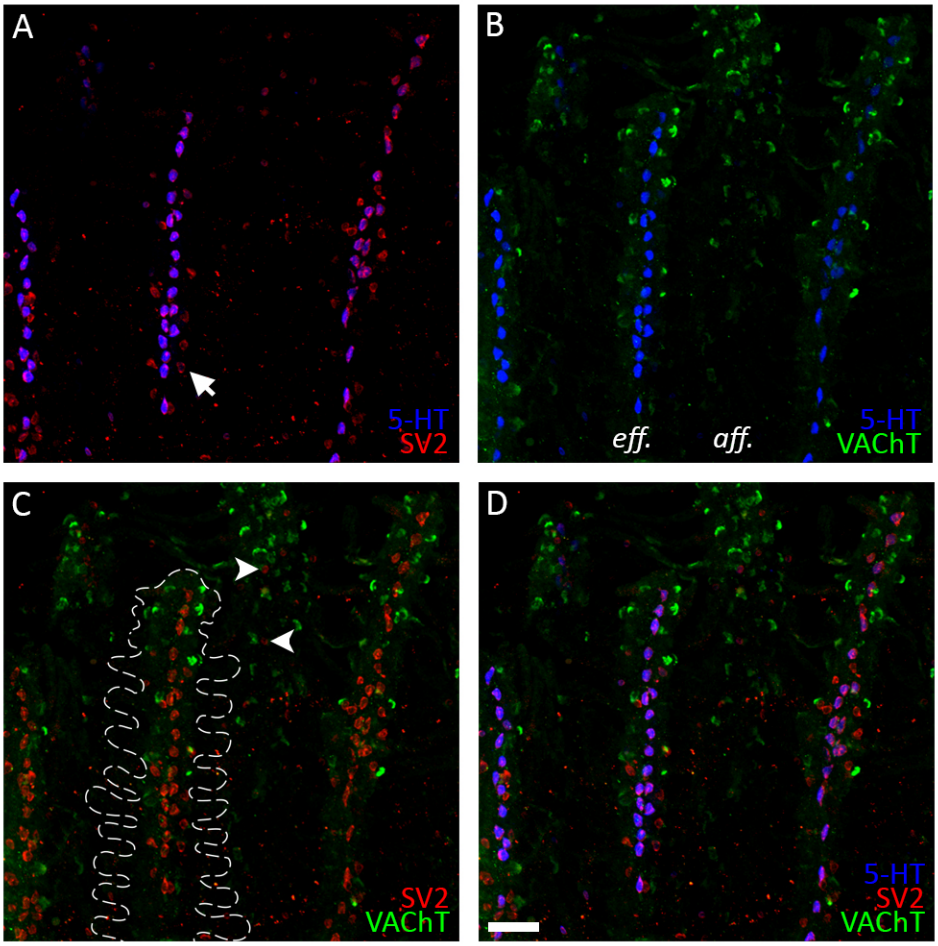
A
5-HT
SV2
B
eff.
aff.
5-HT
VAChT
C
SV2
VAChT
D
5-HT
SV2
VAChT

Figure 2.2. Vesicular acetylcholine transporter (VAChT) immunoreactive cells are smaller than serotonin (5-HT) positive cells, and more numerous along the afferent as compared to the efferent filamental aspect. A) Plot of mean ± S.E.M. number of cells per filament indicates that there were significantly more VAChT-positive cells along the afferent filamental aspect, as measured in the distal 200 µm of the filament ($p < 0.05$, two-sample *t* test, $n = 5$). B) Mean ± S.E.M. diameter of VAChT-positive cells was significantly less than 5-HT immunoreactive cells, as measured at the diameter ($p < 0.05$, two-sample *t* test, $n = 50$).

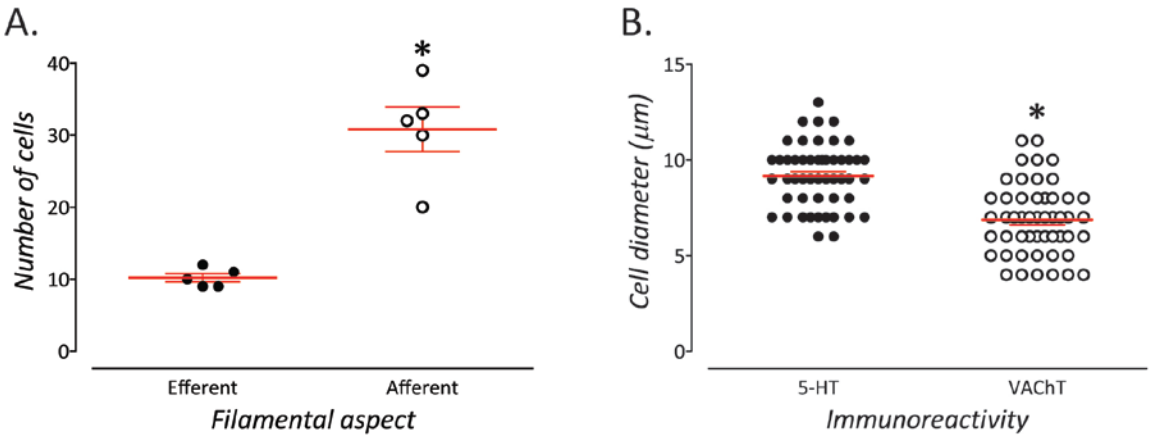
A.
Number of cells
40
30
20
10
0
*
Efferent
Afferent
Filamental aspect
B.
Cell diameter (µm)
15
10
5
0
*
5-HT
VAChT
Immunoreactivity

Figure 2.3. Higher magnification imaging of the efferent filamental aspect confirms that immunoreactivity of serotonin (5-HT, blue) and vesicular acetylcholine transporter (VAChT, green) immunoreactivity occured in separate cell populations. A) Standard labeling pattern of 5-HT and synaptic vesicles (SV2, red) organized along central midline of the filament epithelium. All 5-HT-positive cells colocalized with SV2; however, some SV2 immunoreactive cells did not contain 5-HT (arrow). B) VAChT-positive cells were separate and distinct from 5-HT immunoreactive cells, and were found adjacent to the central midline of the efferent filamental aspect. C) VAChT-positive cells did not colocalize with SV2. D) Overview of 5-HT, SV2, and VAChT immunoreactivity. Scale bar = 10 µm.

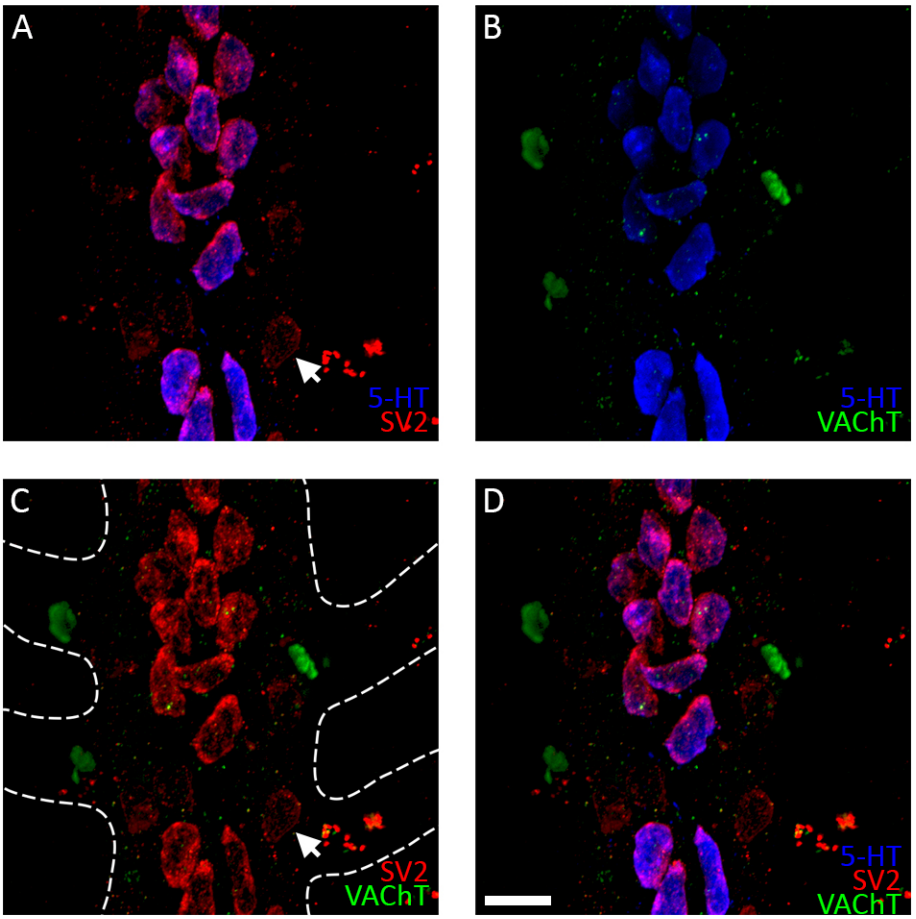
A
5-HT
SV2
B
5-HT
VAChT
C
SV2
VAChT
D
5-HT
SV2
VAChT

Figure 2.4. Cells immunoreactive for the vesicular acetylcholine transporter (VAChT, green) were more numerous on the afferent filamental aspect and intermingle with serotonin (5-HT, blue) immunopositive cells at the distal end of the filament. A) VAChT-positive cells on the afferent side of the filament did not colocalize with the synaptic vesicle marker SV2 (red). In addition, SV2- and 5-HT-positive cells were found on the afferent filamental aspect (arrowhead). B) Image from A rotated 90°. VAChT immunoreactive cells were found predominantly along the afferent filamental aspect and spanned the tip of the filament. Filamental 5-HT-positive neuroepithelial cells (NECs) of the efferent filamental aspect were seen on the left side of the panel. C) 5-HT-positive cells were found throughout the depth of distal end of the filament (arrowheads), and VAChT-positive cells span the distal tip of the filament (arrows). Efferent filamental aspect (*eff.*), afferent filamental aspect (*aff.*). Scale bar = 20 µm.

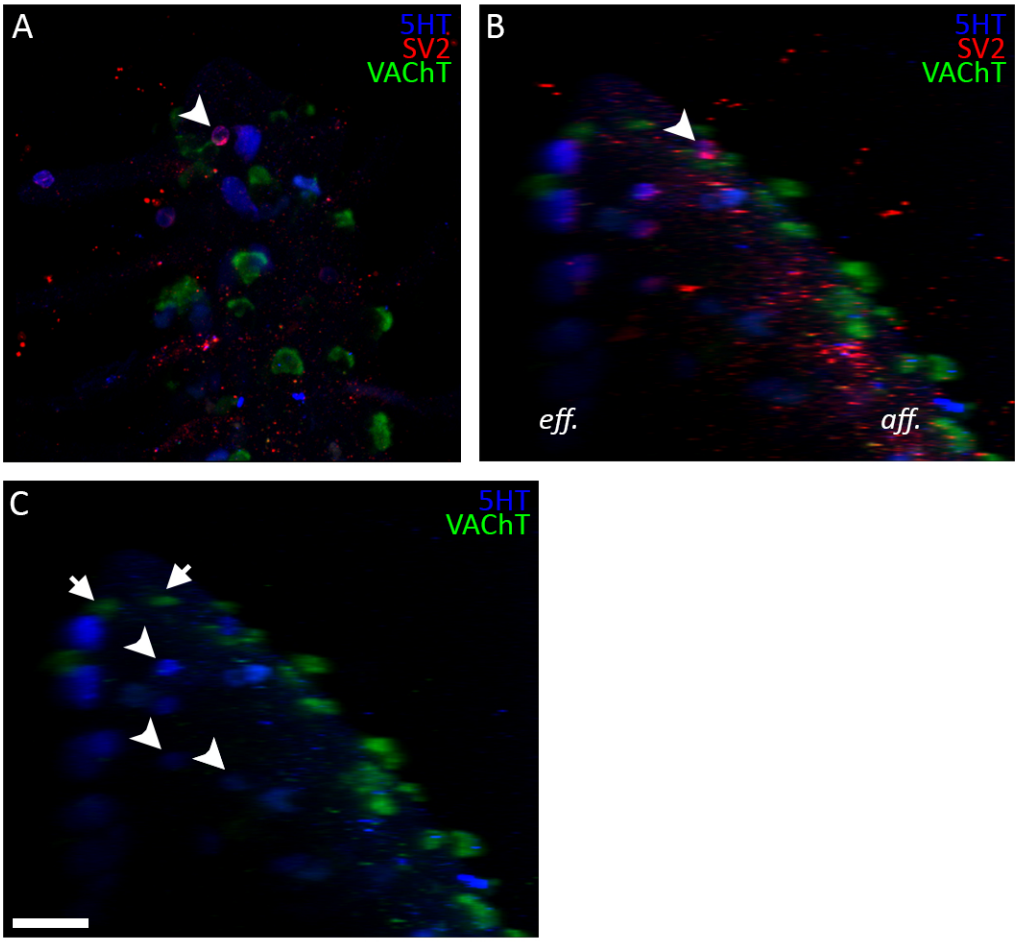
A
5HT
SV2
VAChT
B
5HT
SV2
VAChT
eff.
aff.
C
5HT
VAChT

Figure 2.5. Cells immunoreactive for vesicular acetylcholine transporter (VAChT, green) may be innervated. Bottom panels show transverse view following 90° rotation of upper panels. A) General view of serotonergic (5-HT, blue) neuroepithelial cells (NECs) innervated by nerve fibers labeled with the zebrafish-derived neuronal marker zn-12 (red). B) VAChT immunoreactive cells did not colocalize with 5-HT-positive NECs, and were found at varying depths throughout the efferent filamental epithelium (arrowheads). C) Some VAChT-positive cells came into close proximity of zn-12 immunopositive nerve fibers (arrow), while others did not appear to receive innervation (arrowheads). D) Summary of 5-HT, VAChT, and zn-12 labeling in the zebrafish gill. Scale bar = 50 μm.

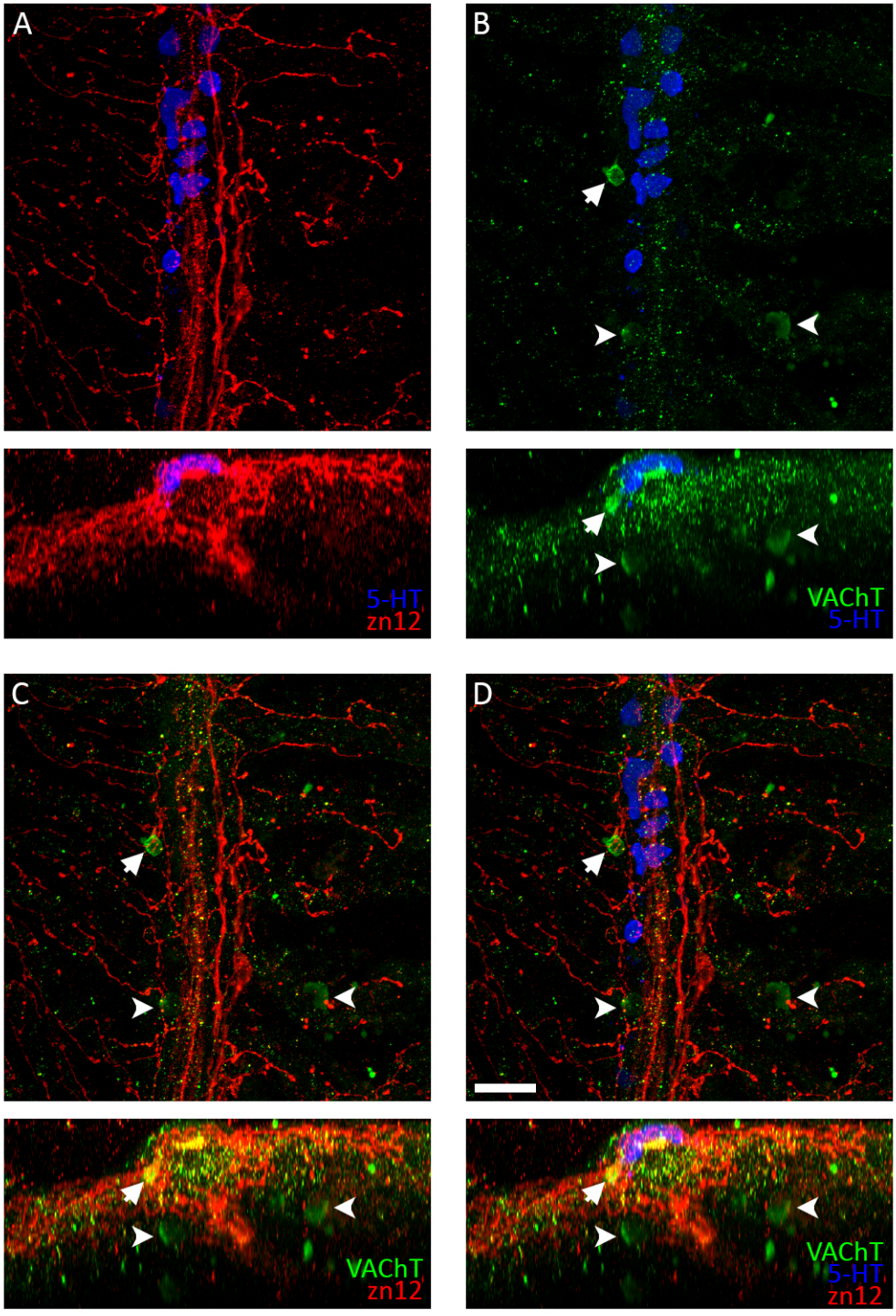
A
B
5-HT
zn12
VAChT
5-HT
C
D
VAChT
zn12
VAChT
5-HT
zn12

Figure 2.6. The afferent filamental aspect contains zn-12 immunoreactive nerve fibers (red), and some of these nerve fibers may innervate vesicular acetylcholine transporter (VAChT, green) immunopositive cells. A) Some VAChT-positive cells are in close proximity (~2 µm) to zn-12-positive nerve fibers (arrow). B) View from A rotated 90°. VAChT-positive cell is directly adjacent to zn-12-positive nerve fiber (arrow). Scale bar = 20 µm.

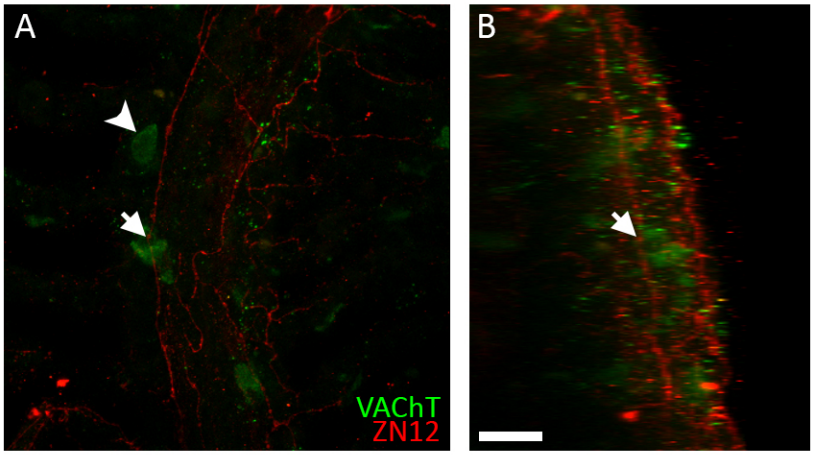
A
VAChT
ZN12
B

Figure 2.7. No vesicular acetylcholine transporter (VAChT, green) -containing cells were observed in the gills of goldfish. Scale bar for A-C = 20 µm, for D-F = 50 µm.

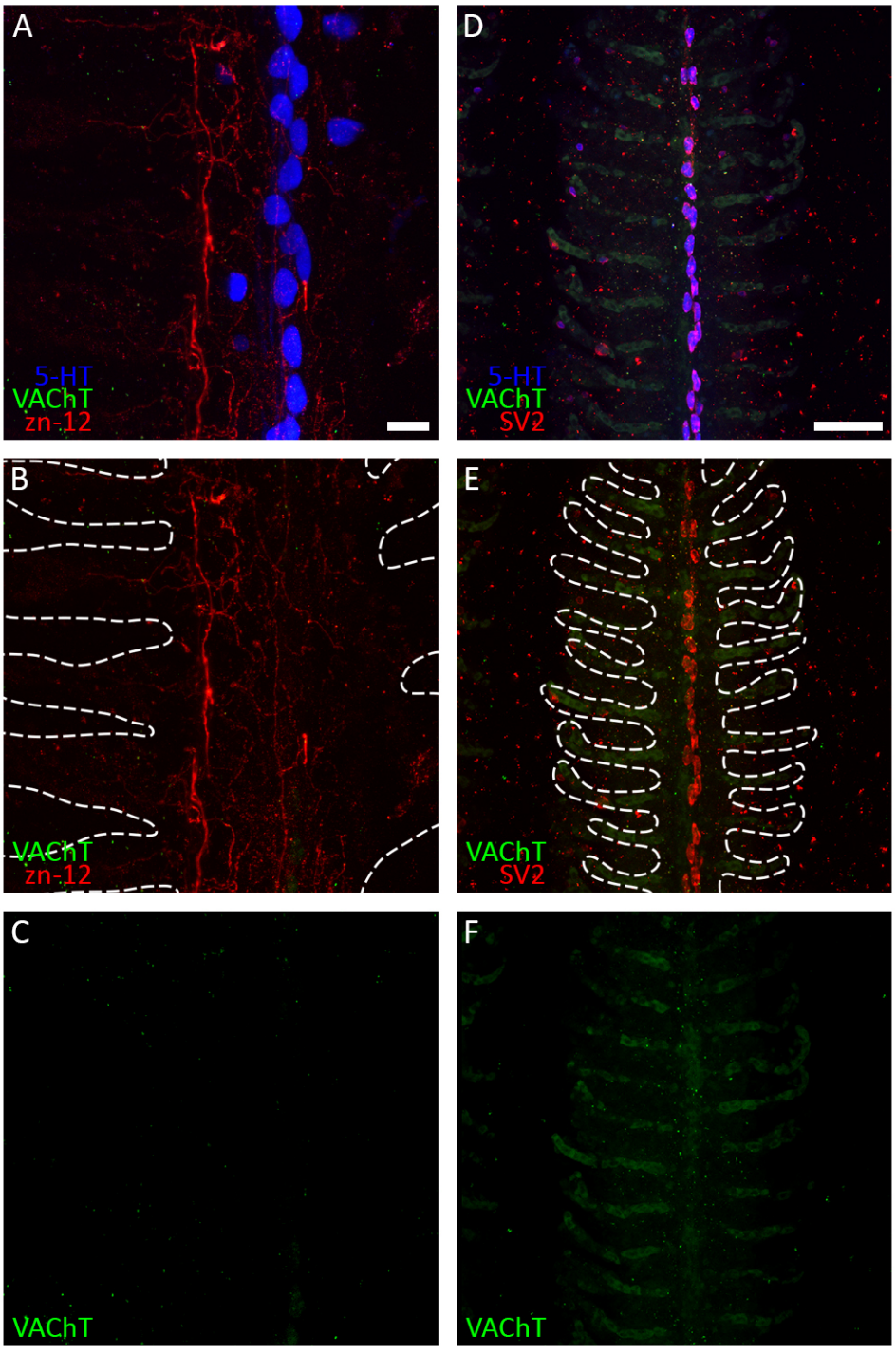
A
5-HT
VAChT
zn-12
D
5-HT
VAChT
SV2
B
VAChT
zn-12
E
VAChT
SV2
C
VAChT
F
VAChT

Figure 2.8. Cartoon depicting distribution of vesicular acetylcholine transporter (VAChT, green)- containing cells relative to serotonergic neuroepithelial cells (NECs, blue) in the gills of zebrafish. 5-HT immunoreactivity is limited to the efferent filamental aspect (eff.), whereas VAChT-positive cells are found on both the eff. and afferent (aff.) filamental aspect. Dotted lines indicate central axis of filament.

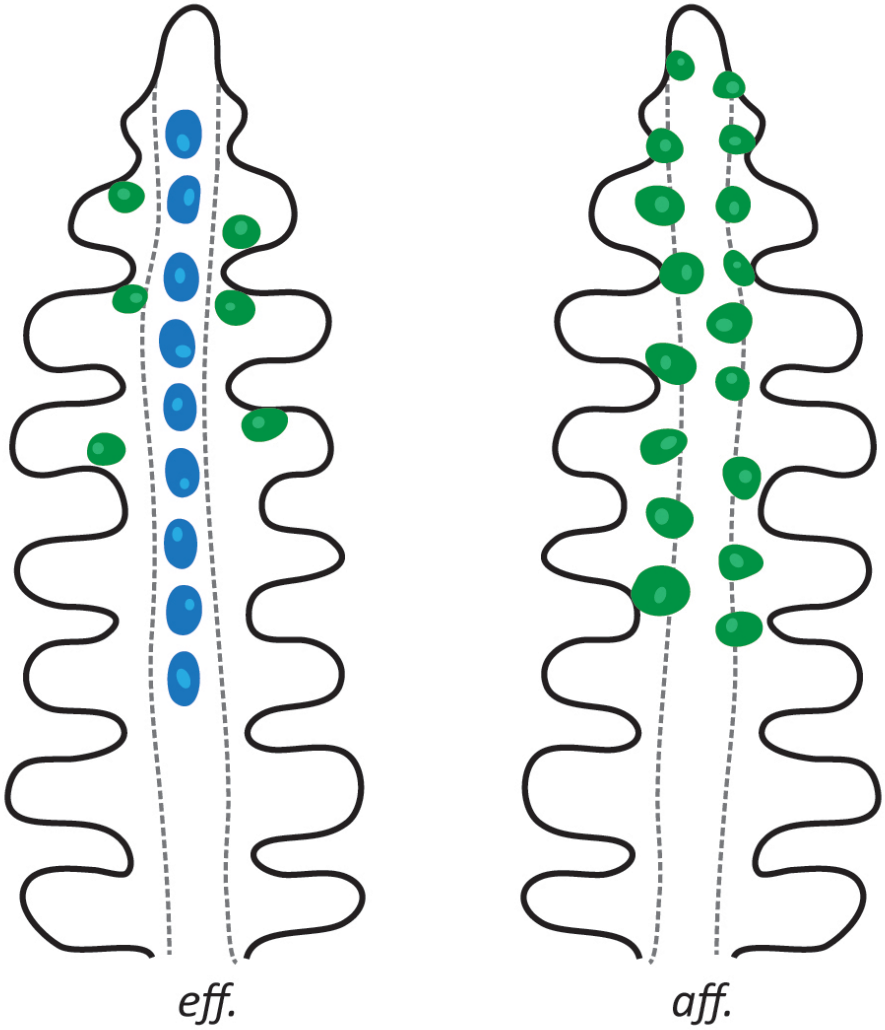
eff.
aff.

Figure 2.9. Nerve fibers of extrinsic origin degenerate in goldfish gill arches kept in explant culture for 48 hours. A) Control arch with zn-12-positive nerve fibers projecting centrally along the filament and out to the lamellae. B) Contralateral arch kept in explant culture for 48 hours shows degeneration of lamellar innervation. C) View from B rotated 90°. Persistent zn-12 labeling shows intrinsic nerve fibers deep within the filamental epithelium. D) Nerve cluster with several zn-12-positive cell bodies (arrowheads) at the base of the filament sends nerve fiber projections into the filament. E) Chain neurons run the length of the filament with multiple cell bodies (arrows). 5-HT-negative/SV2-positive cells lack innervation following degradation of extrinsic nerve fibers (arrowheads). Scale bar = 100µm for A,B,C; 20µm for D, E. Color scheme from E applies to all panels.

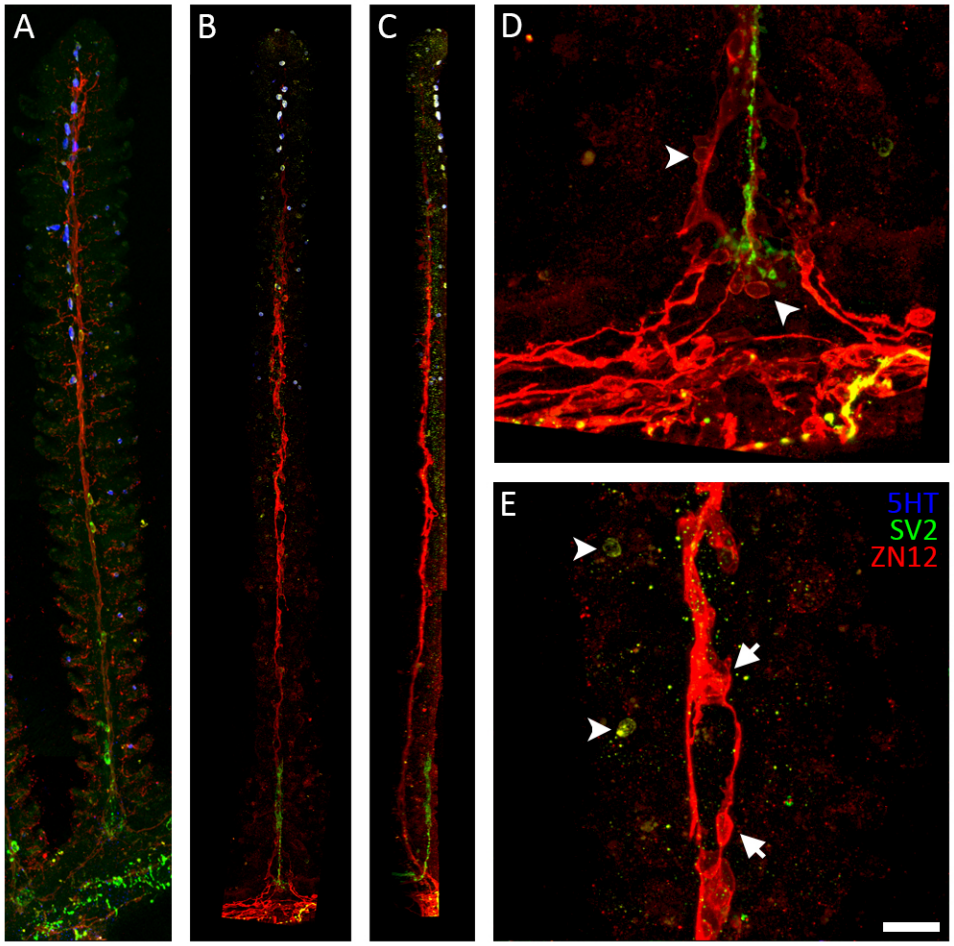
A
B
C
D
E
5HT
SV2
ZN12

Figure 2.10. In goldfish, nerve projections to lamellae and from central chain neurons to filamental neuroepithelial cells (NECs) degenerate following 48 hours in explant culture. A) Control gill arch shows rich innervation of filament and lamellae with zn-12-positive nerve fibers. B) Contralateral gill arch from same fish shows degeneration of all nerve fibers except those associated with central chain neurons. C) Transverse view of control arch shows chain neurons (arrow) with projections to filamental NECs, lamellae, and deeper into the filament (arrowheads). D) Transverse view of explanted arch shows persistence of chain neurons (arrow) and lack of projections to NECs (arrowhead), lamellae, and filament. Scale bar in C applies to A, in D applies to B, = 20µm. Color scheme in B applies to all panels.

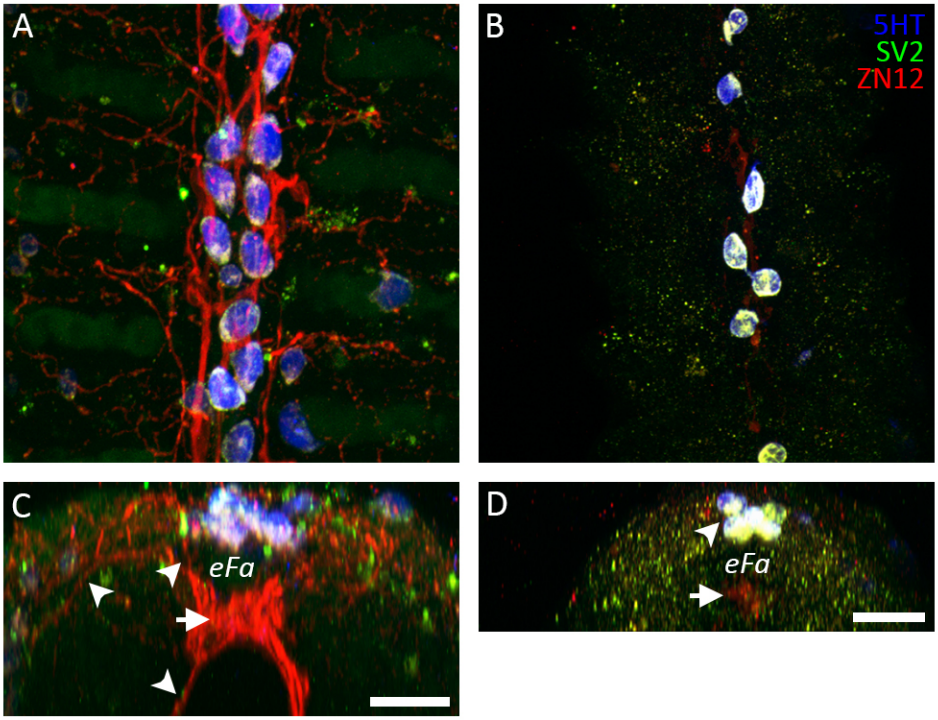
A
B
5HT
SV2
ZN12
C
eFa
D
eFa

3. Characterization of ion channels and O_2 sensitivity in neuroepithelial cells of the goldfish gill

3.1. INTRODUCTION

The ability to detect and respond to changes in environmental O_2 is critically important for the continued survival of air- and water-breathing vertebrates. Production of ATP is dependent upon a constant supply of O_2, thus linking O_2 with maintenance of cellular homeostasis. In mammals, O_2-sensitive chemoreceptors are able to initiate adaptive physiological responses to low O_2 (hypoxia), such as hyperventilation, changes in heart rate and vascular resistance. Among the most studied are the chemosensory type I cells of the carotid body, the primary O_2-sensing organ in mammals (Kumar & Prabhakar, 2012). In water-breathers, such as fish, the neuroepithelial cells (NECs) of the gills are believed to be the primary O_2 chemoreceptors, as they detect changes in O_2 *in vitro* (Jonz et al., 2004; Burleson et al., 2006). NECs originate from the same embryonic tissue that gives rise to the carotid body, and are thus considered to be their evolutionary precursors (Milsom & Burleson, 2007; Jonz and Nurse, 2009; Zachar & Jonz, 2012).

There are a number of advantages to studying O_2 sensing in fish. Fish experience natural fluctuations in water P_{O2} and display pronounced responses to hypoxia, such as hyperventilation and bradycardia (Perry et al., 2009). Moreover, NECs *in vitro* appear to have a higher sensitivity to hypoxia than type I cells. In NECs isolated from zebrafish the half maximal inhibition of plasma membrane K^+ channels occured at a P_{O2} of ~ 60 mmHg (Jonz et al., 2004) − at least 40 mmHg higher than the half maximal response in rat type I cells (Buckler, 1997). In addition, some species, such as the common goldfish (*Carassius auratus*), have evolved tolerance to prolonged exposure to extreme levels of hypoxia or even anoxia (Bickler & Buck, 2007). However, there have been no studies on the cellular mechanisms of O_2 chemoreceptors in goldfish, or any anoxia-tolerant organism, and how these cells may mediate tolerance to extreme environments.

In mammalian type I cells of the carotid body (CB), hypoxic stimuli lead to the inhibition of voltage-independent background K^+ (K_B) channels, and ultimately to the activation of voltage-activated Ca^{2+} (Ca_V) channels and facilitation of Ca^{2+}-dependent neurosecretion (Kumar & Prabhakar, 2012). Several other ion channel types have been identified in the mammalian CB in addition to K_B and Ca_V channels, including voltage-dependent K^+ (K_V) and Ca^{2+}-activated K^+ (K_{Ca}) channels (Peers *et al*., 2010). Both of these channel types have demonstrated O_2 sensitivity in rat (Wyatt & Peers, 1995), rabbit (Sanchez *et al*., 2002), and mouse (Pérez-García *et al*., 2004; Otsuba *et al*., 2006) type I cells. It has been proposed that K_V channels in type I cells may play a role in attenuating membrane depolarization during hypoxia (Pérez-García *et al*., 2004), as they do in some glial cells and neurons (Hoffman *et al*., 1997; Chen *et al*., 2006). Similarly, K_{Ca} channels contribute to rapid repolarization of membranes in mammalian neurons and vasculature (Pérez *et al*., 2013; Roberts *et al*., 2013), though they are also believed to play a role in the initial hypoxic response in the mammalian CB (Peers *et al*., 2010). In addition, a number of molecular O_2 sensors have been proposed that may initiate the chemoreceptor response to hypoxia in type I cells, and these are separated into two categories: membrane-delimited and cytosolic mechanisms (Prabhakar, 2006). However, roles for these molecular sensors appear to be species-specific and remain controversial.

Anoxia tolerant vertebrates have evolved several strategies in order to adapt to extreme O_2 deprivation. For example, goldfish have evolved a relatively high blood O_2 affinity (P_{50} = 2.6 mmHg; Burggren, 1982), allowing them to extract O_2 from their environment more efficiently. Despite these adaptive features in goldfish, comparative studies on goldfish and zebrafish have revealed that both species respond to acute hypoxia (Vulesevic *et al*., 2006; Tzaneva *et al*., 2011), although in these studies zebrafish appear to be more sensitive, and both species have

identical gill and NEC structure (Jonz & Nurse, 2003; Saltys et al., 2006). Thus far, the cellular mechanism of O_2 sensing in fish has been studied most extensively in zebrafish (Jonz *et al*., 2004; Qin *et al*., 2010). Whole-cell currents in zebrafish NECs are dominated by an O_2-sensitive conductance through K_B channels (Jonz *et al*., 2004). In the same way that mammalian models of O_2 sensing show species-specific differences in ion channel expression and molecular O_2 sensors, similar differences may be present in chemoreceptors of aquatic vertebrates.

In this study, we characterized the ion channels expressed in isolated NECs of goldfish and their potential contribution to O_2 sensitivity. Using dialyzed-cell patch-clamp techniques, we discovered a suite of K^+ and Ca^{2+} channel types in NECs, but were unable to identify an O_2-sensitive conductance. Moreover, we demonstrate that NECs with an intact cytosol responded to hypoxia with an increase in intracellular Ca^{2+} concentration ($[Ca^{2+}]_i$) and synaptic vesicle activity. These studies suggest that evolutionary adaptation to prolonged periods of environmental anoxia in water-breathing vertebrates may extend to the level of the respiratory chemoreceptor.

3.2. METHODS

3.2.1. Cell isolation

Experiments were performed on NECs enzymatically isolated from the gills of adult goldfish, *Carassius auratus*. Animals obtained from a local supplier were kept at 18°C in a closed recirculated system. Tissue from 1 or 2 fish yielded cells for one day of experiments. Goldfish were stunned with a blow to the head and killed by decapitation. Whole gill baskets were dissected and immediately placed in ice-cold phosphate-buffered saline (PBS) containing (mM): NaCl 137, Na_2HPO_4 15.2, KCl 2.7, and KH_2PO_4 1.5; pH 7.8 (Jonz *et al*., 2004).

Individual gill arches were then separated under sterile conditions and placed in a wash solution of PBS containing 2% penicillin/streptomycin (Gibco, Life Technologies, Carlsbad, CA, USA). The arches were cleaned of blood and mucus, and transferred to a petri dish containing fresh wash solution for 8 minutes.

The distal tips of the gill filaments were then separated from all eight gill arches and left in 3 mL of 0.25% trypsin/EDTA (Gibco) for 1 hour at 28°C. The tissue was further dissociated mechanically using fine forceps, and by transferring the enzyme/tissue solution to a 15 mL Falcon tube (Fisher Scientific, Waltham, MA, USA) and triturating. Incubation of tissue in trypsin/EDTA or mechanical separation alone did not permit adequate dissociation. Trypsin activity was halted by adding 0.2 mL fetal bovine serum (FBS) (Gibco). Un-dissociated tissue was left to settle for 8 minutes, after which time the supernatant was transferred to a separate 15 mL Falcon tube. This was spun down in a centrifuge (Thermo Scientific, Waltham, MA, USA) at 100 *g* for 5 minutes. The supernatant was removed, and the pellet resuspended in 2 mL PBS. If any tissue was left, it was allowed to settle for 8 minutes, after which time the supernatant was transferred to a separate 15 mL Falcon tube. This was spun down again at 100 *g* for 3 minutes. The supernatant was removed, and the pellet resuspended in an incubating solution of 0.5 mL Leibovitz's (L-15, Gibco) culture medium containing 2% penicillin/streptomycin and 2% FBS. Dissociated cells were then plated in 0.1 mL incubating solution in modifed glass-bottom cell culture dishes (35 mm, Corning, Corning, NY, USA; see Jonz et al., 2004) and incubated at 28°C overnight. Dishes were pre-coated with 0.2 mL poly-L-lysine (Sigma, St. Louis, MO, USA) for 20 minutes, followed by 3 washes of 3 minutes each with filter-sterilized distilled water. Matrigel (BD Biosciences, San Jose, CA, USA) in a 1:3 dilution was then applied to each dish with a cold seriological pipette over ice, and dishes were left at 4°C for 1 hour. Matrigel was

then recovered from the dishes, and dishes were rinsed once with PBS. Cells were fed the following day by the addition of 2 mL L-15 containing 2% FBS. Experiments on dissociated cells were completed within 24-36 hours following dissociation.

3.2.2. Immunocytochemistry

Isolated NECs were plated in dishes fitted with coverslips etched with grids to allow repeated localization of cells of interest following fixation. NECs that adhered to the culture substrate were identified by the addition of 2 $mg \cdot mL^{-1}$ Neutral Red (NR, Sigma), a vital marker used to identify NECs containing serotonin (5-HT) and synaptic vesicles (Jonz *et al*., 2004), to the medium for 8 min. Live cells that took up NR were first imaged using bright field optics. Following NR staining, cells were immediately processed for immunolabelling in order to positively identify them as NECs. Cells were fixed using 4% paraformaldehyde (Sigma) in PBS for 15 minutes at room temperature. Primary antibodies against serotonin (5-HT, Invitrogen) and synaptic vesicles (SV2, Developmental Studies Hybridoma Bank, University of Iowa) were applied to the dishes for 24 hours at 4°C, followed by secondary antibodies targeted to the primary antibodies for 1 hour at room temperature. Fluorescein isothiocyanate (FITC, Invitrogen) was used to label 5-HT immunoreactivity, and Alexa Fluor 594 (Alexa 594, Invitrogen) was used to label SV2. NR-positive cells were imaged using epifluorescence filtered for 488 and 594 nm emission. Imaging was done on an inverted microscope (Axio Vert, Zeiss), and images were captured with a digital camera (CCD Qicam, QImaging, Surrey, BC, Canada) and Northern Eclipse imaging software (Empix Imaging Inc., Mississauga, ON, Canada). The diameter of NR-positive cells was recorded.

3.2.3. Electrophysiology

Dishes were fitted with a chamber (~200-400 μL volume) and mounted on the stage of an inverted microscope (Axio Vert, Zeiss). The recording chamber was perfused under gravity at 4 $mL \cdot min^{-1}$ with extracellular solution (22-24°C). Hypoxia (P_{O2} ~ 11 mmHg) was generated by bubbling solution in a reservoir with 99% N_2 for 30 min prior to recording, as well as blowing 99% N_2 over the recording chamber. Anoxia (P_{O2} ~ 0 mmHg) was generated by adding 2 mM sodium dithionite (Sigma) to the perfusion reservoir while bubbling with 99% N_2 and blowing 99% N_2 over the recording chamber. Extracellular solution containing sodium dithionite was pH adjusted to 7.8 with NaOH.

All voltage- and current-clamp recordings were performed using the whole-cell patch-clamp technique. Experiments were conducted using an Axon Digidata 1550 in conjunction with an Axon MultiClamp 700B microelectrode amplifier (Molecular Devices LLC, Sunnyvale, CA, USA). Stimulus protocols were programmed and recorded using pClamp Electrophysiology Acquisition and Analysis Software (Molecular Devices).

Electrodes were made from borosilicate glass (World Precision Instruments Inc., Sarasota, FL, USA) and pulled on a Narashige PC-10 vertical puller (Narashige International USA Inc., East Meadow, NY, USA). All electrodes were fire-polished before use, with a tip resistance of between 6 and 8 MΩ. Extracellular bath solutions and intracellular electrode filling solutions are summarized in Table 3.1. All extracellular solutions were pH adjusted to 7.8 with NaOH, and all intracellular solutions were pH adjusted to 7.4 with KOH. Electrophysiological recordings were made against an Ag-AgCl pellet immersed in the recording chamber. Data are presented after correction for liquid junction potential error of about 5 mV with either intracellular solution.

NECs were identified for recording using NR, as above. Only cells having a seal resistance of ≥ 1 GΩ, a resting membrane potential (V_m) ≥ -40 mV, and whole-cell membrane capacitance (C_m) of between 2 and 4 pF were used for analysis.

Series resistance was typically < 20 MΩ. Cells were held at a holding potential of -60 mV, and currents were evoked primarily with step depolarizations to various test potentials (see figure legends) for 200 ms at a frequency of 2.5 Hz. Steady-state current was measured at 175 ms. For Figure 3.8A, currents were evoked by changing the membrane potential from -100 mV to +100 mV over a period of 1 s following a ramp protocol. In current-clamp V_m was recorded without current injection (I=0). Recordings were digitized at 10 kHz and filtered at 5 kHz. All data were analyzed using Clampfit software (Molecular Devices), and figures were arranged using Origin 8.6 (OriginLab Corporation, Northampton, MA, USA), Prism 5 (GraphPad Software, La Jolla, CA, USA), and Adobe Illustrator CS6 (Adobe Systems Inc., San Jose, CA, USA).

3.2.4. Carbon fiber amperometry

A carbon fiber electrode (Kation Scientific USA, Minneapolis, MN, USA) was used to measure P_{O2} in the perfusion chamber. All carbon fiber recordings were made relative to an Ag-AgCl pellet. The carbon fiber electrode was polarized to -600 mV in order to detect O_2 molecules (Mojet *et al.*, 1997). Initial current recorded from the air-equilibrated chamber was assumed to be 150 mmHg. Anoxia (0 mmHg) was calibrated by recording current from a solution containing 2 mM sodium dithionite bubbled with 99% N_2.

3.2.5. Measurement of intracellular calcium

Intracellular Ca^{2+} was measured using the ratiometric fluorescent Ca^{2+} chelator Fura-2-acetoxymethyl ester (Fura-2AM, Invitrogen). Cells isolated and plated on glass-bottom culture dishes as above were washed with PBS and incubated with 5 µM Fura-2AM in extracellular solution containing 0.1% pluronic acid (Invitrogen) for 45 min at 28°C. Cells were then washed and incubated in PBS for 45 min at 28°C. NECs were stained by adding 2 $mg \cdot mL^{-1}$ NR for 8 min. Calcium imaging was performed on an upright microscope (Eclipse, Nikon) equipped with a Lambda DG-5 high-speed wavelength changer (Sutter Instruments, Novato, CA, USE) using a digital camera (EXi CCD Camera, QImaging). A constant flow of extracellular solution (4 $mL \cdot min^{-1}$) was maintained with a gravity perfusion system. Hypoxia was generated as above. Dual images (340 and 380 nm excitation and 510 nm emission) were collected and ratiometric data were obtained using Northern Eclipse imaging software (Empix Imaging Inc., Mississauga, ON, Canada). Values for normoxia were obtained as an average of the 340/380 nm excitation ratio ($R_{340/380}$) over the time leading up to hypoxic exposure. Hypoxic values are presented as peak $R_{340/380}$ during hypoxic exposure.

3.2.6. Measurement of vesicular activity

The fluorescence vital dye N-(3-triethylammoniumpropyl)-4-(4-(dibutylamino) styryl) pyridinium dibromide (FM1-43, Invitrogen) was used to observe vesicular activity. Perfusion chambers were added to dishes containing cells isolated as above. NECs were stained using 2 $mg \cdot mL^{-1}$ NR for 8 min. Using gravity perfusion (4 $mL \cdot min^{-1}$), the cells were exposed to normoxic extracellular solution for 3 min followed by either normoxic or hypoxic solution containing FM1-43 (2 µM) for 2 min, and then washed with normoxic solution lacking vital dye

for 1 min. Hypoxia was generated as above. Imaging was done using an inverted microscope (Axio Vert, Zeiss) with a digital camera (CCD Qicam, QImaging) and Northern Eclipse imaging software (Empix Imaging Inc.) within 20 min of FM1-43 exposure. All NR-positive cells were imaged under both brightfield and epifluorescence filtered for 488 nm emission. Images were processed using Image J (National Institutes of Health, Bethesda, MD, USA). Fluorescence intensity was quantified using corrected total cell fluorescence (CTCF), calculated as:

$$CTCF = Integrated\ Density - (Area\ of\ Cell \times Mean\ Background\ Fluorescence)$$

where "Integrated Density" refers to the sum of the grey values of the pixels in a selected area (Burgress *et al*., 2010).

Pharmacological blocking of Ca_V channels was achieved using the general Ca_V channel blocker Cd^{2+} (100 µM, Sigma), and the L-type Ca_V channel blocker nifedipine (50 µM, Sigma). These blockers were added to the perfusion reservoir.

3.2.7. Statistics

Data are presented as mean ± S.E.M. values for voltage- and current-clamp, calcium imaging and FM1-43 experiments. Multiple comparisons were performed using ANOVA followed by the Bonferroni test for FM1-43 data. For calcium imaging, normoxic and hypoxic groups were compared using the paired *t* test. Statistical analyses were performed using software packages Excel (Microsoft, Redmond, WA, USA), Origin 8.6 (OriginLab Corporation), and Prism 5 (GraphPad Software).

3.3. RESULTS

3.3.1. Identification and passive membrane properties of isolated NECs

Isolated goldfish neuroepithelial cells (NECs) were identified *in vitro* using Neutral Red (NR), a vital dye preferentially taken up by acidic granules containing biogenic amines and used previously to identify serotonergic cells, including NECs, in culture (Stuart *et al*., 1974; Youngson *et al*., 1993; Jonz *et al*., 2004). Immunocytochemical analysis showed that 87% (102 of 117) of NR-positive cells were also immunoreactive for 5-HT and SV2 (Figure 3.1A). Measurement of NR/5-HT/SV2-positive cell diameter yielded a frequency distribution with a single mode between 10-11 µm, and an average cell diameter of 10.2 ± 1.3 µm (Figure 3.1B). NR-positive cells in this diameter range were selected for all subsequent experiments. Under voltage-clamp, the mean membrane capacitance (C_m) of these cells was 3 ± 0.9 pF (n = 108), with 90% of cells having a C_m of 2 to 4 pF (Figure 3.2A). In agreement with direct measurement of cell diameter, the ratio 1 µF $(cm^2)^{-1}$ (Solsona *et al*., 1998; Golowasch *et al*., 2009) and the equation for membrane surface area of a spherical cell ($A = 4\pi r^2$), the calculated mean diameter of patched cells was 9.7 ± 1.4 µm (n = 108). Mean resting membrane potential (V_m), measured under current-clamp (I = 0 pA), was -45.2 ± 11.6 mV (n = 69), with 65% of cells having a $V_m \geq$ -40 mV (Figure 3.2B). Mean series resistance (R_s) was 14.2 ± 7.7 MΩ (n = 107), with 82% of cells having an $R_s \leq 20$ MΩ.

3.3.2. Ca^{2+}-dependent and voltage-activated K^+ currents (I_{KCa} and I_{KV})

Depolarizing steps from a holding potential of -60 mV were used in extracellular solution 1 (ECS 1, Table 3.1) to evoke outward K^+ currents at test potentials positive to -30 mV (Figure 3.3). Onset of evoked current showed some delayed rectification below +40 mV (Figure 3.3A, left panel). A current-voltage relationship generated from the mean ± S.E.M. of steady-state

current amplitude from 6 cells is shown in Figure 3.3B (filled circles). The current-voltage relationship shows a prominent shoulder between depolarizing steps to test potentials from −20 to +40 mV (Figure 3.3B, filled circles). This shoulder approximately mirrored inward current through voltage-gated Ca^{2+} (Ca_V) channels, as recorded from 8 cells using Ba^{2+} solution (ECS 3, Table 3.1) (Figure 3.3A, right traces; B, open circles). These characteristics suggest that the outward K^+ current was dependent upon intracellular Ca^{2+}. Ca^{2+}-activated K^+ (K_{Ca}) channels have been described in mammalian O_2 chemoreceptors, such as carotid body type I cells from neonatal and adult rat (Peers, 1990; López-López, 1997), adult rabbit (López-López *et al*., 1993), and in chromaffin cells (Solaro *et al*., 1995).

The Ca^{2+}-activation of outward current was further investigated by preloading the cells with Ca^{2+} (Figure 3.4). Control experiments depolarized the cells with a single step from a holding potential of -60 mV to +100 mV (Figure 3.4A, bottom panel, dotted line). Current evoked with this test pulse constituted total whole-cell current (I_{Total}; Figure 3.4A, top panel). Cells were then preloaded with Ca^{2+} using a 50 ms pre-pulse to 0 mV, exceeding the activation potential of Ca_V channels. Further depolarization to the +100 mV test potential evoked an increased outward conductance. The average conductance (n = 10), measured 5 ms after the initial step to +100 mV, increased significantly in the pre-pulse experiments as compared to control (Figure 3.4B, $P < 0.05$, paired *t* test). The subsequent increase in conductance above the control is thus attributable to current through K_{Ca} channels (I_{KCa}; Figure 3.4A, top panel) (Solaro *et al*., 1995; López-López *et al*., 1997). The transient nature of this increased conductance is likely due to buffering of intracellular Ca^{2+} by EGTA.

The dependence of outward current on Ca^{2+} influx was further investigated by blocking Ca_V channels with 100 μM Cd^{2+} (Figure 3.5). Exposing NECs to Cd^{2+} eliminated the Ca^{2+}-

dependent shoulder from the current-voltage relationship (Figure 3.5B). The mean reduction in outward current at +20 mV upon application of Cd^{2+} was significant ($P < 0.05$, paired *t* test) at 32.1 ± 7.2% (n = 4). This further indicates the Ca^{2+}-dependence of outward K^+ current in the NECs. Application of Cd^{2+} also revealed a transient, voltage-dependent conductance (Figure 3.5A, right traces; B, open circles). The raw current traces generated in the presence of Cd^{2+} are rapidly activating and inactivating, in a manner reminiscent of fast voltage-gated conductance (I_A) through A-type voltage-activated K^+ (K_V) channels observable in the membranes of excitable cells (Bekar *et al*., 2004; Kollo *et al*., 2008). Voltage-activated K^+ current (I_{KV}) appeared to activate at ~ –30 mV (Figure 3.5B, open circles).

Application of the K_V channel blockers tetraethylammonium (TEA, 20 mM) and 4-aminopyridine (4-AP, 5 mM), as well as Cd^{2+} (100 µM) eliminated Ca^{2+}-dependent and voltage-activated outward K^+ conductance (Figure 3.6). The mean reduction in outward current at +20 mV upon application of TEA/4-AP/Cd^{2+} was significant ($p < 0.05$, paired *t* test) at 34.6 ± 8.9% (n = 5). The remaining raw current traces and current-voltage relationship revealed an open-rectifier-type K^+ conductance, as would be carried through background K^+ (K_B) channels (Figure 3.6A, right traces; B, open circles). Such currents have been described in rat type I cells (Buckler, 1997) and zebrafish NECs (Jonz *et al*., 2004) and are O_2 sensitive.

3.3.3. Goldfish NECs do not respond to hypoxia under whole-cell patch-clamp

Measurement of P_{O2} in the recording chamber during perfusion with hypoxic solution using a carbon fiber electrode indicated that bath P_{O2} reached ~ 11 mmHg within 2 minutes before stabilizing (Figure 3.7). Under these conditions, goldfish NECs showed no change in whole-cell conductance when exposed to hypoxia (Figure 3.8A,B). In voltage-clamp

experiments, there was no observable change in the current-voltage relationship between control (Figure 3.8A, filled circles) and hypoxia (Figure 3.8A, red circles) in either ECS 1 (n = 6) or when K_B channels were isolated with ECS 2 and Cd^{2+} (100 µM) (Figure 3.8B, n = 4). Under current-clamp conditions (I = 0 pA), there was no significant membrane depolarization in response to hypoxia (n = 5) (Figure 3.8C).

3.3.4. Intact goldfish NECs respond to hypoxia *in vitro*

The ability of goldfish NECs to respond to hypoxia was further investigated using Ca^{2+} imaging. Cells loaded with Fura-2-acetoxymethyl ester (Fura 2-AM) were exposed to hypoxia (P_{O2} ~ 11 mmHg) and changes in intracellular Ca^{2+} were observed as a shift in the 340/380 nm excitation ratio ($R_{340/380}$) (Figure 3.9). Exposure to hypoxia resulted in a gradual rise in intracellular Ca^{2+} (n = 7) (Figure 3.9A). Peak $R_{340/380}$ during hypoxia was significantly higher than mean $R_{340/380}$ during initial normoxic perfusion ($p < 0.05$, paired *t* test, n = 7) (Figure 3.9B).

In addition, goldfish NECs increased their recycling of synaptic vesicles in response to hypoxia (Figure 3.10). Vesicular activity was observed using the fluorescent vital dye vital dye N-(3-triethylammoniumpropyl)-4-(4-(dibutylamino) styryl) pyridinium dibromide (FM1-43). Uptake of FM 1-43 into excitable cells takes place primarily during the process of vesicular recycling, following neurotransmitter release (Betz *et al*., 1992; Tegenge *et al*., 2012). NECs exposed to hypoxia in the presence of FM1-43 incorporated significantly more dye as compared to normoxia ($p < 0.05$, ANOVA) (Figure 3.10A,B). Blocking Ca_V channels with Cd^{2+} (100 µM) eliminated increased dye uptake during hypoxia, as did application of the L-type Ca_V channel-specific blocker nifedipine (50 µM) (Figure 3.10B).

3.4. DISCUSSION

The present study identified at least four different types of ion channel in the plasma membrane of goldfish NECs, three of which have not previously been observed in the gill chemoreceptors. Though no response to hypoxia was observed in whole-cell patch-clamp experiments, intact NECs responded to hypoxia in calcium imaging and FM1-43 experiments.

3.4.1. Ion channels of goldfish NECs

The electrophysiological properties of respiratory chemoreceptors in water-breathing vertebrates have been studied in a limited number of species (Jonz *et al*., 2004; Burleson et al., 2006; Qin et al., 2010). In zebrafish, whole-cell current is primarily attributable to an O_2-sensitive K^+ conductance (I_{KO2}) through background K^+ (K_B) channels, akin to I_{KO2} through K_B channels observed in mammalian type I cells of the carotid body (Kumar & Prabhakar, 2012). Goldfish express a notably different array of ion channels than zebrafish. Whole-cell patch-clamp recordings from isolated goldfish NECs showed that depolarization activated a Ca^{2+}-dependent K^+ conductance (I_{KCa}). This conductance resembled that of high-conductance Ca^{2+}-activated K^+ (K_{Ca}) channels, as peak I_{KCa} approximately corresponded with inward Ca^{2+} current (I_{Ca}). In addition, I_{KCa} was activated by preloading the cell with Ca^{2+}, and was blocked by micromolar concentrations of Cd^{2+}. The K^+ current remaining after application of Cd^{2+} was rapidly activating and inactivating, and resembled transient "A-type" K^+ conductance (I_A) observed in glial cells and neurons (Hoffman *et al*., 1997; Chen *et al*., 2006). Current through A-type K_V channels has also been observed in the rabbit CB, and contributed to O_2-sensitive K^+ current (Sanchez *et al*., 2002). Further experiments are required to confirm the presence of I_A

currents in goldfish NECs and identify which members of the A-type subfamily of K_V channels are present.

Application of K_V and Ca_V blockers, TEA, 4-AP, and Cd^{2+} further revealed the presence of an outwardly rectifying K^+ conductance, as is observed through background K^+ (K_B) channels (Buckler, 1997; Jonz *et al*., 2004). In NECs of zebrafish and type I cells of the mammalian carotid body, K^+ conductance through K_B channels is O_2-sensitive (Buckler, 1997; Jonz *et al*., 2004; Kumar & Prabhakar, 2012). Though many of these currents have not been previously observed in the gills, detailed pharmacological characterization is required to identify specific members of ion channel subfamilies

3.4.2. Oxygen sensitivity of goldfish NECs

Under whole-cell patch-clamp, NECs of goldfish did not respond to hypoxia (P_{O2} ~ 11 mmHg). This is despite the fact that the level of hypoxia used in this study was significantly lower than that used previously to stimulate zebrafish NECs (P_{O2} ~ 25 mmHg; Jonz *et al*., 2004), which showed a half maximal response at P_{O2} ~ 60 mmHg. We observed no noticeable change to I_{KCa} or I_{KB} in the whole-cell current-voltage relationship under voltage-clamp in goldfish NECs. Moreover, V_m did not change in response to hypoxia under current-clamp (I = 0 pA), as it did in zebrafish (Jonz et al., 2004). The whole-cell patch-clamp technique constitutes breaking of the plasma membrane by suction and dialysis of the cell with artificial intracellular solution (ICS) from the recording electrode. Under these conditions, zebrafish NECs were able to retain the ability to respond to hypoxia (Jonz *et al*., 2004); however, one interpretation of the present data is that, in goldfish, dialyzed cell recording may have had a negative impact on, or even eliminated, critical intracellular signaling mechanisms required for O_2 sensing. This may

be indicative of a key difference between zebrafish and goldfish in terms of the mechanism(s) of O_2 sensing. In the case of zebrafish NECs, their retention of O_2 sensitivity despite loss of natural cytosolic environment suggests that part or all of the mechanism responsible for triggering inhibition of K_B channels is membrane delimited. On the other hand, in goldfish NECs the lack of response to hypoxia under similar conditions may be attributed to the dependence upon a cytosolic O_2 sensing mechanism that is lost during dialysis. In electrophysiological studies of O_2 sensing in mammalian type I cells, the perforated-patch technique is commonly used to avoid loss of cytosolic factors (Wyatt *et al*., 1995; Buckler & Vaughan-Jones, 1998); however, inside-out patch recordings from type I cells have shown that some channels retain their O_2 sensitivity in the absence of the cytosol (Riesco-Fagundo *et al*., 2001). It is possible that application of the perforated-patch technique to goldfish NECs, thus maintaining an intact cytosol, would preserve the response to hypoxia; however, our attempts to apply the perforated-patch technique in goldfish and zebrafish have thus far been unsuccessful.

The presence of a key O_2 sensing factor in the cytosol of goldfish NECs is further indicated by the O_2 sensitivity of intact isolated NECs as observed using Ca^{2+} imaging and FM1-43 uptake experiments. In these experiments, the plasma membrane and cytosol were left undisturbed and NECs were able to respond to the hypoxic stimulus. Exposure of goldfish NECs to hypoxia lead to an increase in intracellular Ca^{2+} concentration ($[Ca^{2+}]_i$). The profile of the increase in $[Ca^{2+}]_i$ in goldfish resembled "type A" responses observed in the NECs of trout in response to ammonia (a respiratory gas in fish; Zhang *et al*., 2011), with a delayed onset and a moderate peak. An increase in $[Ca^{2+}]_i$ is characteristic of the response to hypoxia of mammalian type I cells (Montoro *et al*., 1996; Buckler, 1997; Kumar & Prabhakar, 2012); however, its onset is rapid and more pronounced, and $[Ca^{2+}]_i$ remains elevated for the duration of the hypoxic

exposure. It is possible that modulation of membrane depolarization by K_V and K_{Ca} channels results in the comparatively subtle, delayed profile of $[Ca^{2+}]_i$ increased observed in goldfish NECs. Further investigation is required to determine whether this increase in $[Ca^{2+}]_i$ is dependent on extracellular Ca^{2+} or intracellular Ca^{2+} stores in goldfish NECs.

Vesicular activity also increased in goldfish NECs in response to 2 min of hypoxia, as observed using the fluorescent vital dye FM1-43. As the primary mode of uptake of FM1-43 into the cytosol is through the process of vesicular recycling (Betz *et al*., 1992; Tegenge *et al*., 2012), this indicates an increase in vesicular activity, and presumably neurosecretion, induced by hypoxia. Furthermore, application of the non-specific Ca^{2+} channel blocker, Cd^{2+}, as well as the L-type Ca_V channel blocker, nifedipine, blocked the increase in intracellular fluorescence in response to hypoxia. This demonstrates that vesicular activity in goldfish NECs is dependent upon extracellular Ca^{2+} entry, likely through L-type Ca_V channels. These findings also suggest that the rise in $[Ca^{2+}]_i$ observed in our Ca^{2+} imaging experiments may have been due to influx of extracellular Ca^{2+}.

By contrast, a previous study employing the activity-dependent dye, sulforhodamine 101 (SR101), reported decreased dye uptake by trout NECs *in vivo* following exposure to hypoxia as compared to normoxia (Porteus *et al*., 2012). This study concluded that a decreased presence of dye in the cytosol under these conditions was an indication of suppressed vesicular activity in NECs; however, in Porteus *et al*. (2012), constant stimulation by hypoxia (30 min) may have resulted in unloading of the dye from the cytosol via continuous synaptic vesicle activity, as was demonstrated in neuronal cell cultures (Tegenge *et al*., 2012) and frog neuromuscular junction preparations (Betz *et al*., 1992).

3.4.3. Implications for oxygen sensing and the physiological significance of goldfish NECs

Our proposed model of O_2 sensing in goldfish NECs is summarized in Figure 3.11. A cytosolic O_2 sensor detects a drop in extracellular P_{O2}, resulting in the inhibition of K_B channels (as inferred from previous studies Jonz *et al*., 2004; Burleson *et al*., 2006; Qin *et al*., 2010). This blocks the flow of K^+ ions out of the cell down their electrochemical gradient, which results in depolarization of the plasma membrane. Once V_m reaches ~ −40 mV, L-type Ca_V channels will activate, allowing Ca^{2+} to flow down its electrochemical gradient into the cytosol. At the same time, A-type K^+ channels will activate, providing a means for K^+ ions to begin exiting the cell and repolarizing the membrane. The increase in $[Ca^{2+}]_i$ caused by influx of Ca^{2+} through Ca_V channels allows for interaction of Ca^{2+} ions with primed synaptic vesicles associated with the plasma membrane, facilitating vesicular fusion and release of neurotransmitter. In addition, Ca^{2+} ions will interact with K_{Ca} channels, activating them and further repolarizing the membrane by allowing K^+ ions to flow out of the cell.

We propose that the role of K_{Ca}, and to a lesser degree K_V channels, in the NECs of goldfish is to blunt the cellular response to hypoxia. These channel types, particularly K_{Ca} channels, are known to play a similar role in mammalian neurons and the vasculature (Pérez *et al*., 2013; Roberts *et al*., 2013). This blunting mechanism is possibly further evidenced by the relatively subtle increase in $[Ca^{2+}]_i$ observed in response to hypoxia, as V_m is returned to resting values relatively quickly, thus decreasing the time Ca_V channels are activated. Future experiments aimed at disrupting K_{Ca} and/or K_V channels may illuminate this aspect of the proposed mechanism. Given the evolutionary history of goldfish and other members of the Cyprinidae family (eg. Crucian carp), where prolonged exposure to extreme hypoxia is not

uncommon, such a blunting mechanism would help to protect the NECs from depletion of ATP stores and excitotoxicity.

This study constitutes the first comprehensive characterization of ion channels and O_2 sensitivity of goldfish NECs; however, much work remains to complete the model. Taken together, the Ca^{2+} imaging and FM1-43 data suggest that goldfish NECs require an influx of extracellular Ca^{2+} through L-type Ca^{2+} channels to trigger neurosecretion during hypoxic stimulation. Although we were not able to observe O_2-dependent inhibition of ion channels in patch-clamp recording, our studies suggest that a cytosolic factor is critical for sensing of hypoxia in goldfish NECs. Goldfish have a relatively high blood O_2 affinity (P_{50} = 2.6 mmHg; Burggren, 1982), which allows them to extract O_2 from water into their blood more efficiently. Additionally, a neuroprotective mechanism known as "channel arrest" has been proposed as a mechanism of guarding neurons from anoxia-related excitotoxicity in goldfish and turtle brain (Pamenter *et al*., 2008; Wilkie *et al*., 2008).

Table 3.1. Summary of extracellular perfusing solutions (ECS) and intracellular electrode filling solutions (ICS) used in patch-clamp, Ca^{2+} imaging, and FM1-43 experiments.

Component	Extracellular solution			Intracellular solution	
(mM)	1	2	3	1	2
NaCl	120	95	100	10	10
KCl	5	5	-	120	-
$CaCl_2$	2.5	2.5	-	0.5	-
$MgCl_2$	2	2	2	-	-
Mg-ATP	-	-	-	2	5
HEPES	10	10	10	10	-
EGTA[1]	-	-	-	5	2
Glucose	10	10	10	-	10
TEA[2]	-	20	-	-	-
4-AP[3]	-	5	-	-	-
CsCl	-	-	5	-	120
$BaCl_2$	-	-	10	-	-

1. Ethylene glycol tetraacetic acid
2. Tetraethylammonium
3. 4-Aminopyridine

Figure 3.1. Identification of neuroepithelial cells (NECs) isolated from the goldfish gill. A) The same cell is shown in all four panels. (Upper left) brightfield image of NR-positive cell 24 h after dissociation. (Upper right) after fixation. (Lower left) fluorescence image of serotonin (5-HT) immunoreactivity. (Lower right) synaptic vesicle (SV2) immunoreactivity. Scale bar = 5 µm. B) Frequency distribution of cell diameter measured from NR/5-HT/SV2-positive cells. Measurement of cell diameter of dissociated NECs (n = 102) showed a single mode at 10-11 µm.

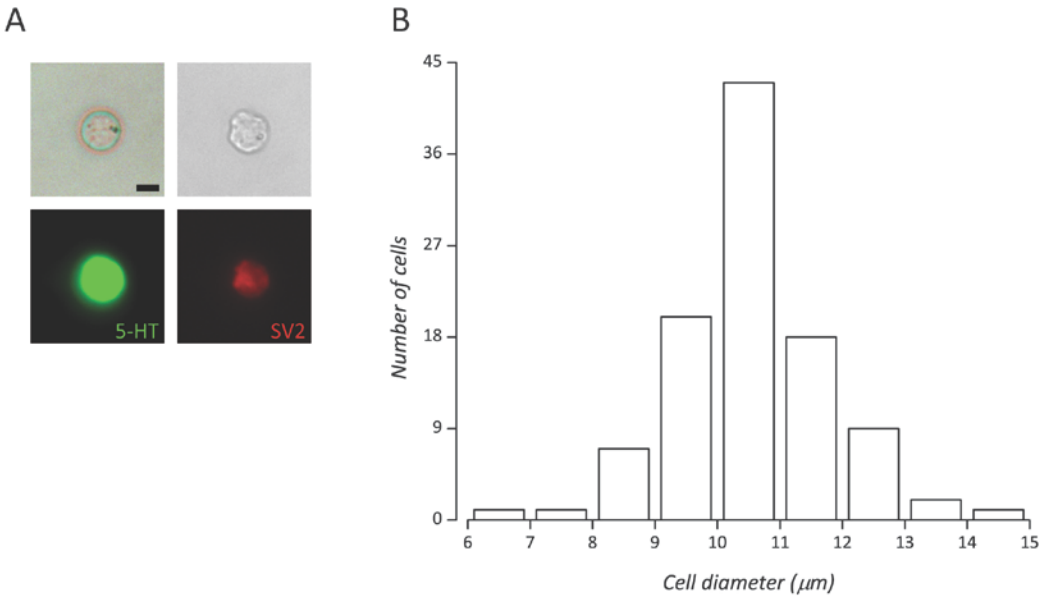
A
5-HT
SV2
B
45
36
27
18
9
0
Number of cells
6
7
8
9
10
11
12
13
14
15
Cell diameter (μm)

Figure 3.2. Passive membrane properties of Neutral Red (NR)-positive cells were used as additional selection criteria for patch-clamp experiments. A) Recording of whole-cell capacitance (n = 115) indicated 90% of cells were between 2-4 pF. B) Recording of resting membrane potential (V_m) under current-clamp (I = 0 pA, n = 65) indicated that 69% of cells had a $V_m \geq -40$ mV. C) Recording of series resistance (R_s, n = 115) showed 82% of cells were under 20 MΩ, indicating minimal series resistance error. NR-positive cells with a whole-cell capacitance of 2-4 pF, $V_m \geq -40$ mV, and recordings with $R_s \leq 20$ MΩ were used in patch-clamp experiments.

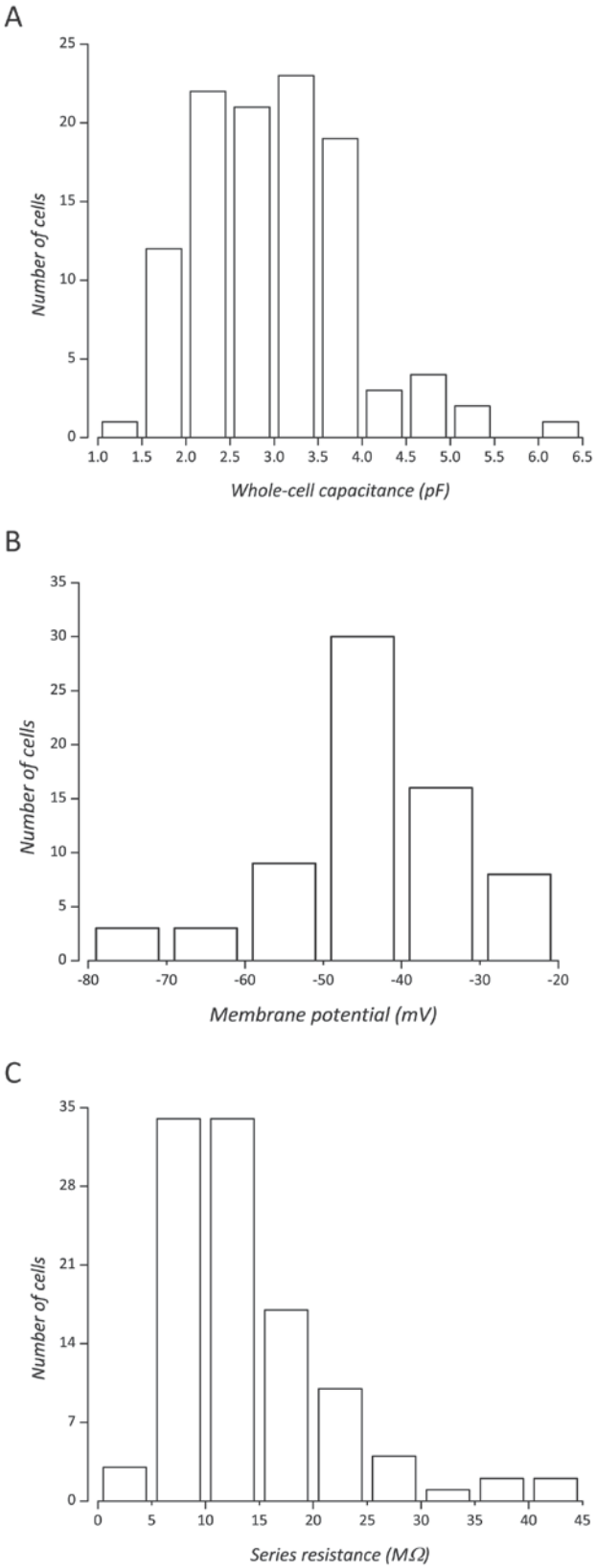
A
Number of cells
Whole-cell capacitance (pF)
B
Number of cells
Membrane potential (mV)
C
Number of cells
Series resistance (MΩ)

Figure 3.3. Neuroepithelial cells of the goldfish gill express Ca^{2+}-activated K^+ (K_{Ca}) channels and voltage-gated Ca^{2+} (Ca_V) channels, as observed in the whole-cell patch-clamp configuration. A) Raw traces from stepwise depolarizations under voltage-clamp, averaged from multiple cells. Left traces (n = 6) show currents evoked in normal extracellular solution (Table 1, ECS 1), with peak conductance at +20 mV and a current profile demonstrating activation imparted by Ca^{2+} dependence. Right traces (n = 8) show currents evoked in ECS containing blockers of outward current (Table 1, ECS 3), and intracellular solution containing Ba^{2+} as a charge carrier (Table 1, ICS 2). Initial activation of inward current occurs at ~ –30 mV, with peak conductance at 0 mV. B) Current-voltage relationship shows mean ± S.E.M. whole-cell current in normal ECS (closed circles) and in Ba^{2+} solution (open circles). Both Ca^{2+}- and voltage-actived components of the outward current are visible, while in Ba^{2+} solution only Ca^{2+} channel activity is shown. Note that peak current of the Ca^{2+}-dependent component of K_{Ca} occurs at a voltage greater than that observed for peak inward current through Ca_v channels.

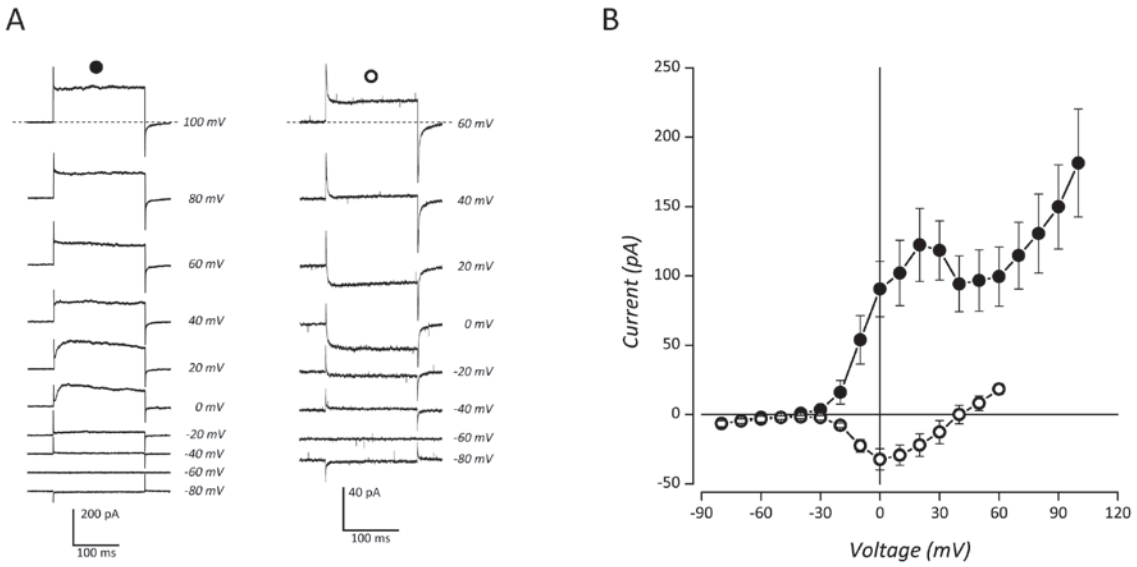
A
100 mV
80 mV
60 mV
40 mV
20 mV
0 mV
-20 mV
-40 mV
-60 mV
-80 mV
200 pA
100 ms
60 mV
40 mV
20 mV
0 mV
-20 mV
-40 mV
-60 mV
-80 mV
40 pA
100 ms
B
Current (pA)
Voltage (mV)
250
200
150
100
50
0
-50
-90
-60
-30
0
30
60
90
120

Figure 3.4. Pre-loading neuroepithelial cells (NECs) of the goldfish gill with Ca^{2+} induces a transient increase in conductance through K_{Ca} channels. A) Raw traces generated from the step protocol in the bottom panel. Top panel shows recording from a single cell. Total whole-cell current (I_{Total}) was generated with a control step from –60 mV holding potential to +100 mV (bottom panel, dotted line). Transient Ca^{2+}-activated K^+ current (I_{KCa}) was generated by preloading NECs with Ca^{2+} using an initial 50 ms step to 0 mV, followed immediately by a step to +100 mV (bottom panel, solid line). Middle panel shows average trace from 10 cells. B) Preloading cells with Ca^{2+} resulted in a significant increase in mean ± S.E.M. outward current immediately following the step to +100 mV ($P < 0.05$, two sample *t* test).

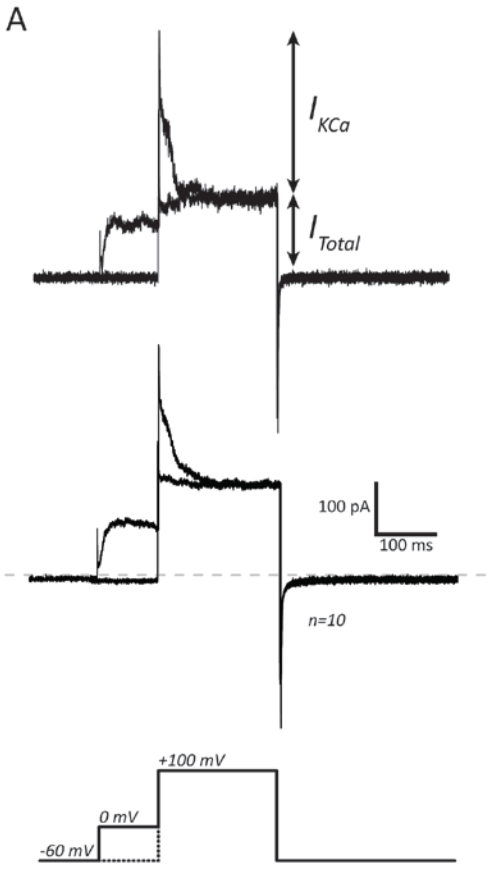
A
I_{KCa}
I_{Total}
100 pA
100 ms
n=10
+100 mV
0 mV
-60 mV

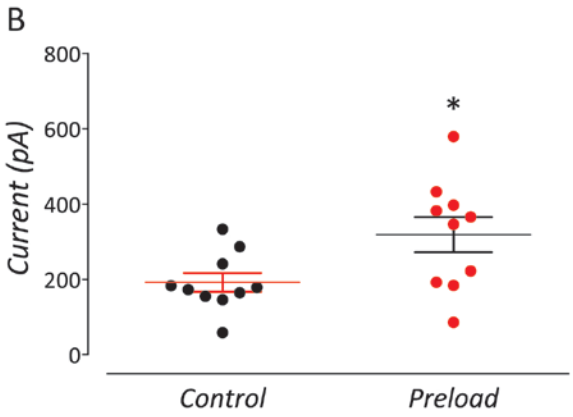
B
800
600
400
200
0
Current (pA)
*
Control
Preload

Figure 3.5. Indirectly blocking Ca^{2+}-activated K^+ (K_{Ca}) current reveals voltage-gated K^+ (K_V) channels. A) Raw current traces elicited by step depolarizations, averaged from multiple cells (n = 4). Left panel shows control traces in normal extracellular solution (Table 1, ECS 1). Right panel shows traces from ECS containing 100 µM Cd^{2+}. B) Current-voltage relationship generated from step depolarizations. Mean ± S.E.M. whole-cell current in normal ECS (filled circles) shows characteristic K_{Ca} profile. Blocking Ca_V channels with Cd^{2+} eliminates the Ca^{2+}-activated component of K_{Ca} and reveals a voltage-gated K^+ conductance (I_{KV}) activating at ~ –30 mV (open circles).

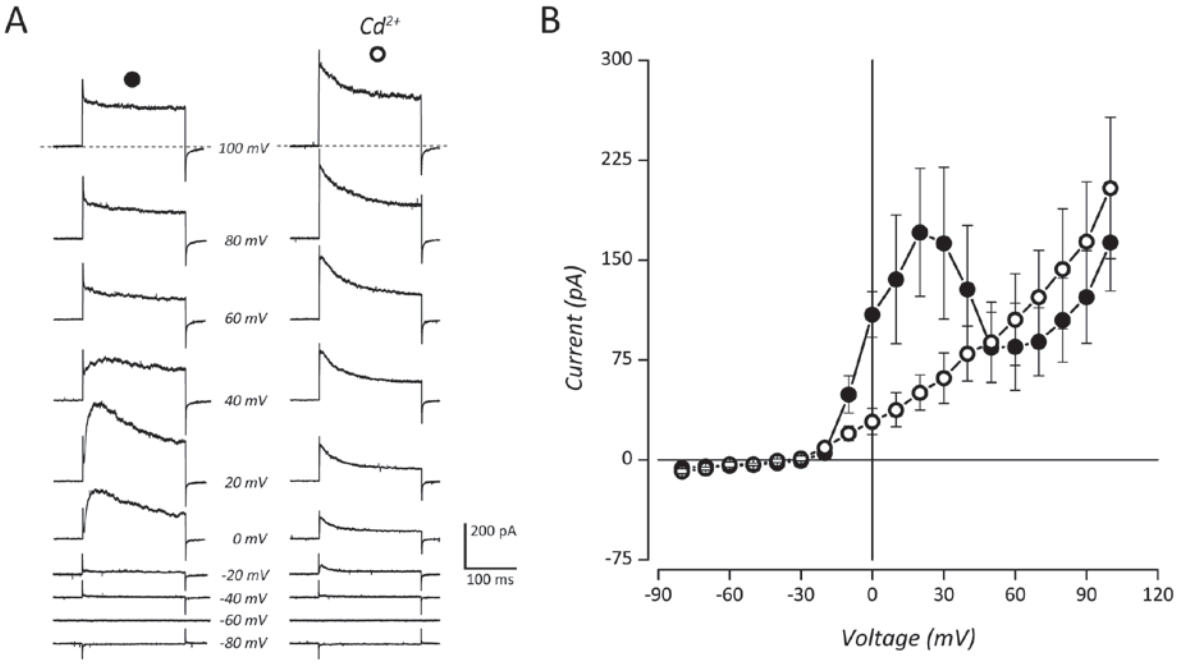
A
Cd2+
100 mV
80 mV
60 mV
40 mV
20 mV
0 mV
-20 mV
-40 mV
-60 mV
-80 mV
200 pA
100 ms
B
Current (pA)
Voltage (mV)
300
225
150
75
0
-75
-90
-60
-30
0
30
60
90
120

Figure 3.6. Blocking Ca^{2+}-activated K^+ (K_{Ca}) and voltage-gated K^+ (K_V) channels reveals background K^+ (K_B) channels. A) Raw current traces elicited by step depolarizations, averaged from multiple cells (n = 5). Left panel shows control traces in normal extracellular solution (Table 1, ECS 1). Right panel shows traces in ECS containing tetraethylammonium (TEA, 20 mM), 4-aminopyridine (4-AP, 5 mM), and Cd^{2+} (100 μM) (Table 1, ECS 2). B) Current-voltage relationship generated from step depolarizations. Mean ± S.E.M. whole-cell current in normal ECS (closed circles) shows characteristic total whole-cell current and K_{Ca} profile. Blocking K_{Ca} and K_V channels reveals outwardly rectifying background K^+ conductance (I_{KB}, open circles).

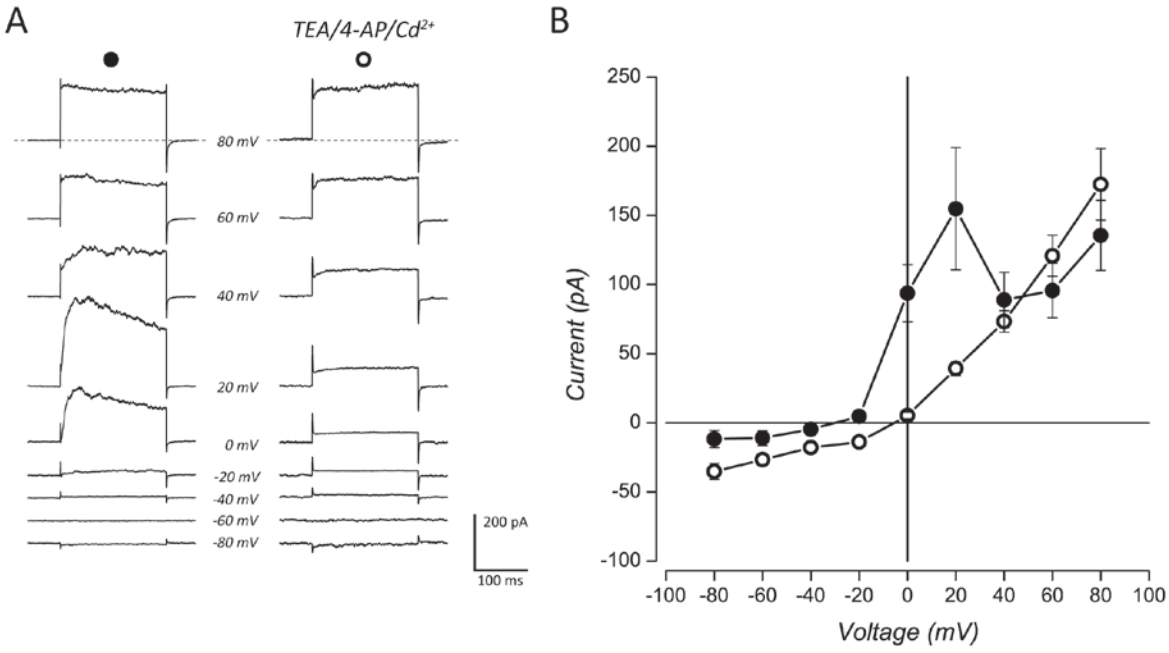
A
TEA/4-AP/Cd2+
80 mV
60 mV
40 mV
20 mV
0 mV
-20 mV
-40 mV
-60 mV
-80 mV
200 pA
100 ms
B
Current (pA)
Voltage (mV)
250
200
150
100
50
0
-50
-100
-100 -80 -60 -40 -20 0 20 40 60 80 100

Figure 3.7. Carbon fiber recording of changes in P_{O2} measured in the recording chamber during perfusion with N_2-bubbled extracellular solution (ECS) to produce hypoxia. Solution within the chamber reached a P_{O2} of ~ 11 mmHg within 2 min.

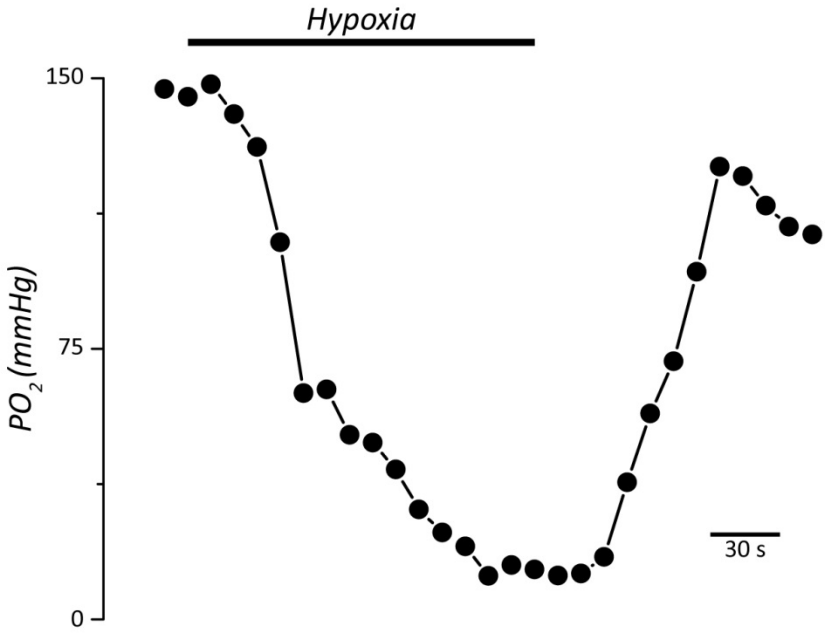
Hypoxia
150
75
0
PO_2 (mmHg)
30 s

Figure 3.8. Hypoxia does not affect whole-cell current or membrane potential in goldfish NECs under voltage- or current-clamp. A) Mean ± S.E.M. current-voltage relationship at 10 mV intervals generated with ramp depolarization from –100 to +100 mV in normal ECS (Table 1, ECS 1). B) Mean ± S.E.M. current-voltage relationship generated with step depolarizations in ECS containing tetraethylammonium (TEA, 20 mM), 4-aminopyridine (4-AP, 5 mM), and 100 µM Cd^{2+} (Table 1, ECS 2; n = 4); inset shows steps to 0, +30, and +60 mV. There was no observable difference in whole-cell current between normoxia (closed black circles), hypoxia (closed red circles), and normoxic wash (open black circles) in either normal ECS, or when current through background K^+ channels (I_{KB}) was isolated. C) Current-clamp (I = 0 pA) recording in normal ECS. Upper panel shows a trace from a single cell. Lower panel shows mean ± S.E.M. of 4 cells. There was no significant change in membrane potential (V_m) during hypoxic perfusion as compared to normoxia.

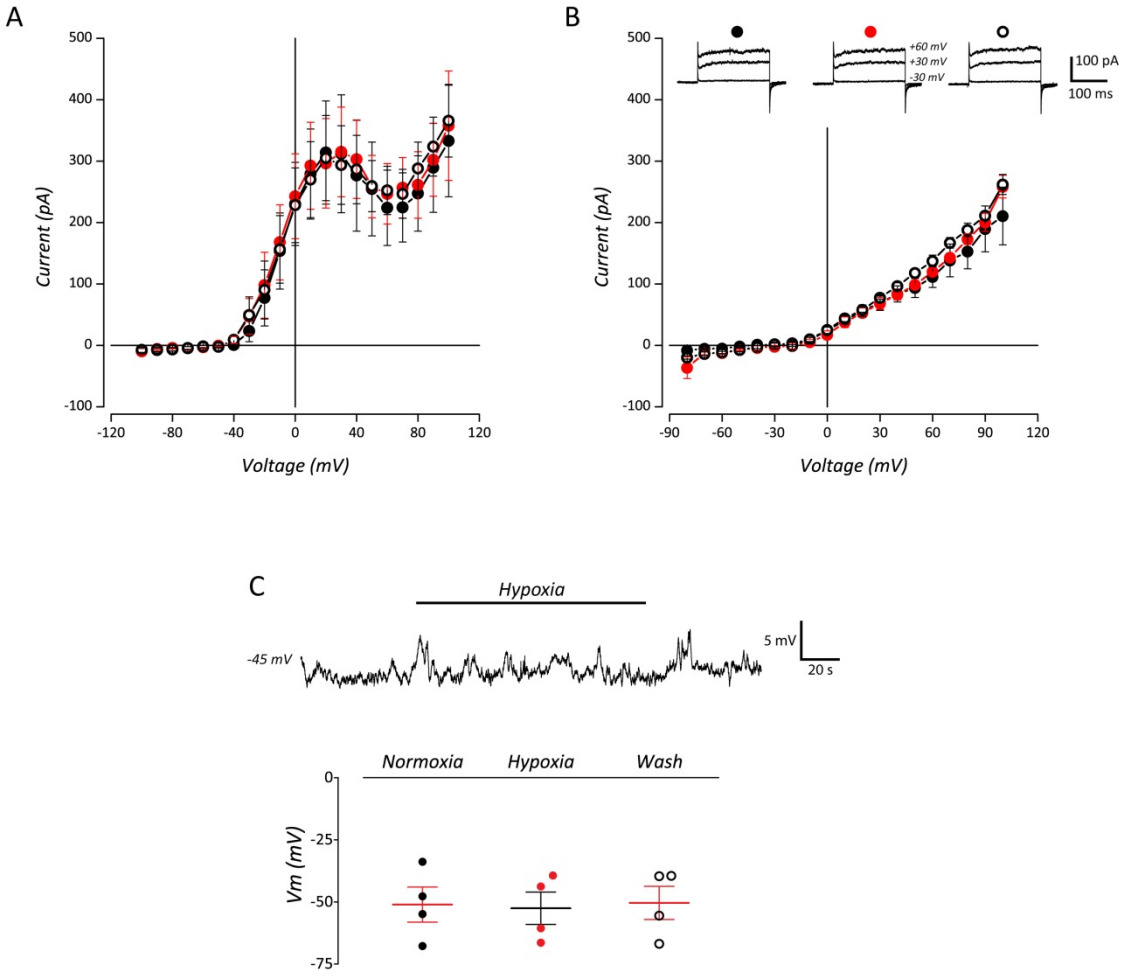
A
B
C
Current (pA)
Voltage (mV)
+60 mV
+30 mV
-30 mV
100 pA
100 ms
Hypoxia
-45 mV
5 mV
20 s
Normoxia
Hypoxia
Wash
Vm (mV)

Figure 3.9. Intracellular Ca^{2+} increases in response to hypoxia in isolated neuroepithelial cells (NECs) of goldfish. Data is presented as Fura-2AM 340/380 nm excitation ratio. (A) Representative trace of NEC responding to hypoxia by increasing intracellular Ca^{2+}, as detected by Fura-2AM binding. Upper panel shows 340/380 nm excitation ratio ($R_{340/380}$), bottom panel shows raw intensities at each wavelength. (B) Plot of mean ± S.E.M. $R_{340/380}$ indicates that intracellular Ca^{2+} rises significantly during hypoxia as compared to normoxia ($P < 0.01$, paired *t* test, $n = 7$).

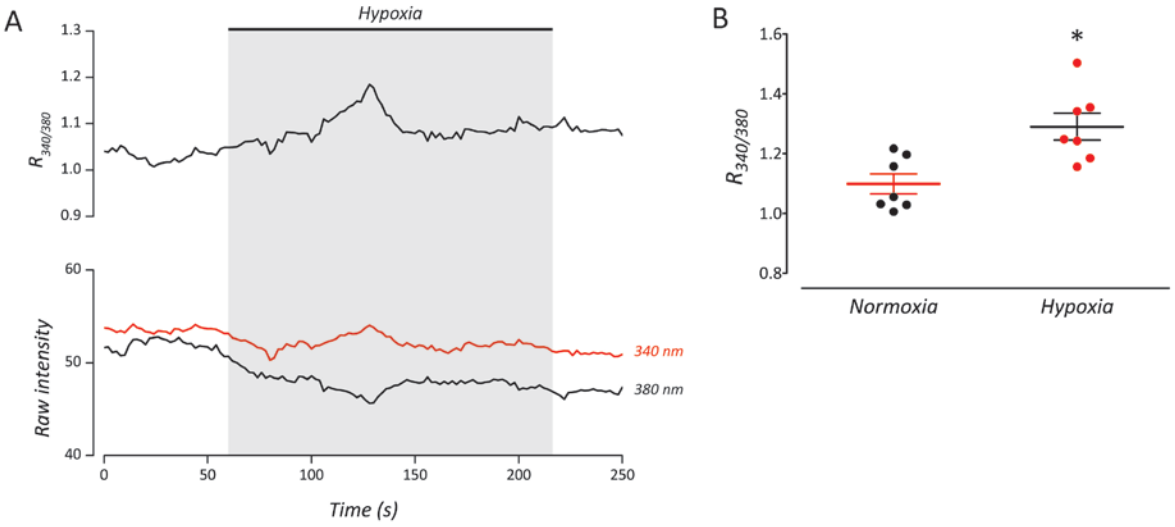
A
Hypoxia
1.3
1.2
1.1
1.0
0.9
$R_{340/380}$
60
50
40
Raw intensity
340 nm
380 nm
0
50
100
150
200
250
Time (s)
B
1.6
1.4
1.2
1.0
0.8
$R_{340/380}$
*
Normoxia
Hypoxia

Figure 3.10. Vesicular activity in isolated goldfish neuroepithelial cells (NECs) increases in response to hypoxia, and is likely mediated by L-type voltage-gated Ca^{2+} (Ca_V) channels. (A) Summary of experimental procedure. Isolated NECs were perfused with normal extracellular solution (ECS) for 3 min. Subsequently, NECs were exposed to either normoxia or hypoxia in the presence of FM1-43 (2 μM) for 2 min. Cells were then washed with normal ECS (Table 1, ECS 1) for 1 min and imaged. (B) Upper panel shows transmitted and fluorescent light images of representative NECs following FM1-43 exposure. Exposure to hypoxia significantly increased mean ± S.E.M. dye uptake in NECs ($P < 0.05$, ANOVA, n = 19) as compared to normoxia (n = 17). Adding Cd^{2+} (100 μM, n = 21) or nifedipine (50 μM, n = 22) to the perfusion reservoir for the duration of the experiment resulted in no significant difference during hypoxic exposure as compared to normoxia.

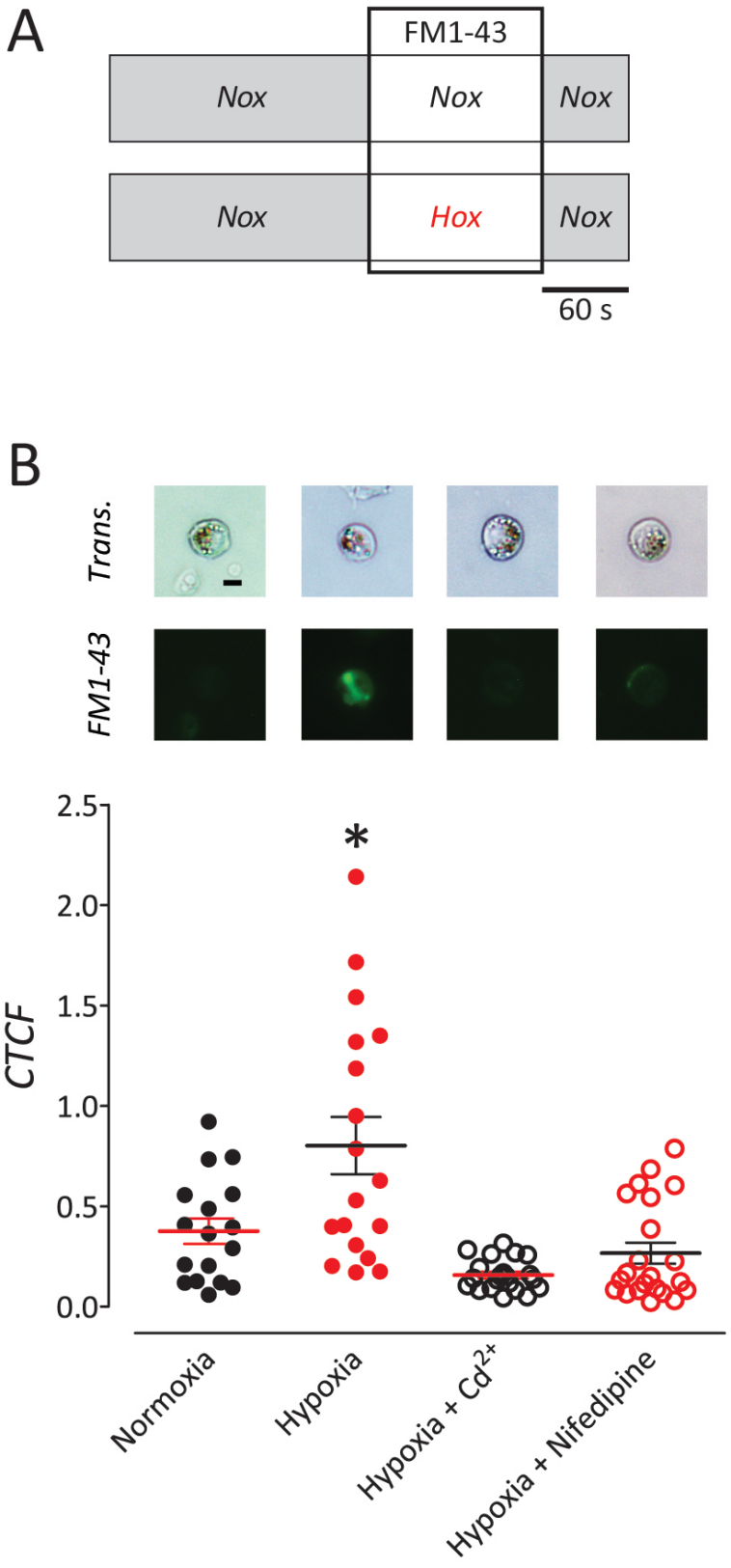
A
FM1-43
Nox
Nox
Nox
Nox
Hox
Nox
60 s
B
Trans.
FM1-43
CTCF
2.5
2.0
1.5
1.0
0.5
0.0
*
Normoxia
Hypoxia
Hypoxia + Cd2+
Hypoxia + Nifedipine

Figure 3.11. Proposed model of cellular O_2 sensing and modulation of membrane potential (V_m) in goldfish neuroepithelial cells (NECs). 1) A decrease in P_{O2} is detected by an unidentified cytosolic molecular O_2 sensing mechanism, inhibiting background K^+ (K_B) channels. 2) Inhibition of K_B channels leads to depolarization of the plasma membrane. 3) The positive shift in V_m leads to activation of rapidly inactivating voltage-activated K^+ (K_V) channels, which allow K^+ ions to flow down their electrochemical gradient out of the cell and contributes to rapid repolarization of the plasma membrane. 4) The initial depolarization of V_m also activates voltage-activated Ca^{2+} (Ca_V) channels, allowing Ca^{2+} to flow down its electrochemical gradient into the cell, increasing intracellular Ca^{2+} concentration ($[Ca^{2+}]_i$). 5) Increased $[Ca^{2+}]_i$ facilitates Ca^{2+}-dependent synaptic vesicle fusion with the plasma membrane and release of neurotransmitter into the synaptic cleft. 6) Increased $[Ca^{2+}]_i$ also allows for interaction of Ca^{2+} with calcium-activated K^+ (K_{Ca}) channels, activating them and causing further repolarization of V_m via efflux of K^+ from the cytosol.

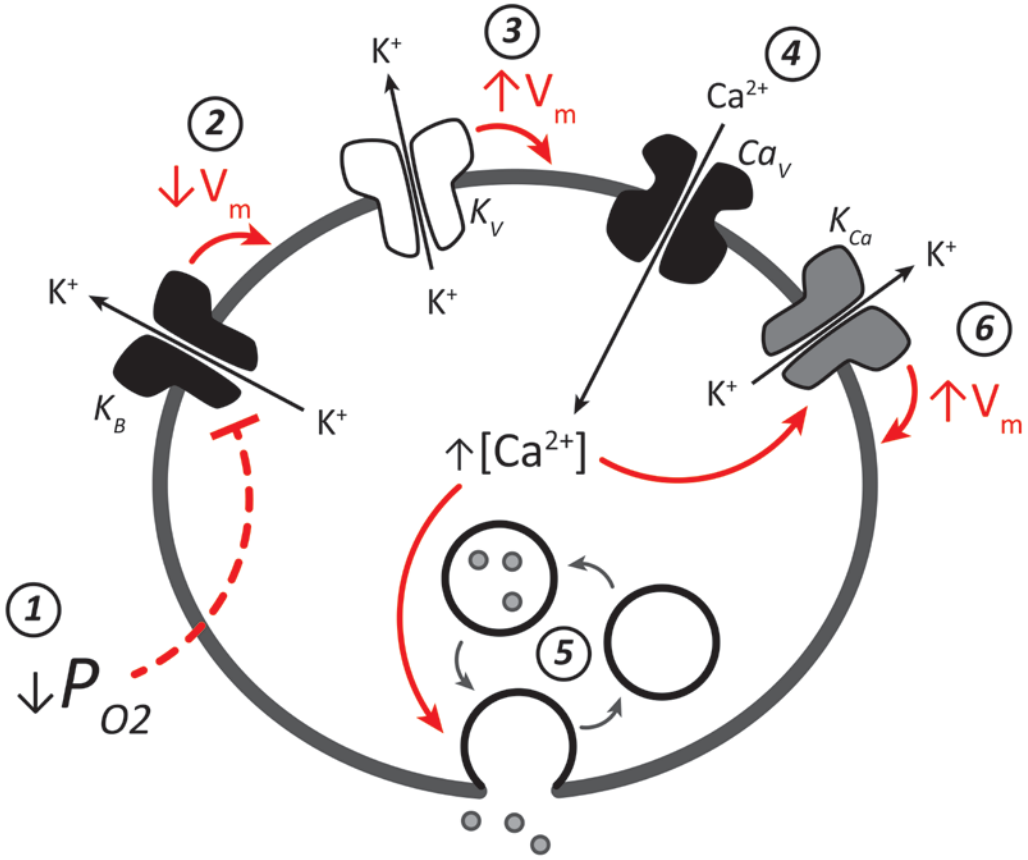
1
↓P O2
2
↓V m
3
↑V m
4
Ca2+
Ca V
5
↑[Ca2+]
6
↑V m
K+
K V
K B
K Ca

4. General Discussion

4.1. Introduction

In this thesis, I have presented results from morphological and physiological experiments directed at better understanding the mechanism(s) of O_2 sensing and response to hypoxia in the gills of zebrafish and goldfish. In Chapter 2, I discussed the presence of novel cell populations in the gills of zebrafish expressing the vesicular acetylcholine transporter (VAChT), and their absence in goldfish. In addition, I uncovered key differences in the pattern of innervation of the serotonergic NECs in the gills of goldfish as compared to zebrafish. In Chapter 3, I presented my discovery of novel ion channel types observed in the NECs of goldfish, as well as experiments investigating the O_2 sensitivity of dialyzed and intact NECs.

In this chapter, I will integrate my findings with the established knowledge in the field of O_2 sensing and the response to hypoxia in aquatic vertebrates. In addition, I will discuss potential adaptive benefits of the neurochemical and biophysical properties my research has uncovered.

4.2. Revised model of O_2 sensing in the gill

A drop in environmental O_2 is detected by the serotonergic neuroepithelial cells (NECs) of the gill (Jonz *et al*., 2004). These NECs contain the neurotransmitter serotonin (5-HT), as well as synaptic vesicles immunoreactive for SV2 (Jonz & Nurse, 2003). In response to hypoxia, the larger, filamental NECs undergo membrane depolarization mediated by background K^+ (K_B) channels (Jonz *et al*., 2004). This depolarization is believed to activate voltage-activated Ca^{2+} (Ca_V) channels, and ultimately trigger Ca^{2+}-dependent synaptic vesicle fusion and neurotransmitter release (Jonz *et al*., 2004), similar to the mechanism described in the mammalian carotid body (CB) (Kumar & Prabhakar, 2012).

In zebrafish, I have discovered a novel source of acetylcholine (ACh) in the gills, as indicated by the presence of VAChT. It is noteworthy that only some of the VAChT-positive cells appeared to receive zn-12 immunoreactive innervation, though this does not rule out innervation by some other population of nerve fibers not labeled by zn-12. ACh is believed to be the primary excitatory neurotransmitter in the CB (Shirahata *et al*., 2007), and is known to play a role in initiating physiological changes in fish, including increased ventilation frequency and heart rate (Burleson & Milsom, 1995b; Shakarchi *et al*., 2012). To affect these kinds of physiological changes in zebrafish, one possibility is that the VAChT-positive cells are O_2 sensitive themselves, responding to hypoxia via extrabranchial nerve fibers. Thus far, no physiological data exists to support the idea that VAChT-positive cells are sensitive to O_2. Alternatively, ACh released from the VAChT-positive cells following efferent signaling from the CNS might act on local vasculature, as has been observed in trout (Sundin & Nilsson, 1997). The VAChT-positive cells were found primarily along the afferent side of the filament, where deoxygenated blood is carried into the gill by the afferent filamental artery. Previous studies implicating ACh in the process known as "lamellar recruitment" showed that exogenous ACh led to decreased perfusion of the lamellae through general vasoconstriction (Booth, 1978). A role for ACh in increasing O_2 uptake during hypoxia in zebrafish might therefore come as the result of its release into the blood stream from the afferent filamental epithelium and action upon cholinergic receptors on arteriolar vasculature on the efferent side of the filament. ACh-mediated contraction of efferent vasculature would lead to increased vascular resistance for blood leaving the lamellae and returning to the efferent filament arteries, increasing time spent perfusing the respiratory surfaces. It is also possible that ACh acts on the afferent filamental artery, though perhaps in a vasodilatory manner via nitric oxide (NO) synthesis (Jin & Loscalzo,

2010). Whether its role is in central signaling or in modulation of local vasculature, ACh appears to be an important component of the zebrafish O_2 sensing model.

In goldfish, ACh does not appear to play a similarly important role in the gills, as I did not detect VAChT-positive cells akin to those I observed in zebrafish. No data exists on the physiological effect of ACh in goldfish, though one study reported observing VAChT immunoreactivity in nerve fibers of the goldfish gill (Porteus *et al*., 2012). The innervation of goldfish NECs showed a few key differences as compared to zebrafish, with filamental NECs receiving primarily extrabranchial innervation. Hypoxic signaling from the goldfish NECs may therefore act primarily on the CNS, causing whole-organism changes such as increased ventilation frequency and heart rate.

The model of O_2 sensing in goldfish further differs from that of zebrafish in the ion channel profile and O_2 sensitivity of the NECs. Whereas current across zebrafish NECs is dominated by an O_2-sensitive conductance through K_B channels, goldfish NECs most notably express a conductance through Ca^{2+}-activated K^+ (K_{Ca}) channels. In the mammalian CB, K_{Ca} channels appear to be O_2-sensitive (López-López *et al*., 1997); however, they are not believed to be primarily responsible for membrane depolarization in response to hypoxia (Peers *et al*., 2010). Additionally, goldfish NECs express fast-activating and inactivating voltage-dependent K^+ (K_V) channels resembling A-type K^+ channels, which have also been observed to be O_2-sensitive in the mammalian CB (Sanchez *et al*., 2002). It has been suggested that the role of K_V channels in the CB is to help in repolarization of the membrane following hypoxic stimulation (Pérez-García *et al*., 2004). In other mammalian excitable cells, K_{Ca} channels are believed to play a similar role (Pérez *et al*., 2013; Roberts *et al*., 2013). As in zebrafish NECs and the mammalian CB, goldfish

NECs also express K_B channels; however, recordings from the goldfish NECs did not show O_2 sensitivity in either unaltered whole-cell current or K_B channels.

When recording using the whole-cell patch-clamp technique, the plasma membrane of a cell is ruptured in order to control voltage and record current across the membrane. This rupture results in the dialysis of the cell with the artificial intracellular solution (ICS) used to fill the recording pipette, thereby eliminating many cytosolic factors. Under these conditions, the NECs of zebrafish retained their O_2 sensitivity (Jonz *et al*., 2004); however, the same does not appear to be true in goldfish NECs. The implication is that the cellular O_2 sensing mechanism in zebrafish NECs seems to rely on some membrane-associated factor(s) that are not lost during dialysis of the cell, whereas goldfish NECs require some cytosolic factor(s). In fact, intact goldfish NECs responded to hypoxia (P_{O2} ~ 11 mmHg) with increased intracellular Ca^{2+} ($[Ca^{2+}]_i$), as well as by increasing synaptic vesicle activity. Furthermore, the increase in synaptic vesicle activity was dependent upon extracellular Ca^{2+} influx through L-type Ca_V channels.

In a previous study, we discussed the effect of chemically-induced anoxia on V_m in the NECs of goldfish (Appendix II; Zachar & Jonz, 2012). Using the whole-cell patch-clamp technique, I observed a gradual membrane depolarization in response to anoxia produced by adding N_2 and the O_2 scavenger, sodium dithionite, to the perfusion reservoir. Exposure to sodium cyanide resulted in a similar membrane depolarization. At the time of publication, I hadn't conducted experiments involving exposure of intact NECs to hypoxic stimuli, leading us to conclude that the response to anoxia, and lack of response to hypoxia, of goldfish NECs indicated a different O_2 sensitivity as compared to the NECs of zebrafish. Indeed, it is possible that the K_B, K_{Ca}, and even K_V channels observed in goldfish NECs may exhibit sensitivity to extreme levels of hypoxia through some membrane-delimited mechanism, or may be O_2

sensitive themselves. Given the response to hypoxia observed in intact goldfish NECs (Chapter 3), and the latency between exposure to dithionite or cyanide and membrane depolarization in whole-cell current-clamp experiments (Appendix II), it is also possible that the responses to dithionite and cyanide I observed were the result of eventual ATP starvation of the cell.

The differences in proposed models of cellular O_2 sensing between goldfish and zebrafish NECs are summarized in Figure 4.1. In goldfish NECs, I propose that hypoxia is detected by some cytosolic factor(s), or a combination of cytosolic and membrane-delimited factor(s), and inhibits outward K^+ current through K_B channels, causing a membrane depolarization. This membrane depolarization activates Ca_V channels, which allow Ca^{2+} to flow into the cytosol, and K_V channels, which briefly release K^+ out of the cell, modulating the initial depolarization. Increased $[Ca^{2+}]_i$ facilitates Ca^{2+}-dependent vesicle fusion, as well as activating K_{Ca} channels. The former leads to neurosecretion, and the latter allows K^+ to flow out of the cell, rapidly repolarizing the membrane. In goldfish, the neurochemical signal generated in this way is then sent to the CNS along extrabranchial nerve fibers and integrated to generate physiological changes in response to hypoxia, such as increased ventilation and heart rate. When exposed to extreme hypoxia (i.e. anoxia), it is possible that the ion channels themselves contribute some O_2 sensitivity in addition to the cytosolic mechanism. In zebrafish, hypoxia is detected by some membrane-delimited factor(s) and leads to inhibition of K_B channels. This causes a membrane depolarization, which activates Ca_V channels and leads to Ca^{2+}-dependent synaptic vesicle fusion and neurosecretion. Neurotransmitter (i.e. 5-HT) released onto intrabranchial nerve fibers may then trigger changes in blood perfusion of the gill by acting on arterial sphincters at the proximal end of the filament, whereas 5-HT acting on extrabranchial innervation would lead to CNS signaling (Jonz & Nurse, 2003). Efferent innervation from the CNS to the VAChT-positive cells

may then trigger ACh release, which may act on local vasculature to increase perfusion of the lamellae. Alternatively, VAChT-positive cells constitute a novel population of O_2 chemosensors which act on cholinergic nerve fibers to modulate physiological reponses to hypoxia (i.e. ventilation, heart rate). It is also possible that, in regions of the gill where VAChT-positive cells and the serotonergic NECs come into close proximity (i.e. the distal tips), ACh released from the VAChT cells may act in a paracrine manner to enhance the response to hypoxia, as it does in the mammalian CB (Wyatt & Peers, 1993).

4.3. Implications for adaptation at the gill and chemoreceptor level

Based on previous developmental and morphological studies, the role of 5-HT as the primary signaling molecule in the hypoxic transduction process in the gills seems clear (Jonz & Nurse, 2003; Jonz *et al*., 2004; Sharakchi *et al*., 2012).

It is particularly noteworthy that I observed VAChT-positive cells in zebrafish, a moderately hypoxia-tolerant organism, and not the anoxia-tolerant goldfish. Zebrafish NECs seem to exhibit a relatively less complex cellular transduction mechanism as compared to the newly characterized goldfish NECs; however, ACh seems to play a more important role in the gills of zebrafish (Sharakchi *et al*., 2012). If one of the primary roles of ACh in the gill is in fact the modulation of vascular tone, as I suggested above and in Chapter 2, then perhaps the absence of VAChT-positive cells in the goldfish gill is indicative that this mechanism does not play a major role in their response to hypoxia. As mentioned previously, goldfish have evolved several adaptations in order to cope with extreme O_2 deprivation, including a high blood O_2 affinity (P_{50} = 2.6 mmHg; Burggren, 1982), which may allow perfusion of the gills to remain unmodified by local vasculature as the organism increases ventilation of the gills and heart rate (and therefore

circulation to the gills) in response to anoxia. A decreased importance for modification of local vasculature may be indicated by the lack of intrabranchial innervation of the goldfish NECs. On the other hand, it may be more important for an organism less tolerant of hypoxia (i.e. zebrafish) to modify local vascular tone in the gills in response hypoxia to ensure maximal blood O_2 saturation.

The NECs of goldfish seem adapted to coping with prolonged periods of exposure to excitatory stimuli (i.e. hypoxia, anoxia). Goldfish belong to the Cyprinidae family and the genus *Carassius*, whose other members include the crucian and common carp. In their natural habitat, these species are regularly exposed to prolonged periods of extreme hypoxia. This evolutionary history has made the goldfish particularly tolerant of prolonged periods of O_2 starvation (Burggren, 1982), but such a constant exposure to a hypoxic stimulus would have many negative implications for O_2-sensitive chemosensory cells. Most importantly, constant stimulation by hypoxia could lead to excitotoxicity, caused by persistent influx of Ca^{2+} (Pamenter *et al*., 2008). In the model proposed in this thesis for O_2 sensing in goldfish NECs (Figure 4.1B), there are two points where this kind of overstimulation is mediated. The role of K_V and K_{Ca} channels in this model is to blunt the hypoxic response, by harnessing both membrane depolarization and Ca^{2+} influx to "apply the brakes". Other neuronal protective mechanisms have been proposed in the brain of goldfish in response to anoxia (Wilkie *et al*., 2008), which set further precedent for this kind of modulation.

If it turns out that, when exposed to anoxia, the K_{Ca} and K_V channels are themselves O_2 sensitive, this would constitute yet another level of modulation, decreasing the effect these channels would have on repolarizing the membrane when presented with anoxia. Sensitivity of K_V channels to hypoxia has been suggested as a mechanism of prolonging the response to

decreased O_2 in mouse CB (Pérez-García *et al.*, 2004). This would again be of adaptive benefit to the anoxia-tolerant goldfish, as a preserved physiological response would become increasingly important as O_2 levels reach ~ 0 mmHg.

It is interesting to note that, despite the anoxia tolerance of goldfish, goldfish NECs bear more similarities to type I cells of the CB, in their complement of ion channels, than the NECs of zebrafish. The significance of this is not yet understood.

4.4. Future directions

Work is required to further illuminate the role of ACh in the gills. While most VAChT-positive cells did not appear to receive zn-12 immunopositive innervation, it is possible that nerve fibers positive for some other antigen may innervate these cells. In addition, investigation of cholinergic receptor types in the lamellae, as well as expression of endothelial nitric oxide synthase (eNOS) may elucidate potential vasoconstrictive or vasodilatory mechanisms for ACh released at the afferent filamental aspect. Finally, it would be very interesting to see if the VAChT-positive cells are themselves O_2 sensitive, as this would constitute a novel population of O_2 chemosensory cells in the gills of fish.

There remains much work to be done to reinforce the proposed cellular model of O_2 sensing in goldfish NECs. If the NECs do in fact rely on some cytosolic factor(s) to respond to hypoxic stimuli, and perhaps some membrane-delimited factor(s) when dealing with anoxia, a method such as perforated patch-clamp might help keep the molecular O_2 sensing mechanism intact. Unfortunately, despite attempts to do so, this technique has not proven feasible in either goldfish or zebrafish because of extremely high series resistance. Additionally, my electrophysiological experiments constitute the first characterization of ion channel expression in

the goldfish NECs; however, more detail is required. For example, though K_V channels appear to belong to the A subtype, systematic characterization using targeted inhibitors of K_V channel subtypes will confirm their identity. Similarly, more steps are required to identify the type of K_B channels present in the goldfish NECs. Application of acidic extracellular solution (ECS) or exposure to halothane will help determine if the K_B channels are of the two-pore acid-sensitive K^+ (TASK) or two-pore halothane-inhibited K^+ (THIK) subtypes, respectively. The FM1-43 experiments demonstrated that synaptic vesicle activity appears to be dependent upon extracellular Ca^{2+}, and that Ca^{2+} influx into the cytosol occurs via L-type Ca_V channels; however, further electrophysiological characterization of the Ca_V channels, as well as pharmacological characterization using calcium imaging will confirm this observation. Finally, further investigation of other sensitizing mechanisms may yield a deeper understanding of the proposed modulation of the hypoxic response in goldfish NECs. For example, increased expression of Na^+ channels, whose inward currents help depolarize membranes, was observed in response to chronic hypoxia in mammalian adrenal chromaffin cells (Stea *et al*., 1992).

4.5. Summary and perspectives

The mechanisms by which an organism responds to O_2 deprivation vary by species, and are influenced by their evolutionary history. In this thesis, I have presented data from the anoxia-tolerant goldfish, and the hypoxia-sensitive zebrafish. In zebrafish, VAChT-positive cells are found predominantly on the afferent side of the filament, and do not colocalize with the synaptic vesicle marker SV2. In some cases, VAChT-positive cells may be innervated by extrabranchial zn-12 immunoreactive nerve fibers. In goldfish gills, I observed no VAChT-positive cells akin to those in zebrafish, but discovered differences in the morphology of

serotonergic NEC innervation. Most notably, the NECs of goldfish do not appear to receive intrabranchial innervation. In addition to these morphological differences, goldfish NECs expressed a complement of ion channels not previously observed in zebrafish, including K_{Ca}, K_V, and Ca_V channels. Like zebrafish, goldfish NECs did express K_B channels; however, current through these channels did not retain its O_2 sensitivity during whole-cell patch-clamp experiments. Intact goldfish NECs were able to respond to hypoxia (P_{O2} ~ 11 mmHg) with an increase in intracellular Ca^{2+}, and increased synaptic vesicle activity. When exposed to anoxia and cyanide, the NECs did exhibit a gradual depolarization. These results indicate that the goldfish NECs likely rely on a cytosolic O_2 sensing mechanism during bouts of hypoxia, and may add to this some membrane-delimited factor(s) when responding to anoxia.

Moving forward, the role of ACh in the gills of zebrafish requires more investigation. I have proposed several mechanisms for the action of ACh, and it would be interesting to examine their validity. In addition, the dearth of information on the effect of ACh in goldfish is surprising, and studies investigating its physiological effect(s) may help understand the findings presented here. Finally, though I have proposed several adaptive roles for the expanded complement of ion channels found in goldfish NECs, it is necessary to expand electrophysiological studies to other species (both anoxia-tolerant and not) in order to truly understand the comparative significance of these findings.

Figure 4.1. Comparison between putative cellular signaling in zebrafish and a proposed mechanism in goldfish neuroepithelial cells (NECs) following hypoxic stimulation. A) Model of cellular O_2 sensing in zebrafish NECs. 1, A decrease in extracellular P_{O2} is detected, likely by a membrane-associated molecular O_2 sensor (Jonz *et al*., 2004). 2, The hypoxic stimulus inhibits K^+ current through background K^+ (K_B) channels, resulting in depolarization of membrane potential (V_m). 3, Membrane depolarization presumably activates voltage-activated Ca^{2+} (Ca_V) channels, leading to an increase in intracellular Ca^{2+} ($[Ca^{2+}]_i$). 4, Increased $[Ca^{2+}]_i$ is believed to facilitate synaptic vesicle fusion and neurosecretion. B) Model of cellular O_2 sensing in goldfish NECs. 1&2 are the same as in (A), except the molecular O_2 sensor appears to rely on cytosolic factor(s). 3, Membrane depolarization activates A-type voltage-dependent K^+ (K_V) channels, leading to an initial repolarization of V_m. 4, Membrane depolarization also activates Ca_V channels, leading to an increase in $[Ca^{2+}]_i$. 5, Increased $[Ca^{2+}]_i$ facilitates Ca^{2+}-dependent synaptic vesicle fusion. 6, Increased $[Ca^{2+}]_i$ also acts on Ca^{2+}-activated K^+ (K_{Ca}) channels, resulting in further repolarization of V_m.

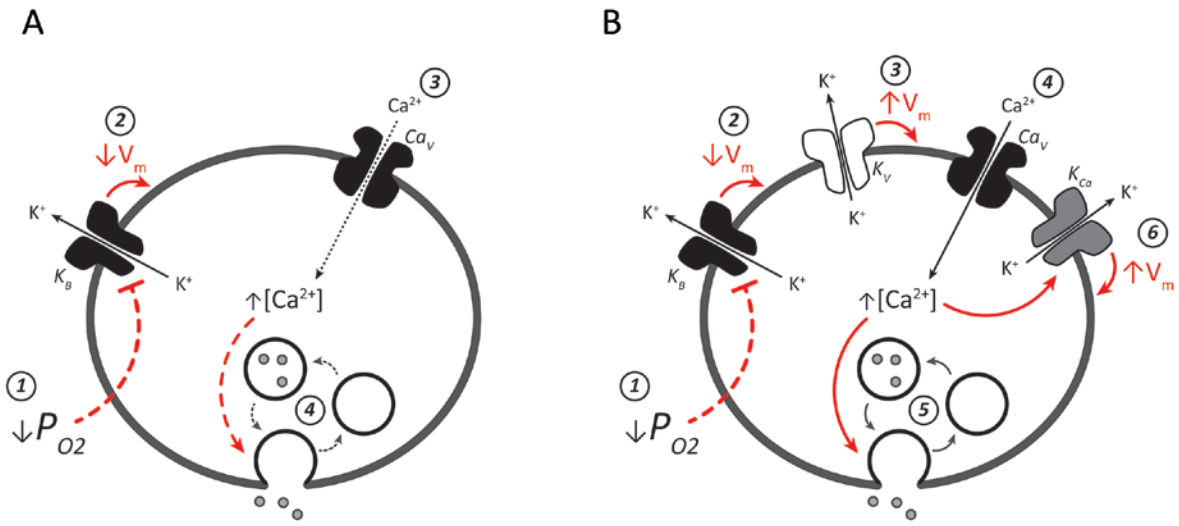
A
B
↓V_m
↑V_m
Ca_V
K_B
K_V
K_Ca
K+
↑[Ca2+]
↓P_O2
1
2
3
4
5
6

5. Appendix I: Vesicular acetylcholine transporter positive control in zebrafish

Reprinted from: Shakarchi, K., Zachar, P.C., Jonz, M.G., 2013. Serotonergic and cholinergic elements of the hypoxic ventilator response in developing zebrafish. J Exp. Biol. 216, 869-880.

Figure 5.1. Positive control for the antibody against the vesicular acetylcholine transporter (VAChT). This experiment, conducted by myself, shows a whole nodose ganglion which was removed from adult zebrafish, prepared for immunohistochemistry, and mounted following the procedures indicated in the Materials and Methods. A single optical section through the ganglion by confocal microscopy indicates the presence of numerous neuronal cell bodies (e.g. arrows) and nerve fibres (e.g. arrowheads). The ganglion is oriented so that the superior aspect is at the top of the image. Scale bar = 10 μm.

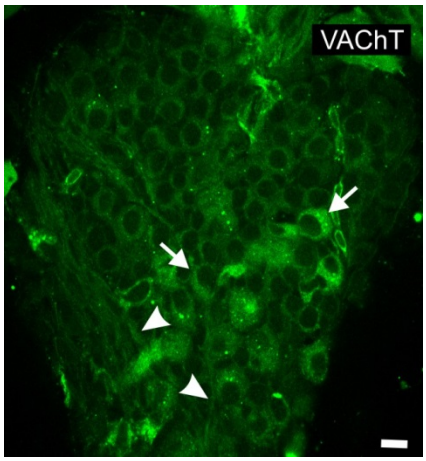
VAChT

6. Appendix II: Oxygen sensitivity of gill neuroepithelial cells in the anoxia-tolerant goldfish

Reprinted from: Zachar, P.C., Jonz, M.G., 2012. Oxgyen sensitivity of gill neuroepithelial cells in the anoxia-tolerant goldfish. Adv. Exp. Med. Biol. 758, 167-172.

6.1. INTRODUCTION

In fish, the challenges of matching oxygen uptake to metabolic demand are compounded by the limited oxygen availability in their surroundings, making these animals uniquely sensitive to hypoxia and ideal for comparative studies in oxygen sensing. Neuroepithelial cells (NECs) are found in the gills of all fish species investigated and are believed to be the primary sites of peripheral oxygen sensing. NECs may store a variety of neurotransmitters within cytoplasmic synaptic vesicles, although serotonin appears to be most common across species. Gill NECs detect changes in either environmental or arterial oxygen partial pressure (P_{O2}) and initiate reflex cardiorespiratory responses, such as hyperventilation (Perry et al., 2009). These cells are, therefore, regarded as evolutionary precursors of peripheral oxygen chemoreceptors in mammals.

The gills of teleost fish are composed of four pairs of arches that give rise to numerous primary filaments. Each filament in turn produces respiratory lamellae, the sites of gas transfer. The NECs are located within the primary filament epithelium facing the incident flow of water as it is pumped through the buccal cavity and over the gills during respiration. This places NECs in a prime location to sample the P_{O2} of inspired water or the nearby arterial circulation (Perry et al., 2009). The gills receive a rich supply of sensory innervation from the glossopharyngeal and vagus nerves (Sundin and Nilsson, 2002). Furthermore, fibres from multiple neuronal populations contact NECs and may receive pre-synaptic input from these cells during hypoxic stimulation (Jonz and Nurse, 2003). The neurochemistry of the NEC-nerve synapse, however, remains largely unresolved (Perry et al., 2009).

The physiological response of NECs to hypoxia at the cellular level has been established in zebrafish (Jonz et al., 2004). A decrease in extracellular P_{O2} inhibits K^+ current through the plasma membrane, representing a mechanism for membrane depolarization and thus transduction

of the hypoxic stimulus. This inhibition is insensitive to classical blockers of voltage-activated K^+ channels, such as tetraethylammonium (TEA) and 4-aminopyridine (4-AP), but sensitive to the drug quinidine (Jonz et al., 2004). These observations indicate that the oxygen-sensitive K^+ current is carried by voltage-independent background K^+ (K_B) channels – as is the case in other cellular models of oxygen sensing (Buckler, 1997; O'Kelly et al., 1999; Campanucci et al., 2003).

While K_B channels may be responsible for the initial depolarization in response to hypoxia, ion channel content and oxygen sensitivity observed in carotid body type I cells of mammalian models presents a more complicated story. For example, in rat type I cells, K_B channels are oxygen sensitive, yet these cells also express calcium-activated (K_{Ca}) and voltage-dependent (K_V) potassium channels (Buckler, 1997; Lopez-Lopez et al., 1997).

In zebrafish, the dominant whole-cell conductance is through K_B channels; however, this may not be the case in other related fish species. Different species of fish exhibit varying tolerances to changes in external P_{O2}, from the relatively hypoxia-intolerant rainbow trout, to the anoxia-tolerant goldfish (Burggren, 1982; Johansen et al., 1984). Differences in tolerance to hypoxia and anoxia may be correlated with different sensitivity or ion channel composition in the NECs of the gill, as NECs of different species retain many morphological similarities regardless of hypoxia tolerance (Saltys et al., 2006). Comparative study across species with varying tolerances is useful in uncovering the relative importance and/or the roles different ion channels might play in modulating the response of NECs to hypoxia. To this end, we are using goldfish (*Carassius auratus*) – an anoxia-tolerant cyprinid fish closely related to zebrafish – to study ion channel expression and oxygen sensitivity in this species.

6.2. METHODS

Physiological characterization of the NECs was done using whole-cell patch-clamp electrophysiology on dissociated cells obtained from gill filaments of goldfish following procedures modified from Jonz et al. (2004). Dissociation of goldfish gill filaments was achieved by immersion in 0.25% trypsin (Invitrogen, Burlington, ON, Canada) and mechanical trituration. Once dissociated, cells were plated on glass-bottomed 35 mm culture dishes (MatTek Corporation, Ashland, MA, USA) coated with Poly-L-lysine (Sigma-Aldrich, Oakville, ON, Canada) and matrigel (BD Biosciences, Mississauga, ON, Canada) and cultured in L-15 medium supplemented with 2% penicillin/streptomycin and 2.5% fetal calf serum (Invitrogen, Burlington, ON, Canada). Dishes containing cells in primary culture were used for patch-clamp recordings within 24-36 hours. Identification of potential oxygen-sensitive NECs was done by introducing 2 mg/ml Neutral Red, a vital marker taken up by acidic granules in the cytoplasm. This technique is commonly used to identify cells containing amines, such as serotonin (Youngson et al., 1993; Jonz et al., 2004). Electrodes were filled with intracellular recording solution consisting of (in mM): KCl (135), NaCl (5), $CaCl_2$ (0.1), HEPES (10), Mg-ATP (2), EGTA (11), and pH adjusted to 7.4 using KOH. Extracellular recording solution consisted of (in mM): KCl (5), NaCl (135), $CaCl_2$ (2), HEPES (10), $MgCl_2$ (2), Glucose (10), and pH was adjusted to 7.8 with NaOH. Recordings were obtained using an Axon Digidata 1440A data acquisition system in conjunction with an Axon Multiclamp 700B microelectrode amplifier (Molecular Devices, Sunnyvale, CA, USA). Signals were sampled at 10 kHz and filtered at 5 kHz. All recordings were corrected appropriately for junction potentials. Hypoxia was generated by bubbling the extracellular solution with 95% N_2. Anoxia was generated by adding 2 mM dithionite (Sigma-Aldrich) to the extracellular solution and maintained by bubbling with

N_2. Cyanide (2 mM) was similarly administered. Tetraethylammonium (TEA, 20 mM) and 4-aminopyridine (4-AP, 5 mM) (Sigma-Aldrich) were applied briefly to inhibit voltage-dependent K^+ channels. All solutions were maintained at a constant pH and were applied to the recording bath under constant superfusion at a rate of 2-4 ml/min.

6.3. RESULTS & DISCUSSION

Exposure of Neutral Red-positive NECs from goldfish to levels of hypoxia similar to those used to study zebrafish NECs (25 mmHg; Jonz et al., 2004) yielded no observable changes in membrane currents or resting potential. In preliminary experiments using chemical anoxia generated by the addition of 2 mM dithionite to the extracellular solution, Neutral Red-positive goldfish NECs were observed to depolarize (Figure 6.1A). Application of 2 mM sodium cyanide elicited a similar response (Figure 6.1B). In both dithionite and cyanide experiments, NECs repolarized upon wash-out with normal solution.

These observations indicate that, while perhaps not responsive to levels of hypoxia conventionally used to assess oxygen sensitivity in chemoreceptive cells of zebrafish (Jonz et al., 2004), goldfish NECs do respond to more severe drops in P_{O2}. This is not surprising, as the blood oxygen affinity in the anoxia-tolerant goldfish is relatively high (P_{50}=2.6 mmHg; Burggren, 1982) as compared to other fish, such as sculpins (P_{50} ranging from 22 to 58 mmHg; Richards et al., 2009) and rainbow trout (P_{50}=22.9 mmHg; Johansen et al., 1984), implying that goldfish NECs need not respond until external P_{O2} levels are much lower. In addition, the finding that cyanide, a potent stimulant of the carotid body, depolarizes the NEC membrane suggests that the mitochondria may play a role in the oxygen sensing mechanism (Wyatt and

Buckler, 2004). This finding is complicated by the nature of cyanide, however, as it is a metabolic inhibitor rather than a chemical known to specifically target oxygen-sensitive cells.

It is evident that a calcium-activated K^+ current (K_{Ca}) is prominent in whole-cell voltage-clamp recordings from goldfish NECs (Figure 6.2). This type of current is reminiscent of rat carotid body type I cells (Lopez-Lopez *et al*., 1997). By contrast, such currents were not reported in zebrafish (Jonz et al., 2004) or channel catfish (Burleson et al., 2006). The present data are also suggestive of a Ca^{2+} conductance across the plasma membrane, as has been reported in gill NECs of trout (Zhang et al., 2011), that precedes activation of K_{Ca} currents. Application of TEA and 4-AP reduced outward current and eliminated the characteristic K_{Ca} 'shoulder' (indicative of K_{Ca} activation) in the whole-cell current-voltage relationship, yielding a profile closely resembling that of an open-rectifier-type background potassium channel (K_B) (Figure 6.2).

K_{Ca} channels have been observed in rat carotid body type I cells, where they may contribute to the resting membrane potential and provide oxygen sensitivity (Peers and Wyatt, 2007). As in type I cells, when the NEC plasma membrane is depolarized by hypoxia (Jonz et al., 2004), voltage-gated calcium channels (Ca_V) would be activated, allowing Ca^{2+} ions to flow down their electrochemical gradient into the cell. Ca^{2+} ions would then activate K_{Ca} channels, further increasing K^+ conductance across the plasma membrane. A role for K_{Ca} channels in goldfish, however, is not presently clear. Such a hyperpolarizing current may suggest a role for K_{Ca} channels in blunting the hypoxic response, or promoting repolarization for subsequent hypoxic stimuli. A similar mechanism of negative feedback has been proposed for cardiac and smooth muscle in mammals (Leblanc et al., 1999; Nelson et al., 2005). Furthermore, future

experiments may reveal if K_{Ca} channels in goldfish NECs are oxygen sensitive, as they are in type I cells, and if they may contribute to oxygen chemotransduction.

Experiments to date have demonstrated that goldfish NECs depolarize in response to severe decreases in extracellular O_2, as generated by dithionite. Additionally, TEA and 4-AP resistant (e.g. K_B) channels believed to be primarily responsible for hypoxia-induced depolarization in zebrafish NECs and carotid body type I cells are present in goldfish NECs. The presence of K_{Ca} channels in goldfish NECs, as observerved in type I cells, raises the possibility that these channels may be involved in modulation or chemotransduction. These data also indicate that the ensemble of ion channels in peripheral chemoreceptors is species-specific in fish and may correlate with natural history or tolerance to hypoxia or anoxia.

Figure 6.1. Current-clamp (I=0) recording of resting membrane potential from goldfish gill neuroepithelial cell (NEC) in primary culture. a) Membrane depolarization of approximately 15 mV in response to chemical anoxia generated by 2 mM dithionite, b) depolarization of approximately 10 mV in response to application of 2 mM sodium cyanide. Resting potentials are indicated to the left of each trace. Scale bars indicate the change in potential vs. time.

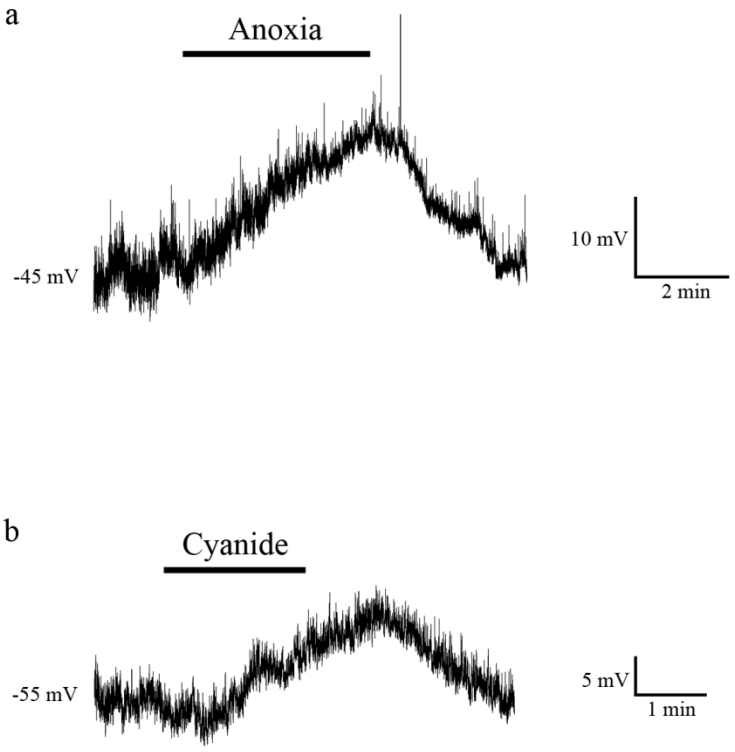
a
Anoxia
-45 mV
10 mV
2 min
b
Cyanide
-55 mV
5 mV
1 min

Figure 6.2. Whole-cell recordings (inset) and current-voltage (I-V) relations generated by sequential steps to a range of test potentials from -80 to +100 mV in 10 mV increments. Cells were held at -60 mV. A characteristic 'shoulder' in the control trace of the I-V indicates the presence of calcium-activated potassium channels (K_{Ca}). Inhibition of voltage-gated potassium channels with TEA and 4-AP reveals the presence of background potassium channels (K_B). Top panels show steps to 0, 30, and 60 mV under control conditions and after application of 20 mM TEA and 5 mM 4-AP.

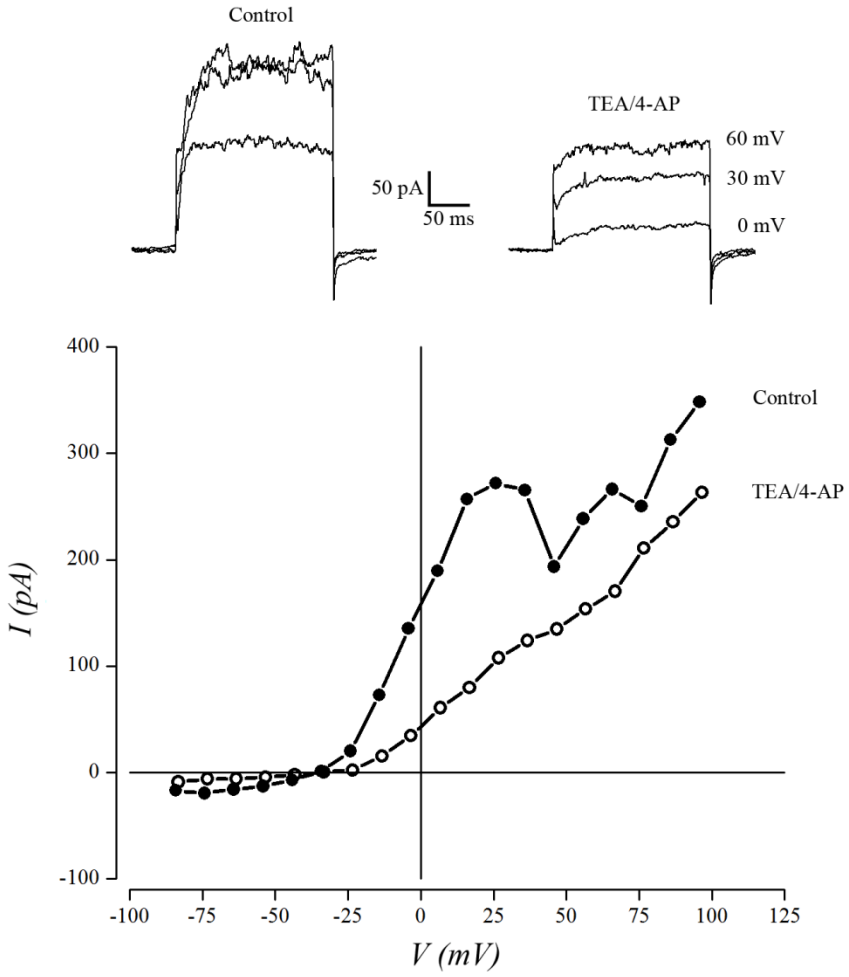
Control
TEA/4-AP
60 mV
30 mV
0 mV
50 pA
50 ms
400
300
200
100
0
-100
I (pA)
Control
TEA/4-AP
-100
-75
-50
-25
0
25
50
75
100
125
V (mV)

7. REFERENCES

Abdallah, S., Perry, S.F., Jonz, M.G., 2012. CO_2 signaling in chemosensory neuroepithelial cells of the zebrafish gill filaments: role of Ca^{2+} and pH. Adv. Exp. Med. Biol. 758, 143-148.

Adriaensen, D., Scheuermann, D.W., 1993. Neuroendocrine cells and nerves of the lung. Anat. Rec. 236, 70-85.

Archer, S.L., Reeve, H.L., Michelakis, E., Puttagunta, L., Waite, R., Nelson, D.P., Dinauer, M.C., Weir, E.K., 1999. O_2 sensing is preserved in mice lacking the gp91 phox subunit of NADPH oxidase. Proc. Natl. Acad. Sci. U.S.A. 96, 7944-7949.

Bailly, Y., Dunel-Erb, S., Geffard, M., Laurent, P., 1989. The vascular and epithelial serotonergic innervation of the actinopterygian gill filament with special reference to the trout, *Salmo gairderi*. Cell Tissue Res, 258, 349-363.

Bailly, Y., Dunel-Erb, S., Laurent, P., 1992. The neuroepithelial cells of the fish gill filament: indolamine-immunocytochemistry and innervation. Anat. Rec. 233, 143-161.

Bayliss, D.A., Sirois, J.E., Talley, E.M., 2003. The TASK family: two-pore domain background K^+ channels. Mol. Interv. 3, 205-219.

Bekar, L.K, Loewen, M.E., Cao, K., Sun, X., Leis, J., Wang, R., Forsyth, G.W., Walz, W., 2004. Complex expression and localization of inactivating K_V channels in cultured hippocampal astrocytes. J. Neurophys. 93, 1699-1709.

Betz, W.J., Mao, F., Bewick, G.S., 1992. Activity-dependent fluorescent staining and destaining of living vertebrate motor nerve terminals. J. Neurosci. 12, 363-375.

Bickler, P.E., Buck, L.T., 2007. Hypoxia tolerance in reptiles, amphibians, and fishes: life with variable oxygen availability. Annu. Rev. Physiol. 2007, 145-170.

Bickler, P.E., Buck, L.T., 2007. Hypoxia tolerance in reptiles, amphibians, and fishes: life with variable oxygen availability. Annu. Rev. Physiol. 2007, 145-170.

Booth, J.H., 1978. The distribution of blood flow in the gills of fish: Application of a new technique to rainbow trout (*Salmo gairdneri*). J. Exp. Biol. 73, 119-129.

Booth, J.H., 1979. The effects of oxygen supply, epinephrine, and acetylcholine on the distribution of blood flow in trout gills. J. Exp. Biol. 83, 31-39.

Brouns, I., Pintelon, I., De Proost, I., Timmermans, J.P., Adriaensen, D. 2009. Diverse and complex airway receptors in rodent lungs. In: Zaccone, G., Cutz, E., Adriaensen, D., Nurse, C.A., Mauceri, A. (Eds.), Airway Chemoreceptors in the Vertebrates: Structure, Evolution and Function. Science Publishers, Enfield, pp. 235-268.

Buckler, K.J., 1997. A novel oxygen-sensitive potassium current in rat carotid body type I cells. J. Physiol. 498, 649-662.

Buckler, K.J., 2010. Two-pore domain K^+ channels and their role in chemoreception. Adv. Exp. Med. Biol. 661, 15-30.

Buckler, K.J., Vaughan-Jones, R.D., 1994. Effects of hypoxia on membrane potential and intracellular calcium in rat neonatal carotid body type I cells. J. Physiol. 476, 423-428.

Buckler, K.J., Vaughan-Jones, R.D., 1998. Effects of mitochondrial uncouplers on intracellular calcium, pH and membrane potential in rat carotid body type I cells. J. Physiol. 513, 819-833.

Buckler, K.J., Williams, B.A., Honoré, E., 2000. An oxygen-, acid- and anaesthetic-sensitive TASK-like background potassium channel in rat arterial chemoreceptor cells. J. Physiol. 525, 135-142.

Buckley, K., Kelly, R.B., 1985. Identification of a transmembrane glycoprotein specific for secretory vesicles of neural and endocrine cells. J. Cell Biol. 100, 1284-1294.

Burgess, A., Vigneron, S., Brioudes, E., Labbé, J.-C., Lorca, T., Castro A., 2010. Loss of human Greatwall results in G2 arrest and multiple mitotic defects due to deregulation of the cyclin B-Cdc2/PP2A balance. Proc. Natl. Acad. Sci. USA. 107, 12564-12569.

Burggren, W.W., 1982. “Air gulping” improves blood oxygen transport during aquatic hypoxia in the goldfish *Carrasius auratus*. Physiol. Zool. 55, 327-334.

Burleson, M.L., Mercer, S.E., Wilk-Blaszczak, M.A., 2006. Isolation and characterization of putative O_2 chemoreceptor cells from the gills of channel catfish (*Ictalurus punctatus*). Brain Res. 1092, 100-107.

Burleson, M.L., Milsom, W.K. 1993. Sensory receptors in the first gill arch of rainbow trout. Respir. Physiol. 93, 97-110.

Burleson, M.L., Milsom, W.K., 1995a. Cardio-ventilatory control in rainbow trout: I. Pharmacology of branchial, oxygen-sensitive chemoreceptors. Respir. Physiol. 100, 231-238.

Burleson, M.L., Milsom, W.K., 1995b. Cardio-ventilatory control in rainbow trout: II. Reflex effects of exogenous neurochemicals. Respir. Physiol. 101, 289-299.

Bushnell, P.G., Steffensen, J.F., Johansen, K. 1984. Oxygen consumption and swimming performance in hypoxia-acclimated rainbow trout *Salmo gairdneri*. J. Exp. Biol. 113, 225-235.

Campanucci, V.A., Fearon, I.M., Nurse, C.A., 2003. A novel O_2-sensing mechanism in rat glossopharyngeal neurons mediated by a halothane-inhibitable background K^+ conductance. J. Physiol. 548, 731-743.

Campanucci, V.A., Nurse, C.A., 2007. Autonomic innervation of the carotid body: role in efferent inhibition. Respir. Physiol. Neurobiol. 157, 83-92.

Chamberland, V., Rious, P., 2010. Not only students can express alcohol dehydrogenase: goldfish can too! Adv. Physiol. Educ. 34, 222-227.

Chen, X., Yuan, L.L., Zhao, C., Birnbaum, S.G., Frick, A., Jung, W.E., Schwarz, T.L., Sweatt, J.D., Johnston, D., 2006. Deletion of Kv4.2 gene eliminates dendritic A-type K^+ current and enhances induction of long-term potentiation in hippocampal CA1 pyramidal neurons. J. Neurosci. 26, 12143-12151.

Dasso, L.L., Buckler, K.J., Baughan-Jones, R.D., 1997. Muscarinic and nicotinic receptors raise intracellular Ca^{2+} levels in rat carotid body type I cells. J. Physiol. 498, 327-338.

Diamond, J., 1955. Observations on the excitation by acetylcholine and by pressure of sensory receptors in the cats' carotid sinus. J. Physiol. 130, 513-532.

Docherty, R.J., McQueen, D.S., 1979. The effects of acetylcholine and dopamine on carotid chemosensory activity in the rabbit. J. Physiol. 288, 411-423.

Donnelly, D.F., 2009. Nicotinic acetylcholine receptors do not mediate excitatory transmission in young rat carotid body. J. Appl. Physiol. 107, 1806-1816.

Duchen, M.R., Biscoe, T.J., 1992. Relative mitochondrial membrane potential and $[Ca^{2+}]_i$ in type I cells isolated from the rabbit carotid body. J. Physiol. 450, 33-61.

Dunel-Erb, S., Bailly, Y., Laurent, P., 1982. Neuroepithelial cells in fish gill primary lamellae. J. Appl. Physiol. 53, 1342-1353.

Eyzaguirre, C., Monti-Bloch, L., 1980. Similarities and differences in the physiology and pharmacology of cat and rabbit carotid bodies. Fed. Proc. 39, 2653-2656.

Finley, J.C., Katz, D.M., 1992. The central organization of carotid body afferent projections to the brainstem of the rat. Brain. Res. 572, 108-116.

Fitzgerald, R.S., Shirahata, M., Ide, T., 1997. Further cholinergic aspects of carotid body chemotransduction of hypoxia in cats. J. Appl. Physiol. 82, 819-827.

Fu, X.W., Nurse, C.A., Wang, Y.T., Cutz, E., 1999. Selective modulation of membrane currents by hypoxia in intact airway chemoreceptors from neonatal rabbit. J. Physiol. 514,139-150.

Fu, X.W., Nurse, C.A., Wong, V., Cutz, E., 2002. Hypoxia-induced secretion of serotonin from intact pulmonary neuroepithelial bodies in neonatal rabbit. J. Physiol. 539, 503-510.

Fu, X.W., Wang, D., Nurse, C.A., Dinauer, M.C., Cutz, E., 2000. NADPH oxidase is an O_2 sensor in airway chemoreceptors: Evidence from K^+ current modulation in wild-type and oxidase-deficient mice. PNAS. 97, 4374-4379.

Golowasch, J., Thomas, G., Taylor, A.L., Patel, A., Pineda, A., Khalil, C., Nadim, F., 2009. Membrane capacitance measurements revisited: Dependence of capacitance value on measurement method in nonisopotential neurons. J. Neurophysiol. 102, 2161-2175.

González. C., Almaraz, L., Obeso, A., Rigual, R. 1994. Carotid body chemoreceptors: from

Guia, A., Wan, X., Courtemanche, M., Leblanc, N., 1999. Local Ca2+ Entry Through L-type Ca2+ Channels Activates Ca2+-dependent K+ Channels in Rabbit Myocytes. Circ. Res. 84, 1032-1042.

Hartness, M.E., Lewis, A., Searle, G.J., O'Kelly, I., Peers, C., 2001. Combined antisense and pharmacological approaches implicate hTASK as an airway O_2 sensing K^+ channel. J. Biol. Chem. 276, 26499-26508.

Herrera, G. M., Etherton, B., Nausch, B., Nelson, M. T., 2005. Negative Feedback Regulation of Nerve-mediated Contractions by KCa Channels in Mouse Urinary Bladder Smooth Muscle. Am. J. Physiol. Regul. Integr. Comp. Physiol. 289, R402-R409.

Hoffman, D.A., Magee, J.C., Colbert, C.M., Johnston, D., 1997. K^+ channel regulation of signal propagation in dendrites of hippocampal pyramidal neurons. Nature. 387, 869-875.

Jin, R.C., Loscalzo, J., 2010. Vascular nitric oxide: formation and function. J. Blood Med. 2010, 147-162.

Jonz, M. G., Nurse, C. A., 2003. Neuroepithelial Cells and Associated Innervation of the Zebrafish Gill: A Confocal Immunofluorescence Study. J. Comp. Neurol. 461, 1-17.

Jonz, M.G., Fearon, I.M., Nurse, C.A., 2004. Neuroepithelial oxygen chemoreceptors of the zebrafish gill. J. Physiol. 560, 737-752.

Jonz, M.G., Nurse, C.A., 2003. Neuroepithelial cells and associated innervation of the zebrafish gill: a confocal immunofluorescence study. J. Comp. Neurol. 461, 1-17.

Jonz, M.G., Nurse, C.A., 2005. Development of oxygen sensing in the gills of zebrafish. J. Exp. Biol. 208, 1537-1549.

Jonz, M.G., Nurse, C.A., 2006. Ontogenesis of oxygen chemoreception in aquatic vertebrates. Respir. Physiol. Neurobiol. 154, 139-152.

Jonz, M.G., Nurse, C.A., 2009. Oxygen-sensitive neuroepithelial cells in the gills of aquatic vertebrates, in Zaccone, G., Cutz, E., Adriaensen, D., Nurse, C.A., Mauceri, A. (Eds.), Airway chemoreceptors in the vertebrates: structure, evolution and function. Science Publishers, Enfield, NH, USA, pp. 1-30.

Jonz, M.G., Nurse, C.A., 2009. Oxygen-sensitive neuroepithelial cells in the gills of aquatic vertebrates. In Airway Chemoreceptors in the Vertebrates, ed. Zaccone, G., Cutz, E., Adriawnsen, D., Nurse, C.A., Mauceri, A., pp.1-30. Enfield, New Hampshire, USA.

Jonz, M.G., Zaccone, G., 2009. Nervous control of the gills. Acta Histochem. 111, 207-216.

Kemp, P.J., Peers, C., Lewis, A., Miller, P., 2004. Regulation of recombinant human brain tandem P domain K^+ channels by hypoxia: a role for O_2 in the control of neuronal excitability? J. Cell Mol. Med. 8, 38-44.

Kimura, H., Nagai, Y., Umemura, K., Kimura, Y., 2005. Physiological roles of hydrogen sulfide: synaptic modulation, neuroprotection, and smooth muscle relaxation. Antioxid. Redox Signal. 7, 795-803.

Kline, D.D., Peng, Y.J., Manalo, D.J., Semenza, G.L., Prabhakar, N.R., 2002. Defective carotid body function and impaired ventilatory responses to chronic hypoxia in mice partially deficient for hypoxia-inducible factor 1 alpha. Proc. Natl. Acad. Sci. U.S.A. 99, 821-826.

Kollo, M., Holderith, N., Antal, M., Nusser, Z., 2008. Unique clustering of A-type potassium channels on different cell types of the main olfactory bulb. Eur. J. Neurosci. 27, 1686-1699.

Kumar, P., Bin-Jaliah, I., 2007. Adequate stimuli of the carotid body: More than an oxygen sensor? Respir. Physiol. Neurobiol. 157, 12-21.

Kumar, P., Prabhakar, N.R., 2012. Peripheral chemoreceptors: function and plasticity of the carotid body. Compr. Physiol. 2, 141-219.

Kusakabe, T., 2002. Carotid labyrinth of amphibians. Microsc. Res. Tech. 59, 207-226.

Lesage, F., 2003. Pharmacology of neuronal background potassium channels. Neuropharmacology. 44, 1-7.

López-Barneo, J., López-López, J.R., Urena, J., González, C., 1988. Chemotransduction in the carotid body: K^+ current modulated by PO_2 in type I chemoreceptor cells. Science 241, 580-582.

López-Barneo, J., Ortega-Saenz, P., Pardal, R., Pascual, A., Piruat, J.I., 2008. Carotid body oxygen sensing. Eur. Respir. J. 32, 1386-1398.

López-Barneo, J., Pardal, R., Ortega-Saenz, P., 2001. Cellular mechanism of oxygen sensing. Annu. Rev. Physiol. 63, 259-287.

López-López, J. R., González, C., Perez-García, M. T., 1997. Properties of ionic currents from isolated adult rat carotid body chemoreceptor cells: effect of hypoxia. J. Physiol. 499, 429-441.

Mandic, M., Todgham, A.E., Richards, J.G., 2009. Mechanisms and evolution of hypoxia tolerance in fish. Proc. R. Soc. B. 276, 735-744.

McQueen, D.S., 1977. A quantitative study of the effects of cholinergic drugs on carotid chemoreceptors in the cat. J. Physiol. 273, 515-532.

Mendelsohn, B.A., Kassebaum, B.L., Gitlin, J.D., 2008. The zebrafish embryo as a dynamic model of anoxia tolerance. Dev. Dyn. 237, 1780-1788.

Mills, E., Jobsis, F.F., 1972. Mitochondrial respiratory chain of carotid body and chemoreceptor response to changes in oxygen tension. J. Neurophysiol. 35, 405-428.

Milsom, W.K., Brill, R.W., 1986. Oxygen sensitive afferent information arising from the first gill arch of yellowfin tuna. Respir. Physiol. 66, 193-203.

Milsom, W.K., Burleson, M.L., 2007. Peripheral arterial chemoreceptors and the evolution of the carotid body. Respir. Physiol. Neurobiol. 157, 4-11.

Milsom, W.K., Reid, S.G., Rantin, F.T., Sundin, L., 2002. Extrabranchial chemoreceptors involved in respiratory reflexes in the neotropical fish *Colossoma macropomum* (the tambaqui). J. Exp. Biol. 205, 1765-1774.

Mojet, M.H., Mills, E., Duchen, M.R., 1997. Hypoxia-induced catecholamine secretion in isolated newborn rat adrenal chromaffin cells is mimicked by inhibition of mitochondrial respiration. J. Physiol. 504, 175-189.

Montoro, R.J., Ureña, J., Fernández-Chacón, R., Alvarez de Toledo, G., López-Barneo, J., 1996. Oxygen sensing by ion channels and chemotransduction in single glomus cells. J. Gen. Physiol. 107, 133-143.

Gonzalez, C., Almaraz, L., Obeso, A., Rigual, R., 1994. Carotid body chemoreceptors: from natural stimuli to sensory discharges. Physiol. Rev. 74, 829-898.
Nurse, C.A., 2010. Neurotransmitter and neuromodulatory mechanisms at peripheral arterial chemoreceptors. Exp. Physiol. 95, 657-667.

O'Kelly, I., Stephens, R. H., Peers, C., Kemp, P. J., 1999. Potential Identification of the O2-Sensitive K+ Current in a Human Neuroepithelial Body-Derived Cell Line. Am. J. Physiol. 276, L96-L104.

Olson, K.R., Dombkowski, R.A., Russell, M.J., Doellman, M.M., Head, S.K., Whitfield, N.L., Madden, J.A., 2006. Hydrogen sulfide as an oxygen sensor/transducer in vertebrate hypoxic vasoconstriction and hypoxic vasodilation. J. Exp. Biol. 209, 4011-4023.

Olson, K.R., Healy, M.J., Qin, Z., Skovgaard, N., Vulesevic, B., Duff, D.W., Whitfield, N.L., Yang, G., Wang, R., Perry, S.F., 2008. Hydrogen sulfide as an oxygen sensor in trout gill chemoreceptors. Am. J. Physiol. Regul. Integr. Comp. Physiol. 295, R669-80.

Ortega-Saenz, P., Pardal, R., Garcia-Fernandez, M., López-Barneo, J., 2003. Rotenone selectively occludes sensitivity to hypoxia in rat carotid body glomus cells. J. Physiol. 548, 789-800.

Ortega-Saenz, P., Pascual, A., Gomez-Diaz, R., López-Barneo, J., 2006. Acute oxygen sensing in heme oxygenase-2 null mice. J. Gen. Physiol. 128, 405-411.

Ortega-Saenz, P., Pascual, A., Piruat, J.I., López-Barneo, J., 2007. Mechanisms of acute oxygen sensing by the carotid body: lessons from genetically modified animals. Respir. Physiol. Neurobiol. 157, 140-147.

Padilla, P.A., Roth, M.B., 2001. Oxygen deprivation causes suspended animation in the zebrafish embryo. Proc. Natl. Acad. Sci. 98, 7331-7335.

Pamenter, M.E., Shin, D.S., Buck, L.T., 2008. AMPA receptors undergo channel arrest in the anoxic turtle cortex. Am. J. Physiol. Regul. Integr. Comp. Physiol. 294, R606-R613.

Pan, J., Copland, I., Post, M., Yeger, H., Cutz, E., 2006. Mechanical stretch-induced serotonin release from pulmonary neuroendocrine cells: implications for lung development. Am. J. Physiol. Lung Cell. Mol. Physiol. 290, L185-93.

Pan,T.F. , Burggren, W.W., 2010. Onset and early development of hypoxic ventilatory responses and branchial neuroepithelial cells in *Xenopus laevis*. Comp. Biochem. Physiol. A. 157, 382-391.

Pardal, R., Ortega-Saenz, P., Duran, R., López-Barneo, J., 2007. Glia-like stem cells sustain physiologic neurogenesis in the adult mammalian carotid body. Cell 131, 364-377.

Peers, C., O'Donnell, J., 1990. Potassium currents recorded in type I carotid body cells from the neonatal rat and their modulation by chemoexcitatory agents. Brain Res. 522, 259-266.

Peers, C., Wyatt, C.N., 2007. The role of maxiK channels in carotid body chemotransduction. Resp. Physiol. Neurobiol. 157, 75-82.

Peers, C., Wyatt, C.N., Evans, A.M., 2010. Mechanisms for acute oxygen sensing in the carotid body. Respir. Physiol. Neurobiol. 174, 292-298.

Pellegrino, D., Sprovieri, E., Mazza, R., Randall, D.J., Tota, B., 2002. Nitric oxide-cGMP-mediated vasoconstriction and effects of acetylcholine in the branchial circulation of the Eel. Comp. Biochem. Physiol. A. Mol. Integr. Physiol. 132, 447-457.

Peng, Y.J., Nanduri, J., Raghuraman, G., Souvannakitti, D., Gadalla, M.M., Kumar, G.K., Snyder, S.H., Prabhakar, N.R., 2010. H_2S mediates O_2 sensing in the carotid body. Proc. Natl. Acad. Sci. U. S. A. 107, 10719-10724.

Pérez, G.J., Desai, M., Anderson, S., Scornik, F.S., 2013. Large-conductance calcium-activated potassium current modulates excitability in isolated canine intracardiac neurons. Am. J. Physiol. Cell Physiol. 304, 280-286.

Pérez-García, M.T., Colinas, O., Miguel-Velado, E., Moreno-Dominguez, A., López-López, J.R., 2004. Characterization of the K_V channels of mouse carotid body chemoreceptor cells and their role in oxygen sensing. J. Physiol. 557, 457-471.

Perry, S.F., Jonz, M.G., Gilmour, K.M., 2009. Oxygen sensing and the Hypoxic Ventilatory Response. Fish Physiol. 27, 193-253.

Plant, L.D., Kemp, P.J., Peers, C., Henderson, Z., Pearson, H.A., 2002. Hypoxic depolarization of cerebellar granule neurons by specific inhibition of TASK-1. Stroke. 33, 2324-2328.

Porteus, C.S., Brink, D.L., Coolidge, E.H., Fong, A.Y., Milsom, W.K., 2013. Distribution of acetylcholine and catecholamines in fish gills and their potential roles in the hypoxic ventilator response. Acta Histochem. 115, 158-169.

Prabhakar, N.R., 2006. O_2 sensing at the mammalian carotid body: why multiple O_2 sensors and multiple transmitters? Exp. Physiol. 91, 17-23.

Prado, M.A., Reis, R.A., Prado, V.F., de Mello, M.C., Gomez, M.V., de Mello, F.G., 2002. Regulation of acetylcholine synthesis and storage. Neurochem. Int. 41, 291-299.

Pumplin, D.W., Getschman, E., 2000. Synaptic proteins in rat taste bud cells: appearance in the Golgi apparatus and relationship to α-gustducin and the Lewis(b) and A antigens. J. Comp. Neurol. 427, 171-184.

Qin, Z., Lewis, J.E., Perry, S.F., 2010. Zebrafish (*Danio rerio*) gill neuroepithelial cells are sensitive chemoreceptors for environmental CO_2. J. Physiol. 588, 861-872.

Regan, K.S., Jonz, M.G., Wright, P.A., 2011. Neuroepithelial cells and the hypoxia emersion response in the amphibious fish Kryptolebias marmoratus. J. Exp. Biol. 214, 2560-2568.

Riesco-Fagundo, A.M., Pérez-García, M.T., González, C., López-López, J.R., 2001. O_2 modulates lrage-conductance Ca^{2+}-dependent K^+ channels of rat chemoreceptor cells by a membrane-restricted and CO-sensitive mechanism. Circ. Res. 89, 430-436.

Roberts, O.L., Kamishima, T., Barrett-Jolley, R., Quayle, J.M., Dart, C., 2013. Exchange protein activated by cAMP (Epac) induces vascular relaxation by activating Ca^{2+}-sensitive K^+ channels in rat mesenteric artery. J. Physiol. (In press).

Roghani, A., Feldman, J., Kohan, S.A., Shirzadi, A., Gundersen, C.B., Brecha, N., Edwards, R.H., 1994. Molecular cloning of putative vesicular transporter for acetylcholine. Proc. Natl. Acad. Sci. 91, 10620-10624.

Saltys, H.A., Jonz, M.G., Nurse, C.A., 2006. Comparative study of gill neuroepithelial cells and their innervation in teleosts and *Xenopus* tadpoles. Cell Tissue Res. 323, 1-10.

Sanchez, D., López-López, J.R., Pérez-García, M.T., Sanz-Alfayate, G., Obeso, A., Ganfornina, M.D., González, C., 2002. Molecular identification of Kvalpha subunits that contribute to the oxygen-sensitive K^+ current of chemoreceptor cells of the rabbit carotid body. J. Physiol. 542, 369-382.

Schweitzer, A., Wright, S., 1938. Action of prostigmine and acetylcholine on respiration. Q. J. Exp. Phys. 28, 33-47.

Shakarchi, K., Zachar, P.C., Jonz, M.G., 2013. Serotonergic and cholinergic elements of the hypoxic ventilator response in developing zebrafish. J Exp. Biol. 216, 869-880.

Shen, R.J., Jiang, X.Y., Pu, J.W., Zou, S.M., 2010. HIF-1alpha and -2alpha genes in a hypoxia-sensitive teleost species Megalobrama amblycephala: cDNA cloning, expression and different responses to hypoxia. Comp. Biochem. Physiol. B. Biochem. Mol. Biol. 157, 273-280.

Shibahara, S., Muller, R., Taguchi, H., Yoshida, T., 1985. Cloning and expression of cDNA for rat heme oxygenase. Proc. Natl. Acad. Sci. U. S. A. 82, 7865-7869.

Shirahata, M., Balbir, A., Otsubo, T., Fitzgerald, R.S., 2007. Role of acetylcholine in neurotransmission of the carotid body. Respir. Physiol. Neurobiol. 157, 93-105.

Smatresk, N.J., Burleson, M.L., Azizi, S.Q., 1986. Chemoreflexive responses to hypoxia and NaCN in longnose gar: evidence for two chemoreceptor loci. Am. J. Physiol. 251, R116-25.

Solaro, C.R., Prakriya, M., Ding, J.P., Lingle, C.J., 1995. Inactivating and noninactivating Ca^{2+}- and voltage-dependent K^+ current in rat adrenal chromaffin cells. J. Neurosci. 15, 6110-6123.

Sollid, J., Nilsson, G.E., 2006. Plasticity of respiratory structures--adaptive remodeling of fish gills induced by ambient oxygen and temperature. Respir. Physiol. Neurobiol. 154, 241-251.

Solsona, C., Innocenti, B., Fernández, J.M., 1998. Regulation of exocytotic fusion by cell inflation. Biophys. J. 74, 1061-1073.

Stea, A., Jackson, A., Nurse, C.A., 1992. Hypoxia and N6,O2'-dibutyryladenosine 3',5'-cyclic monophosphate, but not nerve growth factor, induce Na+ channels and hypertrophy in chromaffin-like arterial chemoreceptors. Proc. Natl. Acad. Sci. U.S.A. 89, 9469-9473.

Straus, C., Wilson, R.J., Remmers, J.E., 2001. Oxygen sensitive chemoreceptors in the first gill arch of the tadpole, Rana catesbeiana. Can. J. Physiol. Pharmacol. 79, 959-962.

Stuart, A.E., Hudspeth, A.J., Hall, Z.W., 1974. Vital staining of specific monoamine-containing cells in the leech nervous system. Cell Tiss. Res. 153, 55-61.

Sundin, L., Nilsson, S., 1997. Neurochemical mechanisms behind gill microcirculatory responses to hypoxia in trout: *in vivo* microscopy study. Am. J. Physiol. 41, R576-R585.

Sundin, L., Nilsson, S., 2002. Branchial innervation. J. Exp. Zool. 293, 232-248.

Sundin, L.I. 1995. Responses of the branchial circulation to hypoxia in the Atlantic cod, *Gadus morhua*. Am. J. Physiol. Reg. Int. Comp. Physiol. 268, R771-778.

Tegenge, M.A., Böhnel, H., Gessler, F., Bicker, G., 2012. Neurotransmitter vesicle release from human model neurons (NT2) is sensitive to botulinum toxin A. Cell Mol. Neurobiol. 35, 1021-1029.

Thompson R.J., Nurse, C.A., 1998. Anoxia differentially modulates multiple K^+ currents and depolarizes neonatal rat adrenal chromaffin cells. J. Physiol. 512, 421-434.

Trevarrow, B., Marks, D.L., Kimmel, C.B., 1990. Organization of hindbrain segments in the zebrafish embryo. Neuron. 4,669-679.

Tzaneva, V., Gilmour, K.M., Perry, S.F., 2011. Respiratory responses to hypoxia or hypercapnia in goldfish (*Carassius auratus*) experiencing gill remodeling. Respir. Physiol. Neurobiol. 175, 112-120.

Tzaneva, V., Perry, S.F., 2010. The control of breathing in goldfish (*Carassius auratus*) experiencing thermally induced gill remodelling. J. Exp. Biol. 213, 3666-3675.

Varas, R., Wyatt, C.N., Buckler, K.J., 2007. Modulation of TASK-like background potassium channels in rat arterial chemoreceptor cells by intracellular ATP and other nucleotides. J. Physiol. 583, 521-536.

Vicario, I., Obeso, A., Rocher, A., López-Lopez, J. R., González, C. 2000. Intracellular Ca^{2+} stores in chemoreceptor cells of the rabbit carotid body: significance for chemoreception. Am. J. Physiol. Cell Physiol. 279, C51-C6.

Vulesevic, B., McNeill, B., Perry, S.F., 2006. Chemoreceptor plasticity and respiratory acclimation in the zebrafish Danio rerio. J. Exp. Biol. 209, 1261-1273.

Wang, D., Zhong, X., Qiao, Z., Gui, J., 2008. Inductive transcription and protective role of fish heme oxygenase-1 under hypoxic stress. J. Exp. Biol. 211, 2700-2706.

Wilkie, M.P., Pamenter, M.E., Alkabie, S., Carapic, D., Shin, D.S., Buck, L.T., 2008. Evidence of anoxia-induced channel arrest in the brain of the goldfish (*Carassius auratus*). Comp. Biochem. Physiol. C. Toxicol. Pharmacol. 148, 355-362.

Williams, S.E., Wootton, P., Mason, H.S., Bould, J., Iles, D.E., Riccardi, D., Peers, C., Kemp, P.J., 2004. Hemoxygenase-2 is an oxygen sensor for a calcium-sensitive potassium channel. Science 306, 2093-2097.

Wyatt, C. N., Buckler, K. J., 2004. The Effect of Mitochondrial Inhibitors on Membrane Currents in Isolated Neonatal Rat Carotid Body Type I Cells. J. Physiol. 556.1, 175-191.

Wyatt, C.N., Pearson, S.A., Kumar, P., Peers, C., Hardie, D.G., Evans, A.M., 2008. Key roles for AMP-activated protein kinase in the function of the carotid body? Adv. Exp. Med. Biol. 605, 63-68.

Wyatt, C.N., Peers, C., 1993. Nicotinic acetylcholine receptors in isolated type I cells of the neuonatal rat carotid body. Neuroscience 54, 275-281.

Wyatt, C.N., Peers, C., 1995. Ca^{2+}-activated K^+ channels in isolated type-I cells of the neonatal rat carotid body. J. Physiol. 483, 559-565.

Wyatt, C.N., Wright, C., Bee, D., Peers, C., 1995. O_2-sensitive K^+ currents in carotid body chemoreceptor cells from normoxic and chronically hypoxic rats and their roles in hypoxic chemotransduction. Proc. Natl. Acad. Sci. 92, 295-299.

Youngson, C., Nurse, C., Yeger, H., Cutz, E., 1993. Oxygen sensing in airway chemoreceptors. Nature. 365,153-155.

Zachar, P.C., Jonz, M.G., 2012. Neuroepithelial cells of the gill and their role in oxygen sensing. Respir. Physiol. Neurobiol. 183, 301-308.

Zachar, P.C., Jonz, M.G., 2012. Oxgyen sensitivity of gill neuroepithelial cells in the anoxia-tolerant goldfish. Adv. Exp. Med. Biol. 758, 167-172.

Zhang, L., Nurse, C.A., Jonz, M.G., Wood, C.M., 2011. Ammonia sensing by neuroepithelial cells and ventilatory responses to ammonia in rainbow trout. J. Exp. Biol. 214, 2678-2689.